THESIS

IMPROVED CATALYST REGENERATION PROCESS TO INCREASE POISON REMOVAL AND IMPROVE PERFORMANCE RECOVERY

Submitted by

Rodrigo Bauza

Department of Mechanical Engineering

In partial fulfillment of the requirements

For the Degree of Master of Science

Colorado State University

Fort Collins, Colorado

Spring 2021

Master's Committee:

Advisor: Daniel Olsen

Brett Windom
Jerry Johnson

ABSTRACT

IMPROVED CATALYST REGENERATION PROCESS TO INCREASE POISON REMOVAL AND IMPROVE CATALYST PERFORMANCE

Internal combustion engines are partly responsible for increasing amounts of carbon dioxide, nitrogen, carbon monoxide, hydrocarbons, aldehydes, and particulate matter in the atmosphere.

These emissions have detrimental health effects on humans and negatively impact the environment by contributing to the formation of acid rain and photochemical smog. Large bore two-stroke natural gas engines are used commonly for power generation, and in order to meet the National Emissions Standards for Hazardous Air Pollutants set by the Environmental Protection Agency, engine manufacturers commonly select oxidation catalysts as the exhaust aftertreatment of choice. These catalysts degrade over time due to thermal, chemical, and mechanical reasons. Lubrication oil makes its way through the combustion chamber and onto the catalyst, degrading the unit. To estimate the degradation rate of the units and to find the best restoration method, two identical alumina-platinum oxidation catalysts were used in a dual setting, combining a field degradation engine and a laboratory testing engine. The lubrication oil from the cylinder makes its way to the catalyst and creates a layer of volatile hydrocarbons at the very surface that reduces the surface area and catalytic activity of the unit. Moreover, the additives from the oil, such as sulfur, phosphorus, and zinc actively poison the crystallites and minimize the reduction efficiency of the units. The wash-coat is turned

into a powder and analyzed, showing sulfur is the most prevalent poison, constituting approximately 8.97% of the wash-coat when the units are degraded. Phosphorus constitutes roughly 2.55%, and zinc makes up less than 0.50% of the wash-coat and is the most superficial poison. Sulfur is not only the most prevalent but also penetrates deeper into the wash-coat than the rest of the poisons, but phosphorus is seen to interact chemically with the platinum crystallites, suggesting a stronger de-activation by phosphorus.

Platinum is more active in its metallic form, and the catalyst of interest improves in performance after being chemically reduced in a 5% hydrogen purge at 450°C, indicating the platinum crystallites were oxidized in the aging process. The units were aged, then restored with the industry standard washing procedure, then aged again until reaching non-compliance with the emissions standards set by the Environmental Protection Agency, and then restored a second time with a modified version of the industry standard washing process. In order to find the best restoring process, variations of the industry standard chemical wash are tested, and the result proves unsuccessful to modify the washing procedure. Moreover, the industry standard washing process is enhanced by adding two new steps, carbon baking and crystallite restoration. The combination of both baking and washing is tested with elemental and performance analysis. The laboratory elemental analysis suggests the baking restoration steps should be added before washing, which is in agreement with the performance bench testing results. The levels of sulfur and phosphorus are respectively brought down to 0.692% and 0.689% after applying the modified restoration process to the units, and zinc is reduced to 0.048% of the wash-coat. However, the slipstream

performance results with real exhaust from a Cummins QSK19G do not fully agree with the addition of the baking steps to the industry washing standard restoration, likely because the combined restoration was tested on a catalyst that had been previously washed and re-aged, which is known in the industry to produce less successful restoring results. The catalysts can be aged and restored two to three times before the reduction efficiency increase from the restoration is not great enough to financially motivate catalyst users to restore the units instead of replacing them.

ACKNOWLEDGEMENTS

I would like to first thank my parents, Rodrigo and Carmen, and my siblings for the unconditional support provided throughout my years at CSU living far away from home. My close friends too deserve my entire appreciation by making this experience so much more enjoyable. These years of intense studying were also the most fun years I have had, all thanks to them.

Thanks to Dr. Olsen for being a cornerstone in this research project by providing guidance and advice during the entirety of the project. Not only did he perform his duty responsibly, but he seems to effortlessly give the best of himself to his students and advisees. Thanks to Pat McCurdy for his guidance with elemental analysis. And a great amount of appreciation goes to Mark James, James Tillotson, Kirk Evans, Patrick Stauffer, Clayton Eisenach, and Matt Willman for their help with emissions testing and the catalyst washing box experiment, and for making the day to day something to look forward to with their professional guidance and sense of humor.

TABLE OF CONTENTS

LIST OF TABLES

LIST OF FIGURES

LIST OF ACRONYMS

- AU: Atomic units
- AGES: Advanced Gas Engine Solutions
- BE: Binding energy
- CASINO: Monte Carlo Simulation of Electron Trajectory in Solids
- CC: Carbonate
- CO: Carbon monoxide
- CO_2: Carbon dioxide
- EC: Elemental carbon
- EDS: Energy dispersive X-ray detector
- EPA: Environmental Protection Agency
- FID: Flame ionization detector
- HC: Hydrocarbons
- ICE: Internal combustion engines
- kV: Kilovolts
- NESHAP: National Emissions Standards for Hazardous Air Pollutants
- NO_x: Nitrogen oxides
- OC: Organic carbon
- PC: Pyrolyzed char formed
- PM: Particulate matter
- PPM: Parts per million
- PPMD: Parts per million dry

- SCR: Selective catalytic reducers
- SEM: Scanning electron microscope
- SSU: Sulfur scavenger unit
- TEM: Transmission electron microscopy
- TPR: Temperature programmed reduction
- TWC: Three-way catalyst
- VOC: Volatile organic compounds
- XPS: X-ray spectroscopy
- XRD: X-ray powder diffraction

1. Introduction

1.1 Exhaust emission control

Internal combustion engines (ICE) are mostly responsible for increasing amounts of carbon dioxide (CO_2) to our atmosphere, as well as nitrogen oxides (NO_x) carbon monoxide (CO), hydrocarbons (HCs), aldehydes, and particulate matter (PM) [1]. The inhalation of such has detrimental respiratory effects. For example, CO and NO have a high affinity for hemoglobin, depriving the body from carrying oxygen to body tissues, and NO_x is one of the causative agents of acid rain and photochemical smog [2, 3]. In order to reduce the amount of these emissions, the Environmental Protection Agency (EPA) sets the National Emissions Standards for Hazardous Air Pollutants (NESHAP), which constantly push engine manufacturers to come up with efficient exhaust after-treatment methods. Engine characteristics determine such limits, e.g., for a large bore lean burn two-stroke engine, the requirement states 58% as the minimum CO reduction efficiency achieved, or a maximum concentration of 12 ppmd of formaldehyde at 15% O_2 in the post-catalyst exhaust to be present [4]. Secondary air injection systems, exhaust gas recirculation, particulate filters, and catalytic converters are a few of the main contemporary methods to reduce pollutant emissions [5]. This paper focuses on the latter.

One can select between selective catalytic reducers (SCR), oxidation catalysts and three-way catalytic converters (TWCs). Furthermore, “a catalyst is a material that increases the rate of a chemical reaction while not itself undergoing any permanent change” [6]. A catalytic converter works by utilizing chemical properties of different

noble metals through their interaction with the exhaust. In order to promote catalyst activity, the noble metal is *sprinkled* into a very porous alumina wash-coat that is about 20μm thick and has a surface area of 100 to 200 m^2/g; this extensive surface area is sufficient to allow close to 100% conversion of the contaminants [7]. Typically, a metallic or ceramic substrate in the shape of a honeycomb, or corrugated sheet, holds the wash-coat.

Utilizing selective catalytic reducers (SCR), NO_x can be reduced to N_2 and water by adding a reducing agent to the exhaust stream that goes into the catalyst, the most common reductant being ammonia (NH_3). The following equations describe the reduction process [7, 8]:

$$4NO + 4NH_3 + O_2 \rightarrow 4N_2 + 6H_2O$$

$$2NO_2 + 4NH_3 + O_2 \rightarrow 3N_2 + 6H_2O$$

$$NO + NO_2 + 2NH_3 \rightarrow 2N_2 + 3H_2O$$

Thermal decomposition of urea forms ammonia and more carbon dioxide as a byproduct. Ammonia is rather toxic and more difficult to store than urea, so it is common for urea to be added to the exhaust stream instead. The following equation describes the reduction process using urea.

$$4NO + 2(NH_2)_2CO + O_2 \rightarrow 4N_2 + 4H_2O + 2CO_2$$

On the other side, oxidation catalysts can be used in order to oxidize CO and HC_s and convert them to CO_2 and water. Common precious metals present in oxidation catalysts include platinum and palladium, or a combination of the two, though platinum is more prevalent for oxidation catalysts operating at lean conditions [7].

A single catalyst unit can simultaneously reduce NO_x and oxidize CO and HC_s at stoichiometric conditions. Due to the removal of all three contaminants this is named the three-way catalytic converter, TWC. Figure 1 shows that this type of catalytic converter achieves high levels of conversion of all three pollutants when the engine operates within 0.7% of the stoichiometric combustion air fuel ratio (AF). When operating lean, it acts as an oxidation catalyst, and when running rich it reduces NO_x. It is difficult to maintain constant stoichiometric conditions in practice, so AF is typically controlled by oscillating between rich and lean conditions. Additionally, there is a proven conversion benefit from oscillating between slightly rich and lean combustion due to oxygen storage and release within the catalyst [7].

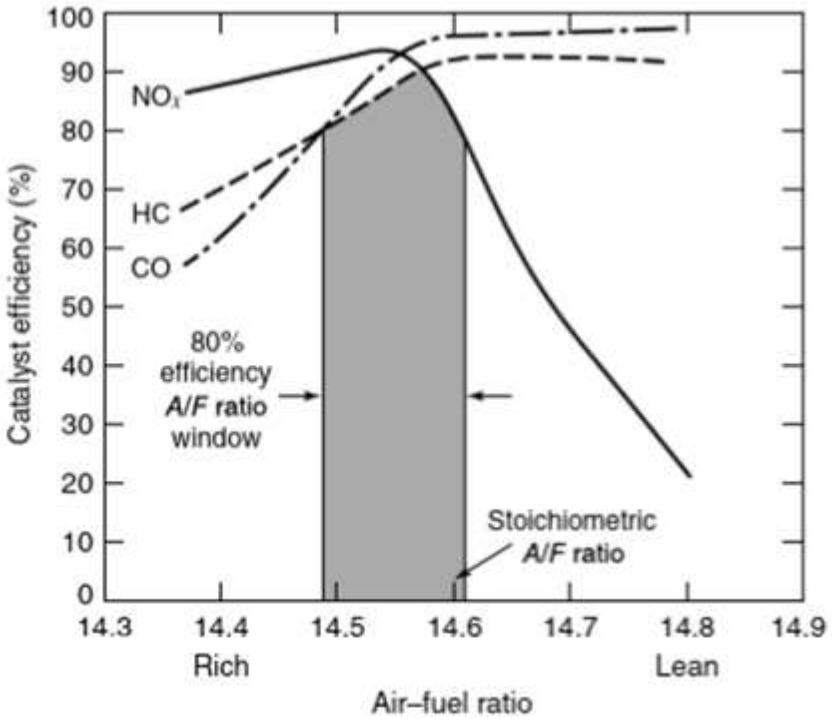

Figure 1: Conversion efficiency of a three-way catalyst as a function of AF ratio [7]

1.2 Degradation

The loss of active catalyst sites can be classified as chemical, mechanical, or thermal; chemical deactivation includes poisoning and oxidation of the crystallites, thermal deactivation accounts for sintering, and mechanical deactivation comprises fouling and attrition.

On one hand, the blockage of active catalyst sites due to the deposition of species in the fluid phase on the surface of the catalyst is known as fouling. A way of determining fouling is to measure pressure drop across the catalyst, as they have a positive correlation [9]. Additives in the lubrication oil and fuel, impurities (e.g. H_2S) in the fuel, carbon, and coke can make it to the catalyst and induce fouling [9, 10]. Similarly, poisoning is related to the chemisorption of reactants and products on active catalyst sites, and “has operational meaning; that is, whether a species acts as a poison depends upon its adsorption strength relative to the other species competing for catalytic sites.” An element might be an oxidizing agent in some cases, or act as a poison in others [9]. However, fouling excludes processes where chemisorption occurs; the blockage is merely physical. Poisoning, thus, causes a more intrinsic damage as chemical reactions are involved. Common poisons for oxidation catalysts are sulfur, phosphorus, zinc, silicone, and calcium [9, 11, 12, 13]. According to C.H. Bartholomew et al., sulfur can cause fouling and poisoning, and when fouling it can block at least one active catalyst site and up to four surface metal sites [9]. Refer to Figure 2, extracted from Davies to see a schematic of how sulfur interacts with the substrate and the wash-coat. A sulfur atom is strongly adsorbed and blocks atoms of metal substrate, M, and therefore also blocks atoms of crystallites or active catalyst sites, A [10].

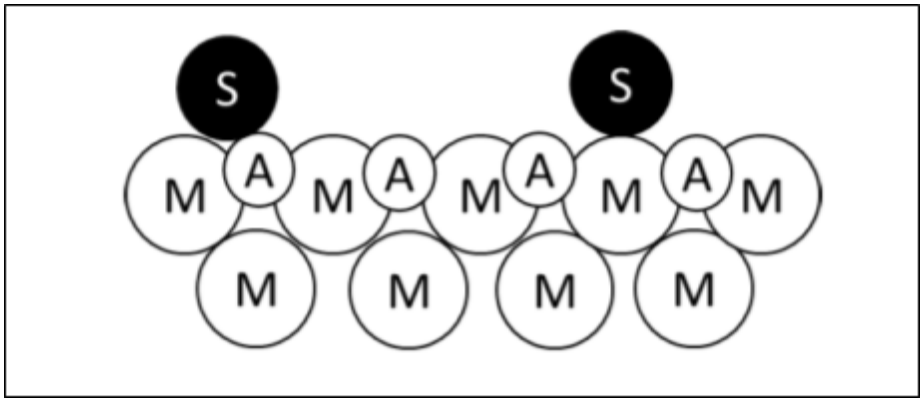

Figure 2: Sulfur fouling on the substrate and wash-coat [10]

When poisoning, sulfur atoms modify the metallic nearest neighbor, and possibly the second nearest neighbor, but the “short range electronic modification of the metal” [14] does not extend beyond five atomic units [9].

Multiple elements can cause fouling and poisoning, and their sources are not always obvious. The anti-knocking properties of lead and its damaging effects with regard to three-way catalysts are known but lead still plays a small role even when the fuel is unleaded; unleaded fuel carries over about 10 mg of lead per liter of fuel from the distribution system. Similarly, phosphorus, zinc, and sulfur are used in lube-oil additives [7], but they differ in that sulfur and phosphorus cause fouling as they interact with the surface of the catalyst; however, zinc depends on phosphorus in order to adhere to the surface and block sites and cause more damage, but it cannot do it on its own [10], and zinc has proven to have negligible interaction with oxidation catalysts built with alumina, ceria, and platinum. Furthermore, sulfur has been partially regulated in some commercial applications [15].

With regard to poisoning, the toxicity of a poison depends on the combination of several variables, such as molecular size, electronegativity, adsorption strength, shielding, and removal by gasification [14]. These variables are not independent of each other but the weighted average of them is what gives the final outcome. The adsorption strength depends on the heat of adsorption of each compound, in kJ/kmol, which is modified by temperature and residence time; therefore, some of these poisons foul the catalyst with more ease; sulfur and carbon are examples of these. Shielding makes reference to the number of ligands that surround the atom of the poison. Shielded structures are less toxic than unshielded ones; this is the reason why sulfur compounds such as sulfur oxide and sulfate ions are less toxic than elemental sulfur and hydrogen sulfide. When it comes to shielding, as Calvin H. Bartholomew states, "the order of decreasing toxicity for sulfur compounds is S, H_2S, $S0_2$, $S0_3$, SO_4^{2-}" [11, 14].

On the other hand, though carbon has an electronegativity comparable to that of sulfur, it is considered less toxic. This has two main explanations. First, their geometry is significantly different; carbon has a smaller atomic radius than sulfur and phosphorus: 0.77 atomic units (AU), versus 0.99 AU, and 1.04 AU, respectively. Second, the toxicity decreases if the poison can be removed by gasification with O_2 or H_2 [9]. Carbon is therefore a less toxic poison due to a smaller atomic radius and the removal by oxygenation or hydrogenation, forming carbon dioxide and methane, respectively. Sulfur can also be *partially* eliminated with gasification, 10% O_2, at high temperatures of 500°C [15]. Therefore, taking all these factors into account, the toxicity order seems to be P > S > Zn > C; but according to the author's knowledge, this is not proven nor is it clearly stated in the literature, and will be addressed herein.

In addition, poisoning effects might disappear when one removes the poison from the stream, which defines whether this poison is permanent or temporary [11]. This depends on the noble metal, wash-coat, and temperature combination. Please refer to Figure 3 to see an experiment presented by Neyestanaki et al., where an alumina-palladium-barium catalyst interacts with the combustion of methane with and without added sulfur [11]. One can see here that sulfur, under such conditions, acts as a temporary poison.

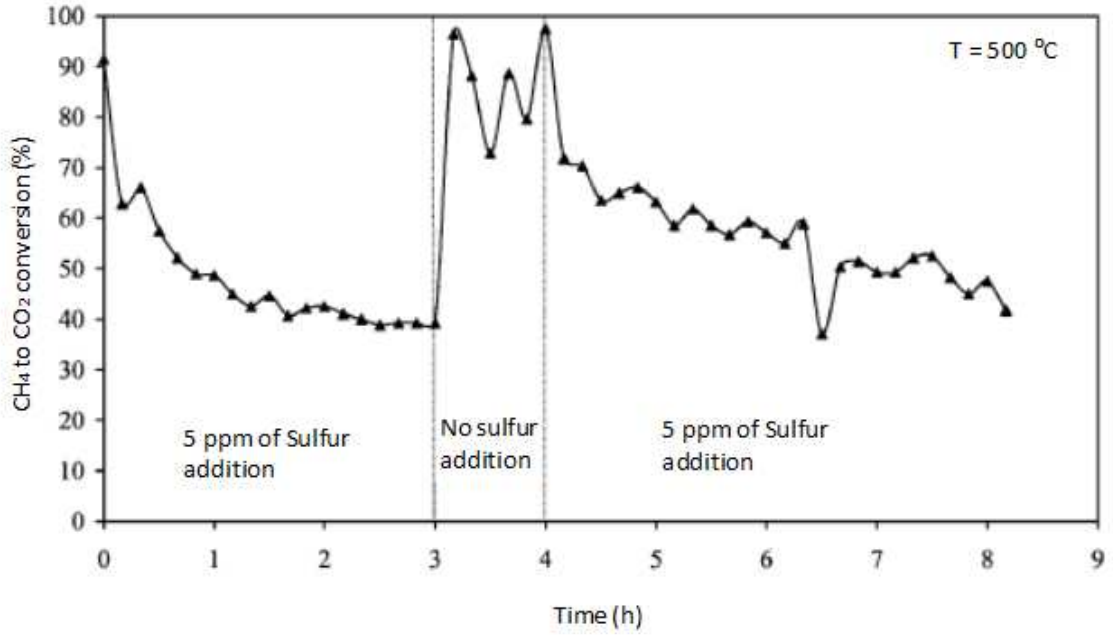

Figure 3: Conversion percent of methane to carbon dioxide in an alumina-palladium-barium catalyst at 500°C [11]

Moving away from chemical degradation and on to thermal degradation, thermal degradation is caused solely by temperature. The small precious metal particles that are dispersed in the wash-coat are commonly called crystallites [11]. At the high operating temperatures, crystallite growth is promoted as these are able move until they

eventually coalesce with one another, causing the loss of surface area of the precious metals and therefore loss of catalytic conversion. This is called (metal) sintering and it depends on the temperature, rate of heating, and particle size, among other variables [10]. For these reasons, “the noble metals are dispersed as finely as possible… which prevents particle to particle metal contact and suppresses sintering” [7]. The wash-coat suffers sintering too, as the transport of material induces a loss of porosity and encapsulation of some of the active noble metals [11]. Any loss of surface area is substantial, as these units are built with high surface areas in order to increase the amount of interaction between exhaust gases and crystallites. On the same line, the noble metal of choice can be oxidized in the aging process. Platinum is considered to be less reactive when oxidized, and this is opposite for palladium [11].

In addition, there is a trade-off for increasing the temperature of the catalyst environment. When the engine starts, exhaust gases are flowing freely through the catalyst with no apparent conversion, but the catalyst becomes more efficient as temperature increases; once the catalyst reaches a conversion effectiveness of 50%, it reaches the so-called *light-off temperature* [7]. This happens because higher temperatures promote oxidation reactions and the breaking of chemical bonds [10]. Consequently, it is better in the short term for catalysts to operate at a high temperature, but it degrades the unit in the long term. Due to degradation, the light-off temperature has an upward trend; the more the catalyst is degraded, the higher the light-off temperature [10, 16, 17].

The last type of degradation mentioned is mechanical degradation, which includes attrition and fouling. With respect to the first, different materials compose the wash-coat

and the substrate, and as temperatures fluctuate, the different coefficients of expansion deteriorate this interface [16]. Over time, this can cause attrition, which is “the size reduction and/or breakup of catalyst granules or pellets” [11], and it is easily observable under a microscope. This chronic process is irreversible [16]. One thing the author wants to point out is the looseness of the wash-coat. As one moves the catalyst unit around, pieces of loose wash-coat easily fall off as a light-colored powder. This is not the result of attrition, as it happens even with brand-new unused units, and it happens so much that it would be hard to notice with the naked eye if the rate of particles that fall off the unit increases with attrition.

1.3 Restoring options

The elevated costs of catalyst replacement motivate the study of their restoration. Several restoration methods have been tested, but to the knowledge of the author there is not conclusive information available from research showing the effects of such restoration methods on the washccoat and crystallites. Isolated tests have been executed, but the idea behind this paper is to test these methods in combination and come up with a complete restoration procedure that extends the life of the catalyst yet does not induce more damage.

1.3.1 Catalyst flipping

Different poisons and particulate settle in different areas of the catalyst. Phosphorus selectively settles in the entrance of the catalyst and in the upper most level of the wash-coat, particularly in the first few millimeters, but with enough exposure time it takes over not only the inlet but the entirety of the catalyst surface [10, 11, 15]. On the

other hand, zinc can be found sitting on the surface along with particulate matter on diesel catalysts. It is not a part of the wash-coat, but rather sits on it [11]. In addition, according to the personnel from a local catalyst washing company owned by Siemens, ash forms in the very front of the catalyst depending on the type of fuel and aging time. For these reasons it is common to flip the catalyst over and turn the original entrance region into the new exit region, as the irregular pores allow new paths of exhaust flow and catalyst exchange, where the different poisoned areas give room for *cleaner* active sites, from poisons, carbon, and fouling.

1.3.2 Catalyst baking

Each poison comes in different forms, depending on their interaction. The baking removal temperature of a poison depends on the form of interest of the poison. When running rich, the sulfur from the additives forms hydrogen sulfide. But in an oxidation catalyst, the oxidation of sulfur dioxide forms sulfur trioxide, SO_3, and this compound is stable until approximately 700°C [11]. The formed SO_3 can react with the noble metal, but it can also affect the wash-coat. In the case of alumina, the reaction with SO_3 can form aluminum sulfate species, which are stable until they reach 650°C. Similarly, carbon leaves the surface of the catalyst at approximately 450°C according to several studies [8, 17, 18]. Other studies indicate that carbon leaves the surface at 500°C, while phosphorus levels remain constant [15]. Removal of carbon at 500°C takes place, as it is above 450°C, but it is strongly discouraged as indicated by Marceau et al., who indicate using transmission electron microscopy (TEM) and X-ray powder diffraction (XRD), that sintering starts to occur above 400°C. TEM consists in an electron gun shooting electrons at very thin samples for them to be transmitted through. Similar to

regular light microscopy, but it uses electrons instead of visible light allowing higher magnification and resolution [19]. XRD allows excited electrons from a filament to knock away the inner shell electrons of the sample and emit photons [19, 20]. Their data is summarized in Table 1 [21]. Here, the crystallites of an alumina-platinum catalyst are analyzed as a function of temperature. The increase in the average particle size on the left column of Table 1 shows crystallite growth occurs, and the dispersion refers to the percentage of metal exposed, platinum in this case. “The selective chemisorption of gases, principally hydrogen and carbon monoxide, provides a measure of the exposed metal” and “after excessive heating in various atmospheres or in vacuum, the extent of gas adsorption decreases” [22]. The less metal surface is exposed, the less dispersion, and therefore the less catalytic activity. Redispersion of the platinum is possible if chlorine is present in its precursor, but chlorine is also able to pass from the crystallites to the alumina wash-coat and decrease the oxidation of hydrocarbons, so there is a trade-off [11]. Therefore, the temperature of the catalyst ought to stay below 450°C to impede sintering.

Table 1: Particle size and dispersion of a degraded alumina-platinum catalyst [21]

Ageing Temperature (°C)	Average Particle Size (Å)	Dispersion (%)
400	30	41
450	40	40
490	50	24
550	90	18
600	100	12

1.3.3 Hydrogen reduction

Platinum is more active in its metallic form, and the crystallites might get oxidized in the catalyst aging process [11, 22]. Oxidation of platinum can be reversed with an H_2 reduction. To the knowledge of the author this is a common study, but it has never been used to restore a catalytic converter, even though it has been used in the manufacturing process [22]. Figure 4 shows the consumption of H_2 versus temperature [23]. These are the results of a temperature programmed reduction study (TPR) with a reducing mixture of 5% H_2 in an argon balance during a temperature sweep. The TCD signal parameter indicates the usage of a thermal conductivity detector to measure the consumption of H_2. For this catalyst, the three curves indicate consecutive reduction and oxidation cycles, with the least oxidized experiment being most easily reduced, curve a, which peaks at 560°C with a consumption of 1.2 mmol H_2/g_{CeZr} [23]. This TWC is composed of platinum, ceria, zirconium, and alumina.

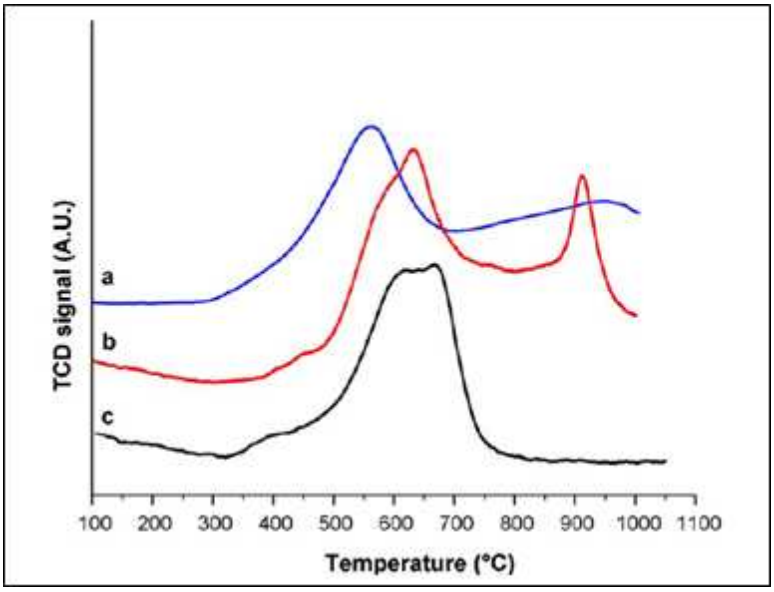

Figure 4: TPR of a three-way catalyst for a sample that has been oxidized and reduced once, twice, and thrice, for curves a, b, and c, respectively [23]

This and several other reduction studies suggest the ideal reduction temperature is different for each catalyst, and the reduction peaks near 500-600°C [22, 23]. However, the consumption of H_2 initiates in between 400°C and 450°C in most cases, just as it is seen in Figure 4 [23, 24, 25].

1.3.4 Catalyst washing

Chemical washing is another option to restore and prolong the life of a catalyst. Submerging a catalyst in tetrachloroethylene for 30 minutes is successful at partially reactivating the catalyst [10]. The downfall of chemical washing is that it can also attack the wash-coat and the substrate, so it is compulsory to use weak acids, such as acetic acid or oxalic acids [11]. In fact, some studies show concern of the crystallites being leached away with acidic baths [16]; this will be studied herein. The idea is to find a washing procedure with a strong enough acid to remove the poisons, but weak enough not to interact with the wash-coat. In theory, temperature, agitation, pH level, and soak time should affect the effectiveness of the washing procedure [16].

A local company dedicated to catalyst washing, Dresser Rand Enginuity, used to provide catalyst washing services. They stopped providing such a service after they were acquired by Siemens, and this transition happened while this research project was ongoing. Another company that dedicates to wash and sell catalytic converters is Advanced Gas Engine Solutions (AGES), and both have been contributors to this project by providing use of their facilities.

The most common catalyst washing process is considered in this document as the industry standard and it involves washing the units with a base, a weak acid, and rinsing

it with deionized water. Adapted from Hackleman et al., Table 2 shows detailed information about the industry standard washing procedure.

Table 2: Industry standard washing procedure performed by Dresser Rand

Bath sequence	Soak time	pH	Temperature (°C)
Caustic Soda	4 hours	12.64	23.7
Deionized water	1 hour	11.82	21.8
Acetic acid	30 min	2.78	21.7
Deionized water	30 min	11.82	21.8

The main body of the washing process offered by different companies is similar, but there are small differences, and for confidentiality purposes no names will be given in the following descriptions. The information was obtained by directly contacting the different businesses, and the main differences lie on the renewal frequency of the chemical baths, the ability to test the reduction efficiency before and after washing the unit, the drying method, and whether the unit sits in a stationary chemical pool or if there is added recirculation of the chemical fluid through the catalyst unit. Table 3 shows a summary of the differences among processes. Testing the reduction efficiency before washing the unit allows the user to evaluate whether washing the unit is necessary or beneficial. After washing several units, they can estimate the maximum achievable improvement in the reduction efficiency. According to the personnel at AGES, it is not

gainful to wash an oxidation catalyst unit if it needs an improvement of more than approximately 15%, in which case the unit can be recycled. Furthermore, testing a unit after washing ensures the delivery of a working catalyst to the customer. The remaining differences will be evaluated in the upcoming chapters.

Table 3: Catalyst washing differences among different companies in the US.

Company	A	B	C
Baths	Acetic acid (10%) and sodium hydroxide (5%)	Acetic acid (10%) and sodium hydroxide (5%)	Acetic acid (10%) and potassium hydroxide (9%)
Recirculation	No	No	Yes
Baking to dry	No	Yes (at 420°F)	Yes (unspecified temperature)
Baking to remove carbon	No	No	No
Bath renewal frequency	pH based and visual inspection	Every customer	Every unit
Rinse water	De-ionized and re-used	De-ionized and fresh	De-ionized and fresh
Rinsing times	2 after caustic soda, 1 after acid	2 (once after wach chemical bath)	2 (with recirculation, once after each chemical bath)
Testing of catalyst unit	Visual inspection of blocked cells	In-site with gas bottles	No testing done periodically

1.5 Previous work

A more detailed explanation of the equipment used is shown in the experimental sections, but there is vital information the reader should know in order to better understand the previous work performed. XPS and SEM stand for X-ray spectroscopy and scanning electron microscopy, respectively. XPS reveals the composition and percentage of all elements in the sample, while SEM prompts pictures which show concentration trends based in colors and is able to generate a magnified image and show morphology. XPS and SEM are discussed further in chapter 2 [10, 26].

This project has been ongoing for several years, so it can be non-trivial to differentiate between previous and new work presented in this paper. Figure 5 contains a description of the major tasks achieved during the entirety of the project and clarifies contributions from this work.

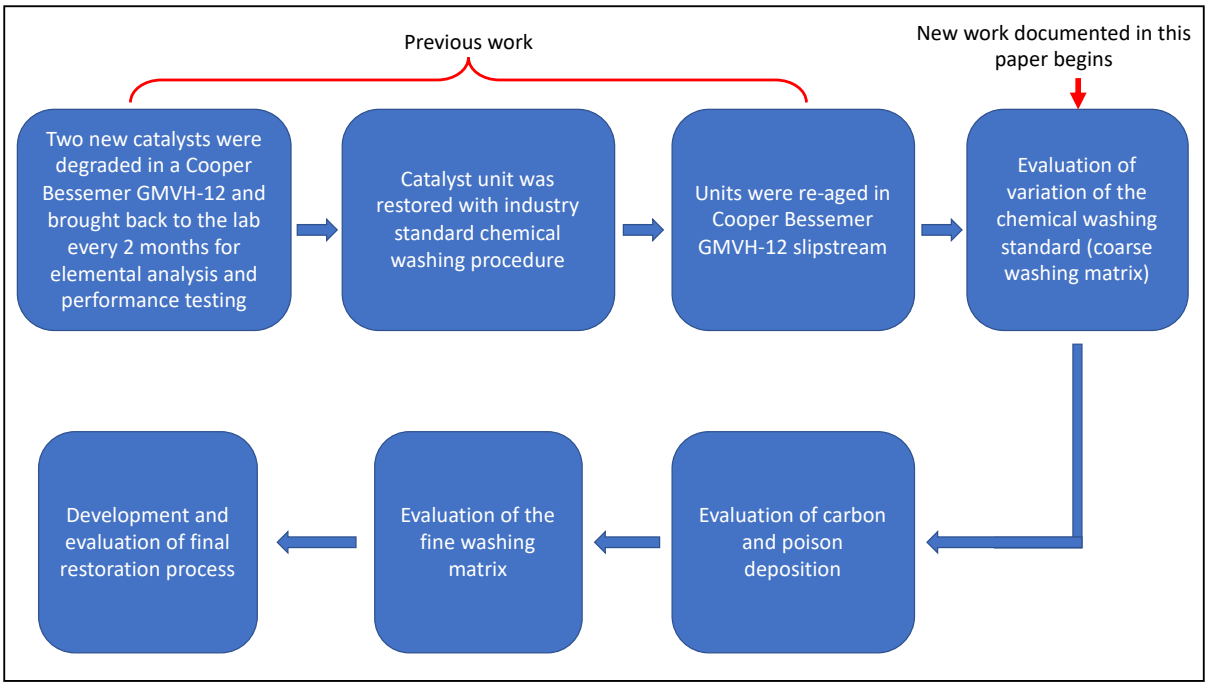

Figure 5: Project timeline and major tasks

1.5.1 Characteristics of the catalyst and aging process

Several types of catalyst structures exist. The one used for this project is built with corrugated steel as the substrate, which holds an alumina wash-coat with small particles of platinum in it [17]. It is common to use alumina for the wash-coat since it acts as a sulfur scavenger. Moreover, the alumina wash-coat is mixed with lanthanum in order to avoid sintering and help with poisoning, as it increases the storage of sulfur by the wash-coat, allowing less sulfur to interact with the crystallites. Cerium has a similar effect on the wash-coat and precious metals but was not been observed in this case [11, 17].

Figure 6 displays the catalyst sheet distribution [17]. Corrugated substrate is alternated with flat sheets, and the wash-coat layer is applied to every concavity as that is where exhaust flows. The areas where the corrugation presses tightly against the flat sheet

contain little to no wash-coat based on how the units are built, as exhaust does not flow there. Therefore, when one removes a substrate sheet from the catalyst for analysis and looks at it from the top, one always sees the wash-coat layer deposited in the valleys, and no wash-coat in the peaks formed by the corrugation, so from now on we will refer to the valleys as the areas where alumina wash-coat is deposited and exhaust flows.

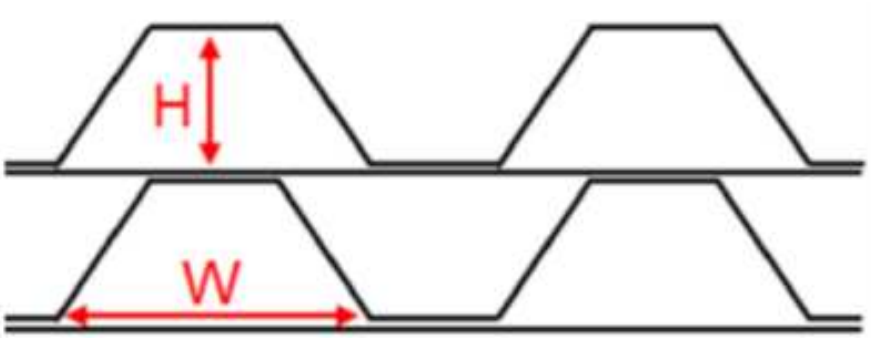

Figure 6: Substrate sheet distribution of our oxidation catalysts [17]

Catalyst degradation requires extended periods of exhaust flow through the unit, so though a laboratory set-up is needed when testing, it is practical for a catalyst to be aged in the field. For this reason, two catalyst units were aged in cycles until they no longer met the requirements established by the NESHAP, 58% CO reduction efficiency and a maximum of 12 ppm of formaldehyde.

The testing cycles consisted of aging the units for two-month periods in a slipstream of a large bore two-stroke natural gas engine, and then taking them back to the lab engine for emissions testing. The tests consist of temperature sweeps between 150°C and 435°C at 150000 hr^{-1}, and space velocity (inverse of residence time) sweeps between 20,000 hr^{-1} and 200,000^{-1} at 287°C [10, 16, 17]. Both catalyst units were first *degreened*, which involved baking them for 24 hours in a kiln at 650°C before

connecting them to the field slipstream. This allowed the research to fast forward in the aging process and focus on poison deposition instead of sintering, as the degreening process simulates the degradation spike observed when brand new catalysts are placed in the field and produces comparable amounts of sintering as those occurring naturally in the initial stages of field degradation [2, 10, 17].

The field engine used for aging is a two-stroke Cooper Bessemer GMVH-12, stationary natural gas engine. This large bore engine is turbocharged and has a displacement of 35 L per cylinder. With a bore and stroke of 355 mm it provides 2013 kW (2700 hp) of power at 330 rpm. On the other hand, the engine chosen for lab testing is the Cummins QSK19, a 4-stroke natural gas engine with a total displacement of 19 L, and bore and stroke of 159 mm, which delivers 350 kW (470 hp) at 1800 rpm [10]. Modified from Kristen Davies, Table 4 shows the specifications for both engines.

Table 4: Engine specifications for catalyst aging and lab testing [10]

Engine Specifications		
Manufacturer and model	Copper Bessemer GMVH-12	Cummins QSK19G
Displacement	35 L per cylinder	19 L
Bore	355 mm	159 mm
Stroke	355 mm	159 mm
Rated Power	2013 kW at 330 rpm	350 kW at 1800 rpm 335 kW at 1500 rpm
Fuel	Pipeline natural gas	

1.5.2 Surface analysis

One of the units was dismantled to remove a substrate sheet for materials testing after each two-month testing cycle, and then it was reassembled for further aging in the field, while the other unit remained intact. After the third testing a pitot tube showed that the exhaust flow rate was reduced and was delaying the aging process, for which reason a blower was added; the blower almost doubled the flow of exhaust that went through the catalyst [10]. In order to evaluate surface composition, the sheets were cut into suitable sized samples for XPS and SEM analysis. Modified from Hackleman's, Figure 7 shows a schematic example of how the aged sheets were cut in six different locations to determine whether the poisons were distributed unevenly, as the theory suggests.

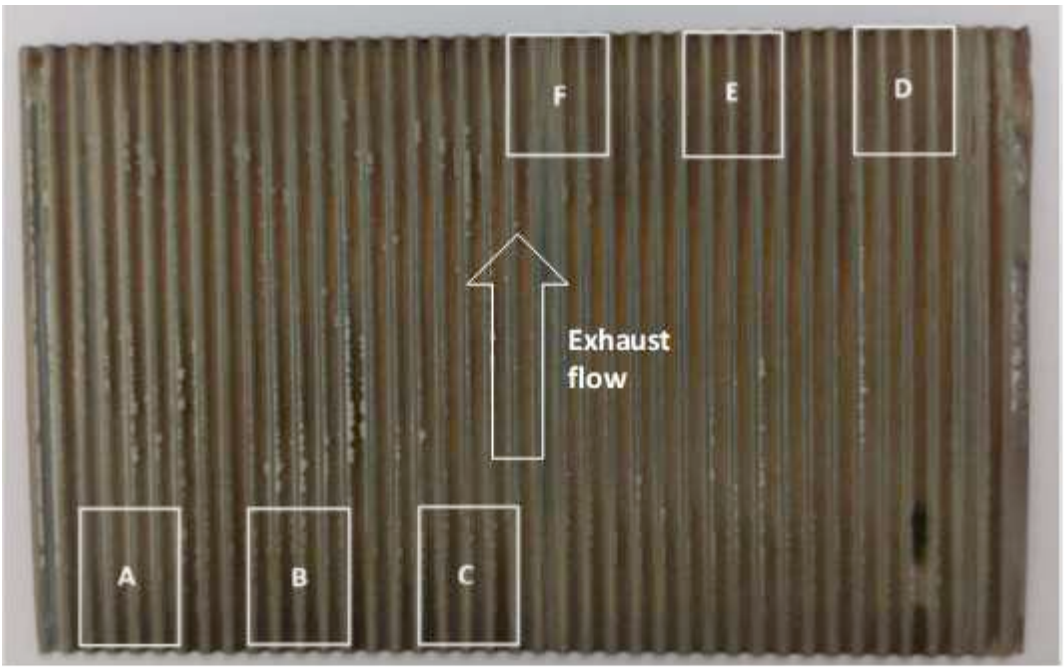

Figure 7: Example schematic of the 6 different cuts from each catalyst sheet to determine the distribution of poisons [16]

XPS and SEM analysis shows there is no significant difference in the amount of sulfur near the inlet or outlet after aging. Phosphorus and zinc, however, accumulate quickly near the inlet of the catalyst sheet, with a following buildup rise near the outlet [16, 17]. Phosphorus and zinc were expected to show linked trends, as zinc depends on phosphorus to attach to the catalyst surface. Baumgardner et al. also mentions sulfur quickly reaches a saturation level, while phosphorus and zinc keep on building on the surface; this can be clearly seen in Figure 8 [17].

In Figure 8 the idea of catalyst exchanges appears. This refers to the aging time thus far and will be explained in more detail later. Each point along the line indicates a different testing cycle. Furthermore, given enough degradation time in the field, carbon from the exhaust piles up and interferes with the spectroscopy equipment used for materials testing. This carbon layer makes it impossible to see the other poisons and is therefore removed. This was not an issue until reaching the fourth testing cycle. The selected carbon removal method was baking. Baking at 450°C for one hour was selected at first since it removed most of the carbon without apparent removal of other poisons [10, 17]. The temperature for this baking procedure ought to be kept on the lower side in order to avoid causing more sintering and the bake-out of other poisons, but the baking time can increase depending on the amount of carbon buildup [11].

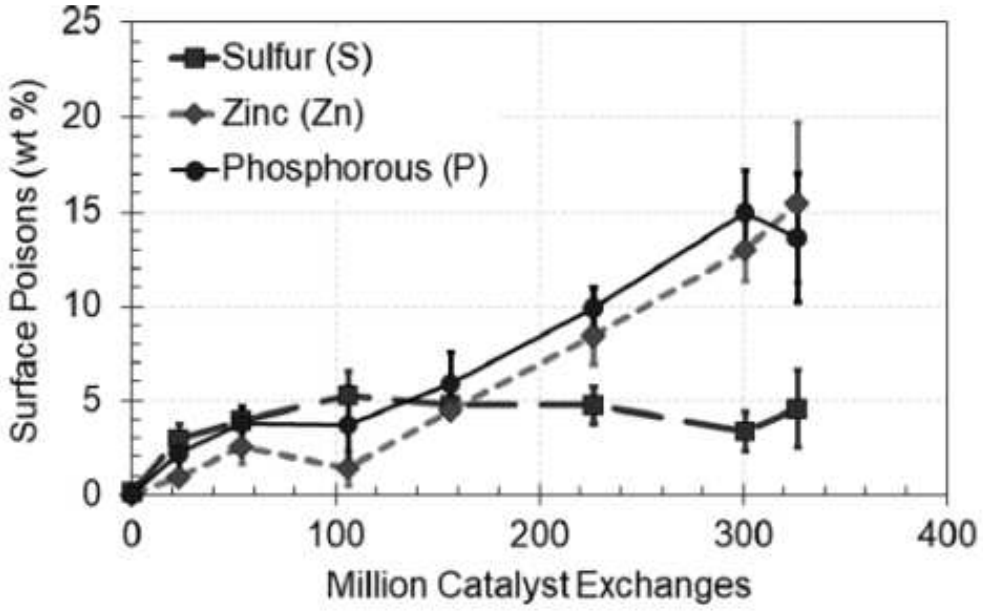

Figure 8: Sulfur, zinc, and phosphorus buildup as a function of time, where only sulfur indicates saturation [17]

1.5.3 Emissions testing

In addition to the surface analysis, emissions testing is necessary to evaluate the degradation level of a catalyst unit. The main comparison factors to keep in mind are the reduction efficiency and the light-off temperature [10]. The reduction efficiency contrasts pre- and post-catalyst levels, and for this reason an automated toggle valve was installed to alternate between pre- and post-catalyst values when testing in the lab, paying special attention to CO, methane, ethane, ethylene, propylene, propane, formaldehyde, and volatile organic compounds (VOCs); where the VOCs refer to the addition of ethylene, propylene, and propane, and these where measured with a five-gas analyzer and a Fourier transform infrared (FTIR) spectrometer [10]. Furthermore, the main catalyst efficiency tests consisted in temperature and residence time sweeps. The common term to describe residence time is its inverse, space velocity (SV) [10]. A

faster SV indicates a shorter interaction between exhaust gases and active catalyst sites. Moreover, the number of catalyst exchanges is more useful than time to determine degradation, as it takes into account size of the catalyst and the characteristics of the flow. In summary:

$$SV = \frac{\dot{V}}{V_{cat}}$$

$$CatEx = t * SV,$$

where $\dot{V}$ represents the standard volumetric flow of the exhaust, V_{cat} the volume of the catalyst unit, *CatEx* the number of catalyst exchanges, and *t* stands for the total degradation time [10, 16]. The post-catalyst emissions initially showed 6 ppm of formaldehyde, and it took 180 million exchanges for the catalyst to be non-compliant with the 12 ppm formaldehyde limit, which for a generic engine does not take more than a couple months of continuous operation at a SV of 150000 h-1. However, the industry lifespan of these catalysts at typical operating parameters found in the industry is 8 to 12 months, since the 58% CO reduction efficiency limit delays the deactivation [17]. Often in the field CO reduction efficiency is used as a surrogate to assess degradation because formaldehyde requires an FTIR spectrometer, not typically available to field service personnel.

The temperature and space velocity sweeps show propylene levels are the most affected by poisoning, and that higher than usual operating temperatures help postpone deactivation. The average operating temperatures were recorded to be 220 $\pm$ 4°C, but the temperature sweeps show the catalyst is significantly more efficient at 315°C; however, there is no significant improvement to operate at temperatures higher than

315°C. To achieve this temperature with the Cooper GMVH engine, the catalyst would need to be moved upstream of the turbocharger, which it is not advised; Baumgardner stated, it “is generally considered too mechanically risky due to the possibility of debris being carried over to the turbocharger” [17].

Furthermore, there is a clear trend in the reduction efficiency going downwards and light-off temperature going upwards as the aging process goes on (From Baumgardner et al., refer to Figure 9). The tests for other species show the same trend. The brand-new catalyst emissions test, denoted baseline test, is not successful at reducing propane, methane, or ethane, with reduction efficiencies below 20% at the maximum tested temperature. This is expected with this type of oxidation catalysts and will be discussed no further [17].

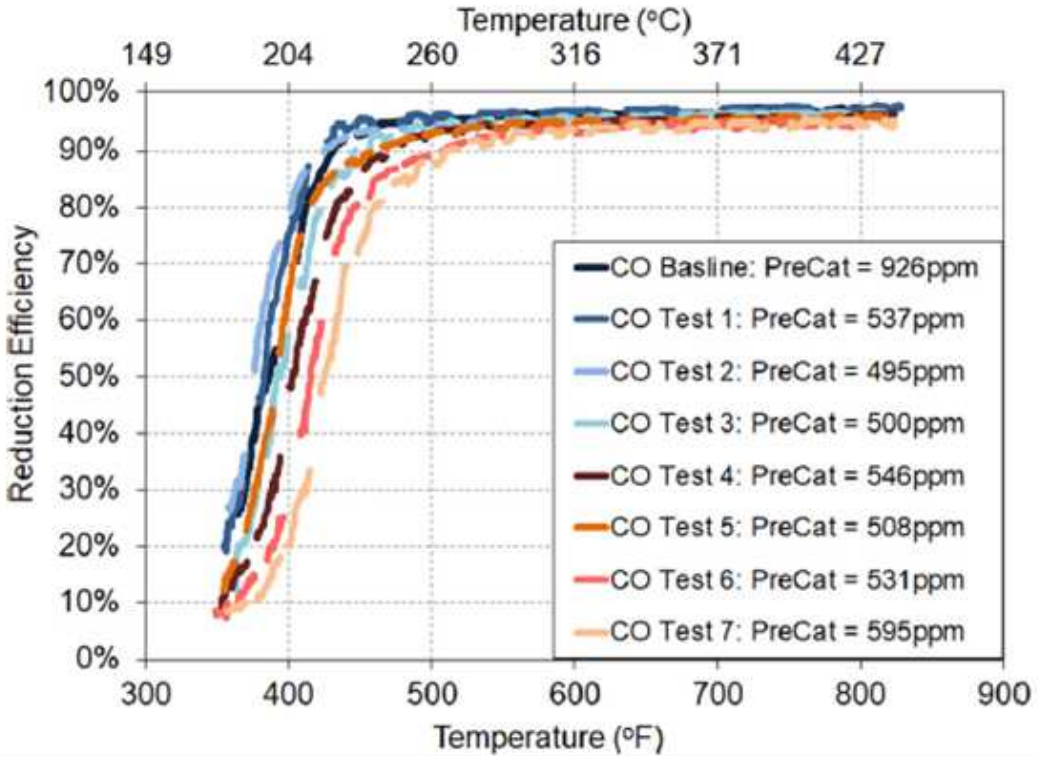

Figure 9: Reduction efficiency for CO emissions during temperature sweep for various aging levels [17]

1.5.4 Oil analysis

Besides examining the poisoning levels and analyzing the surface with XPS and SEM, the source of the poisons was investigated. In a study presented at the Gas Machinery conference Olsen et al. showed that the amount of PM in the emissions of a Cooper-Bessemer GMV-4TF two-stroke is directly related to the amount of lube-oil from the cylinder lubrication ports, shown in Figure 10. The PM emission levels are in the same order of those of a tier four diesel engine, but the lean operating conditions and the fuel suggest that it is not soot what is poisoning the catalyst [2].

Furthermore, an OCEC analysis was performed. This test makes use of the difference in the phase change temperature between volatile organic carbon (OC) and more stable elemental carbon (EC), as a stepped temperature increase can set them apart. The OCEC analysis shows that the carbon in the exhaust is about 99% OC, which corresponds to the hydrocarbons from the oil. Some of these samples were analyzed with XPS, and the results indicate that hydrocarbons compose most of the PM trapped in the filter. In conclusion, large, condensable hydrocarbons from the cylinder lubrication ports compose most of the PM of this LBNG engine.

Moreover, using a dilution tunnel and based on measurements performed in the laboratory on the GMV-4TF engine, Baumgardner et al. measured that 10% of the oil added to the cylinders fails to burn or return to the sump down the cylinder walls, and ends in the exhaust as suspended oil droplets that form PM. XPS measurements of the rate of poison deposition are consistent with the PM deposited onto the catalyst from lube-oil carryover. These are depicted in Figure 11 [2, 17, 27]. The rate of poison

deposition therefore depends heavily on the lubrication rate, so it will change based on the engine performance settings, lubrication system, and type of oil.

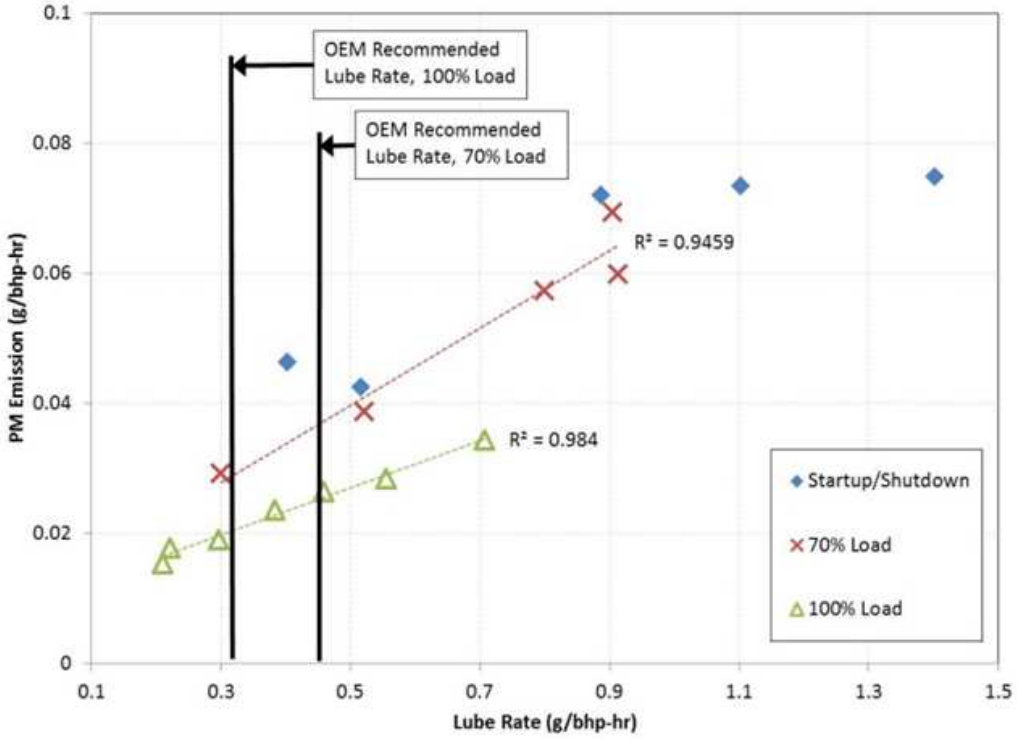

Figure 10: Positive correlation between brake specific PM and lubrication rate [2]

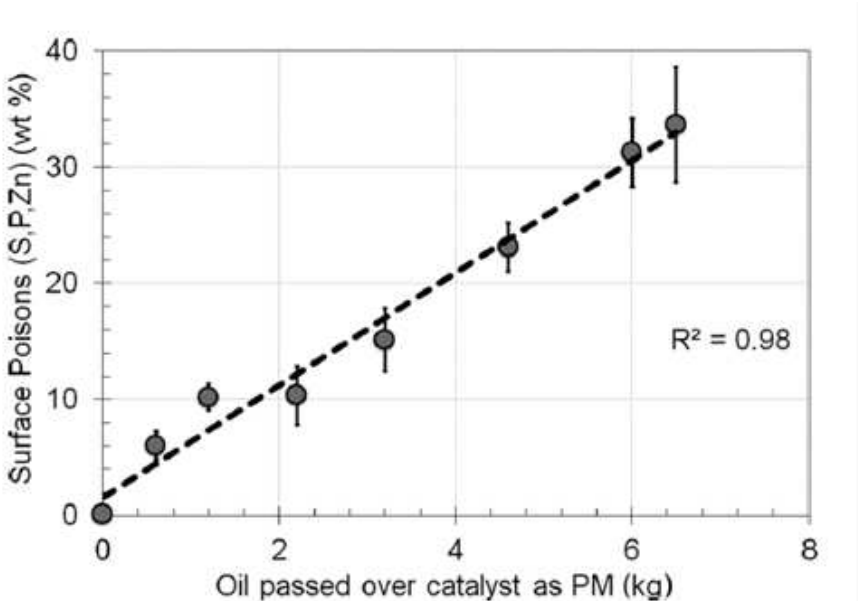

Figure 11: Sum of all poisons as a function of PM [17]

1.5.5 Chemical washing, industry standard

As mentioned before, Dresser Rand and AGES provide catalyst washing services. One of the aged catalyst units was washed at Dresser Rand with the industry standard, Table 2, and then underwent the exact same aging procedures and testing cycles. They were aged and tested until the catalyst became non-compliant with the NESHAP limits previously stated [4].

Surface analysis on the samples was also performed in order to evaluate the efficiency of the wash. Carbon had been accumulated again and made it hard to see the other poisons with XPS and SEM, but the carbon bake-off procedure in order to see the other poisons was slightly different this time. Instead of baking the carbon off with the previous procedure (at 450°C for one hour), the cut samples were baked at 425°C for seven hours. This is the result of the search of an efficient carbon bake-out method, since a baking time of one hour is no longer sufficient for the larger amounts of carbon deposited over more time spent in the field. Instead of increasing the baking time only, an iterative method with a rather lower temperature was selected. The samples were baked for one hour at 450°C, and then iteratively for two hours periods at 425°C until the variation of carbon concentration shows to be 1% or less with XPS. Though longer, the preliminary tests show that seven hours at 425°C proves sufficient, and this can be seen in Figure 12 [16].

The XPS analysis shows the industry standard wash reduces amounts of phosphorus and zinc in large proportions near the inlet, but sulfur remains unaffected in this area. Sulfur reduction occurs near the outlet of the catalyst. This test reconfirms the link between phosphorus and zinc mentioned previously, that zinc depends on phosphorus

to attach to the wash-coat [10, 16]. Moreover, it also shows phosphorus as the most abundant. This is observed in Figure 8 up until 300 million catalyst exchanges, and in Figure 13, which shows the amounts of each poison, both near the inlet and outlet, before and after washing the samples with the industry standard procedure. Phosphorus, zinc, and sodium seems to be the decreasing order of poison species concentrations [16].

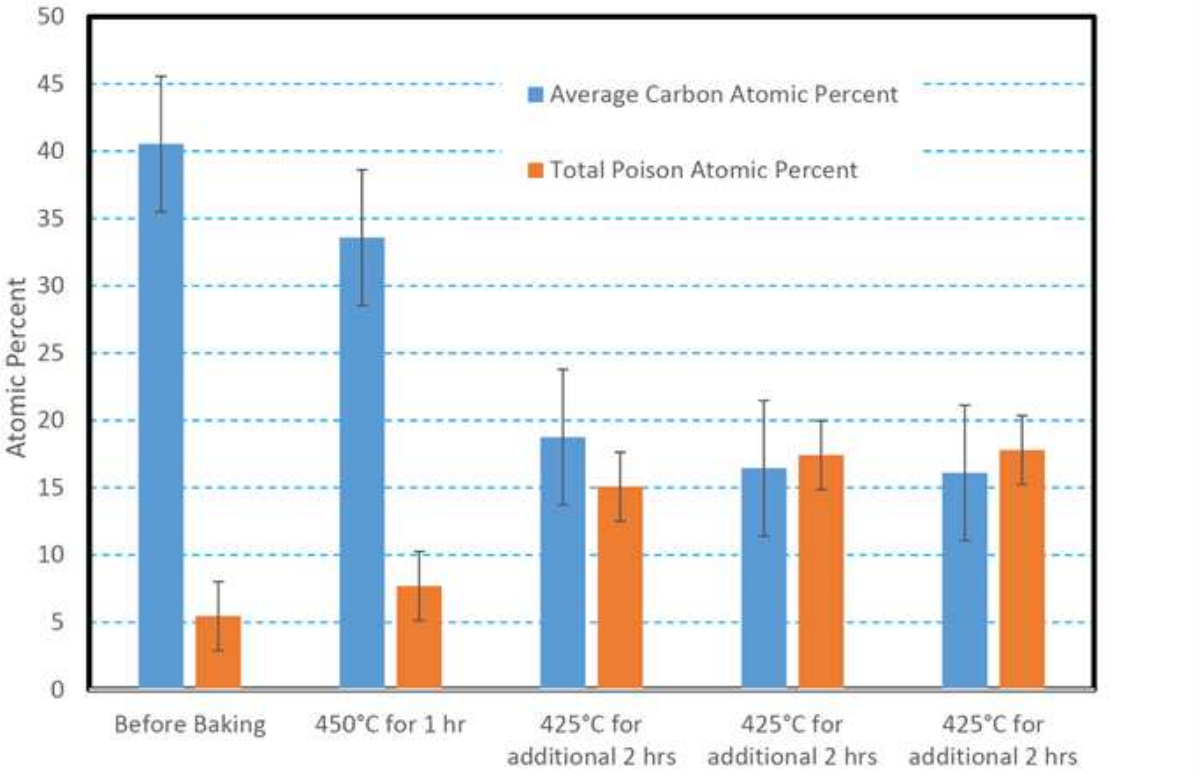

Figure 12: Secondary bake-out procedure to get rid of the masking effects of carbon

Sodium appears in this analysis too, and after thoughtful analysis it was declared to come from the caustic soda bath. Other options were discarded, e.g. the coolant, since its other components did not carry over. Furthermore, the total amount of pre-wash poisons was 18% excluding sodium, and it dropped to about 4% after being washed [16]. These results are reflected when testing emissions, as the reduction efficiency

improves substantially, but it does not achieve the same reduction levels of a new catalyst. Refer to Figure 14 to see the CO light off curves for pre- and post-wash experiments; similar trends are observed for formaldehydes and VOCs [16].

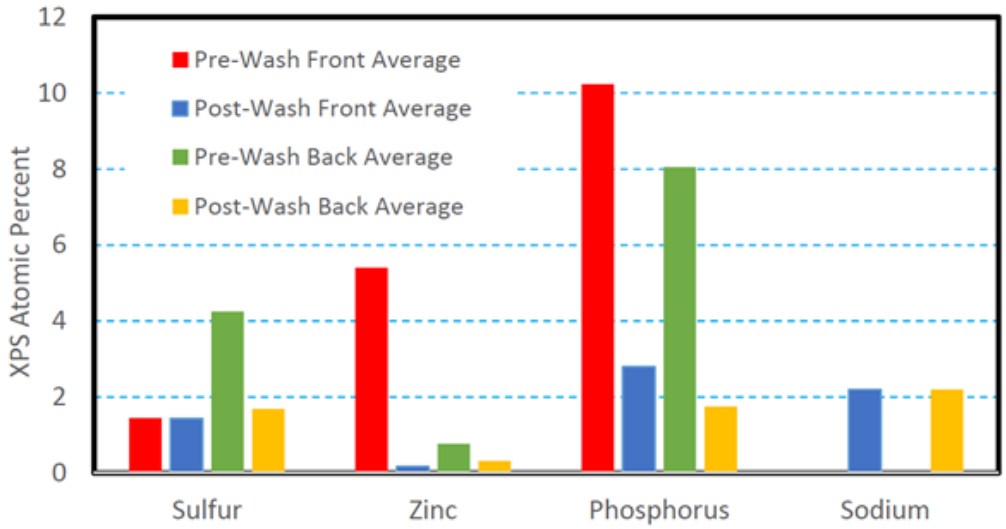

Figure 13: Atomic percentages of each poison near the inlet and outlet of the catalyst, including pre-was and post-wash results [16]

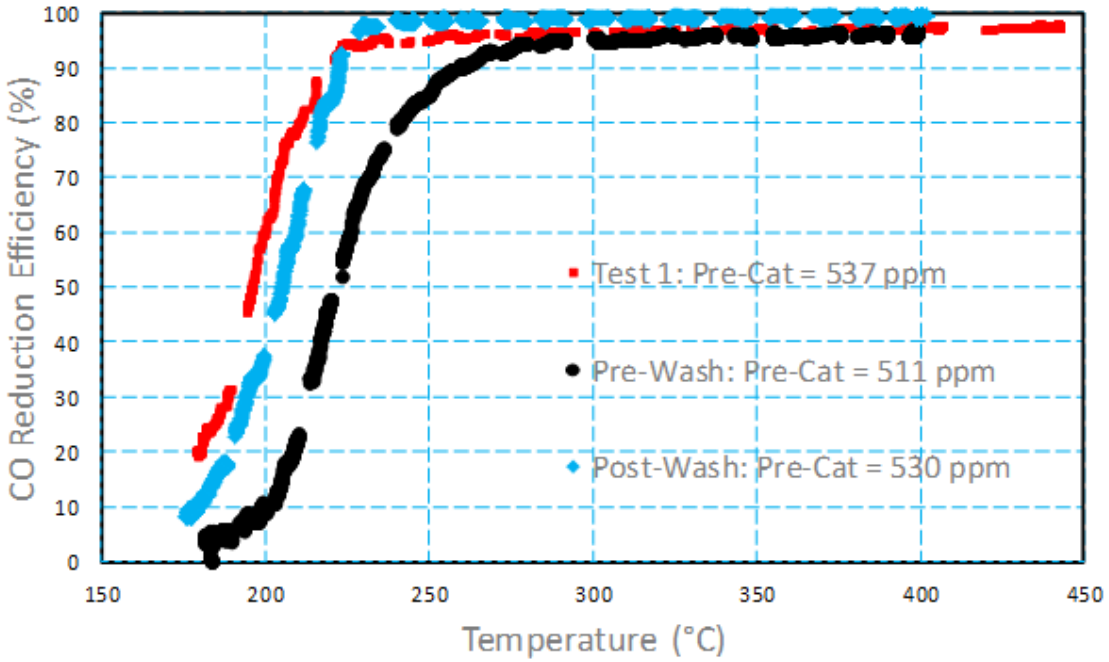

Figure 14: Light off curves for CO pre- and post-wash tests [16]

The main observable difference between exhaust species graphs is the maximum reduction efficiency obtained. The maximum reduction for CO is 100% as seen in Figure 14, for formaldehydes it is 90% and for VOCs it is about 75%. Propane, ethylene, and propylene comprise VOCs, and the amount of propane in VOCs might be accountable for the lower reduction, as these are less reactive alkanes and require higher energies to be oxidized due to the hydrocarbon bonds [28]. Overall, the light-off temperature did not reach new catalyst levels, but the average improvement in light-off temperature based on CO, formaldehydes, and VOCs reductions is approximately 19°C.

The post-wash poison deposition rates are similar to those of a new catalyst. It takes approximately three testing cycles, each of two months, for the catalyst to no longer comply with the CO NESHAP requirements, which gives a total of approximately six months of extended life with the industry standard wash.

Please recall that for a new catalyst there is an expected lifespan of 8 to 12 months, and that the washing costs represent about 10% of those of a new catalyst. Refer to Figure 15 to see the poison deposition rates of a new catalyst versus a washed unit [16]. The rate of post-wash poison deposition is higher, so the restoration does not achieve new catalyst reduction levels and gets poisoned faster, though there is a lot of variation in the collected data.

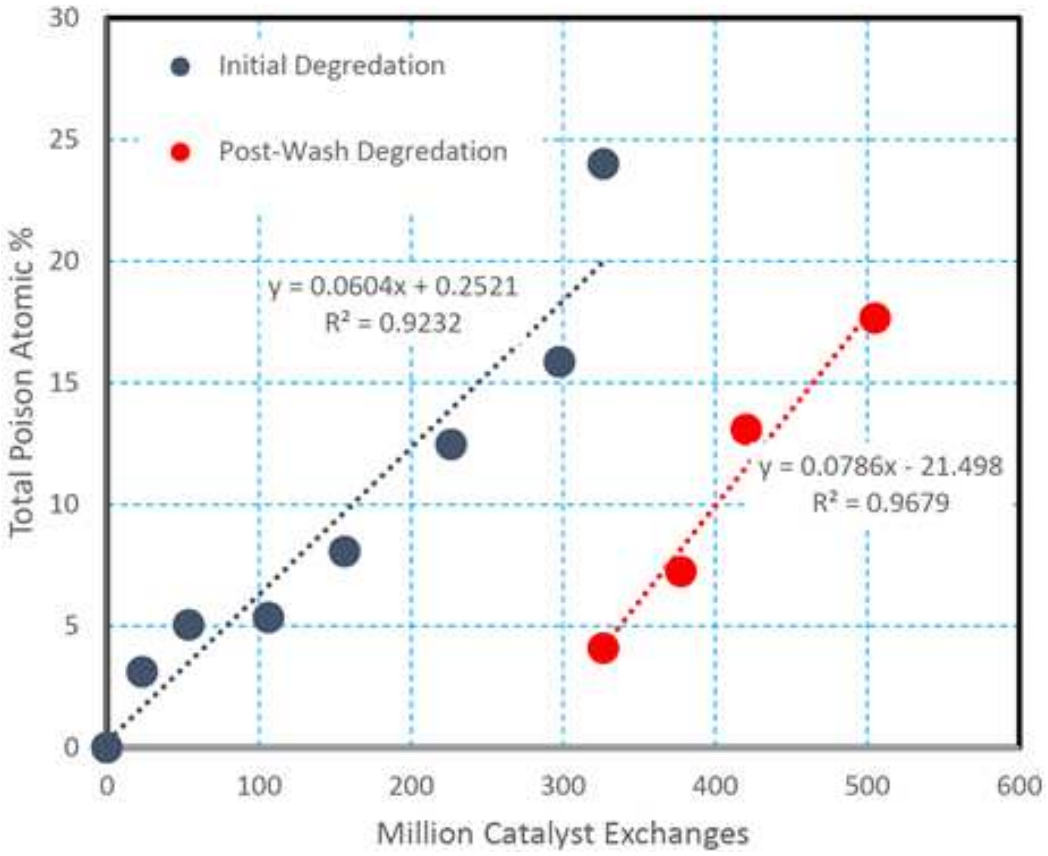

Figure 15: Poison deposition rate of washed and unwashed catalysts [16]

1.5.6 Coarse washing matrix

The most common way of restoring catalysts in the industry is to soak them in chemical baths that are strong enough to remove the poisons, but weak enough to keep the wash-coat and noble metals in good conditions at the end of the washing process. The industry standard washing procedure uses acetic acid and caustic soda and is summarized in chapter 1 (Table 2). A coarse washing matrix is developed to improve the industry standard washing process by further investigating four variables in the washing process: temperature, agitation rate, pH levels, and soaking times.

Table 5: Coarse washing matrix [29]

Experiment	Temperature (°F)	Agitation (rpm)	pH	Time
W1	167	0	0	0
W2	0	50 - 100	0	0
W3	0	0	13.4 (Caustic soda), 2.1 (Acetic Acid)	0
W4	0	0	0	x2
W5	167	50 - 100	13.4 (Caustic soda), 2.1 (Acetic Acid)	x2
W6	167	50 - 100	0	0
W7	0	0	13.4 (Caustic soda), 2.1 (Acetic Acid)	x2

There is a W8 experiment that is not included in Table 5. It is the same as the industry standard wash, but with fresh rinse water instead of a reused water bath, due to the high pH measured in reused water.

All of these washes are performed in a small scale by cutting down a strip of corrugated sheet metal from the catalyst unit. Moreover, in order to get rid of some of the carbon that interferes with the XPS scans, the samples are baked for seven hours at 425°C before performing the appropriate washing experiment.

Using both XPS and SEM the effectiveness of each washing experiment is evaluated by comparing the atomic percent of poisons removed, but mainly focusing on the integrity

of the wash-coat. For example, the back and front samples are affected differently by the washes [29]. Figure 16 from Hackelman et al. shows a photograph of front and back samples after being washed with experiment W3 that shows how the samples are affected differently by the same washing process, and Figure 17 shows the SEM electron layered image taken of the wash-coat of those samples. Please observe the difference in smoothness of the wash-coat. Using EDS the scan in Figure 18 shows that the integrity of the wash-coat of the back samples is compromised when stronger chemical baths are used (e.g. experiment W3), as this removes pieces of the alumina coating with the precious metals and exposes the steel substrate [29].

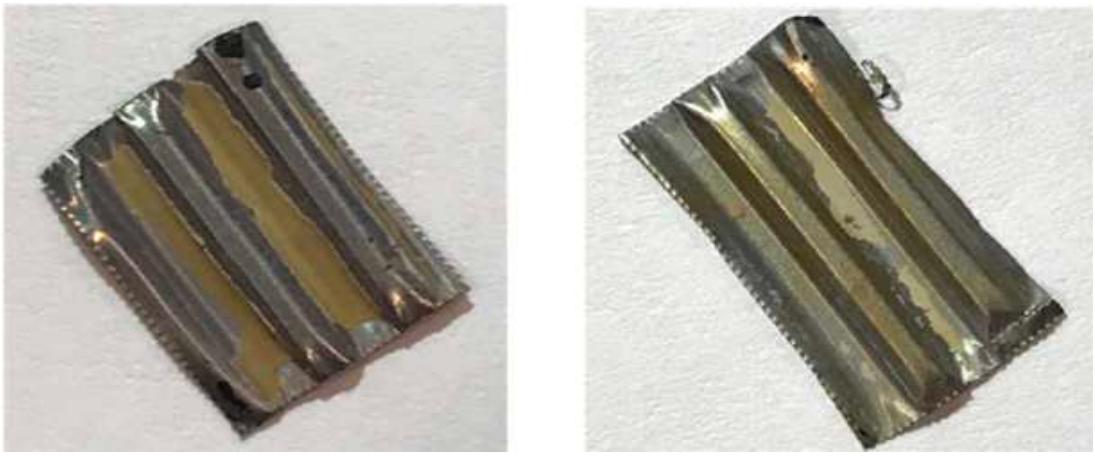

Figure 16: Front (left) and back (right) W3 samples [29]

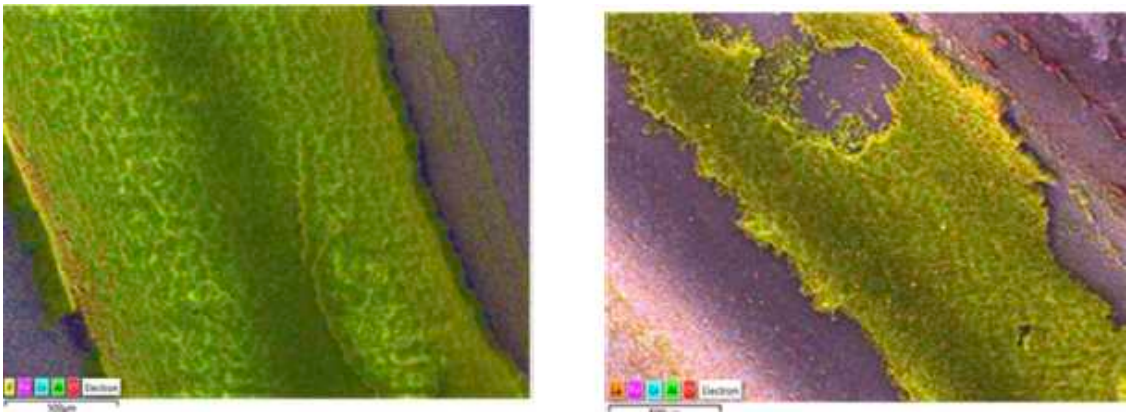

Figure 17: SEM scan of front (left) and back (right) W3 samples [29]

Figure 19 is a modified version of what was previously reported by Hackleman, it compares the removal of sulfur, phosphorus, and zinc for the different washing experiments, and it includes the error propagation for such experiments. Based on the amount of poison removal and integrity of the wash-coat after washing, it was determined that the temperature of the baths evaluated in the coarse washing matrix is too high, the difference in pH of the baths damages the wash-coat, and agitation does not damage the wash-coat and shows slightly larger amounts of poison removal. However, the error propagation shows that the amount of poison removal is statistically equivalent for most washes.

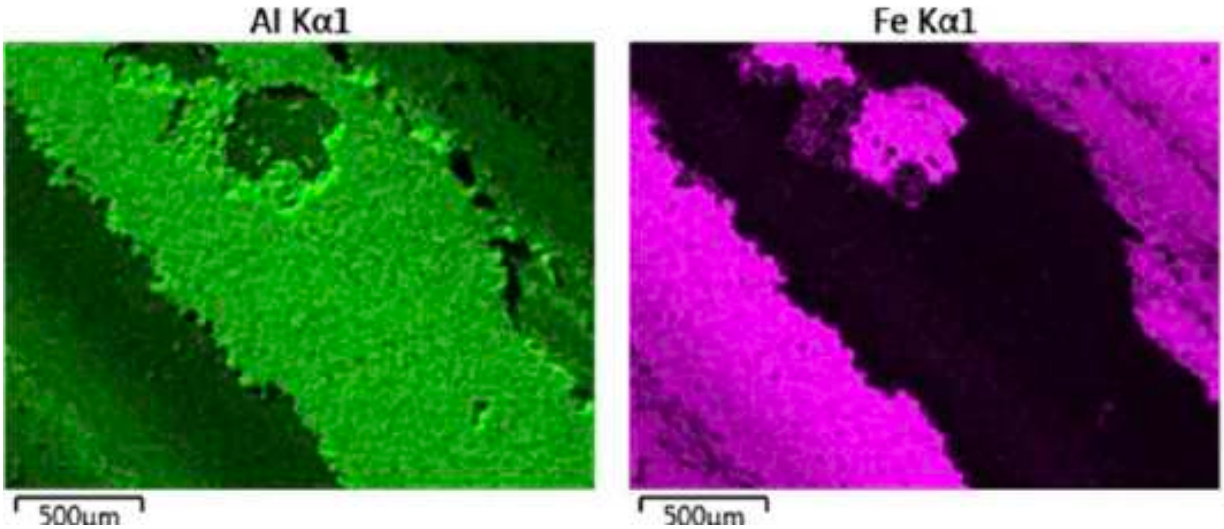

Figure 18: EDS analysis of the back sample washed with experiment W3 showing that the integrity of the wash-coat is compromised [29]

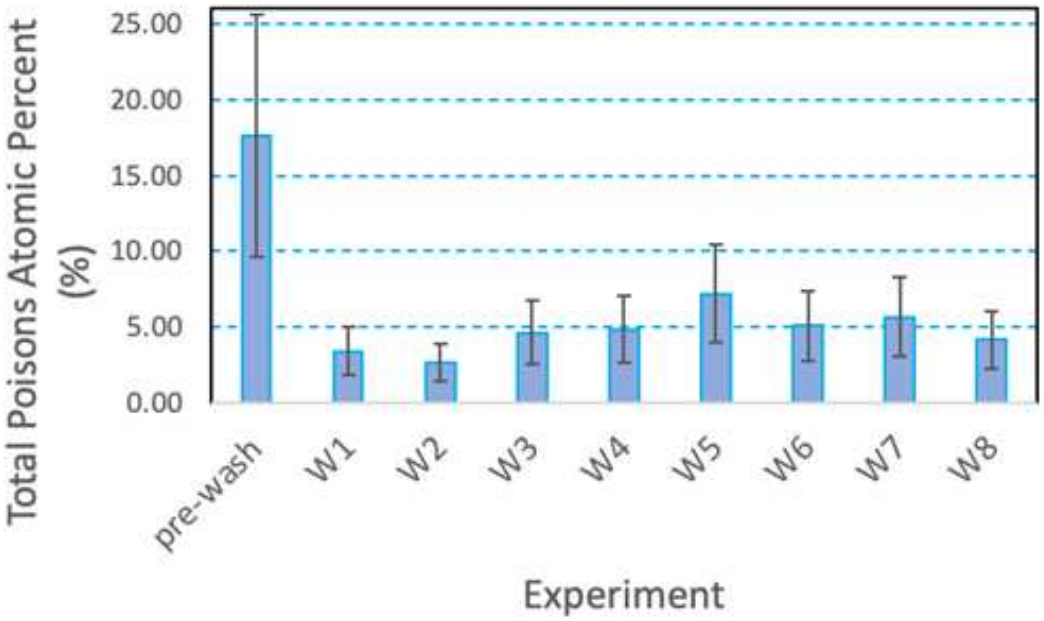

Figure 19: Comparison of the combined reduction of all poisons [29]

Thesis overview

This research focuses on the detailed analysis of poison deposition onto the catalyst, studies the damages caused by the restoration methods, and aims to provide the industry with an efficient step-by-step catalyst restoration procedure, including improved chemical washing and baking methods. The research questions are as follows:

- What is the source of the poisons?
- What is the distribution of the poisons on the wash-coat surface and how deep do they go into the catalyst unit?
- What is the damage level of crystallites and is their degradation reversible?
- What are the steps to efficiently restore a catalytic converter without further damage?

- What can one do in order to extend the life of a catalyst and postpone their restoration?

2. Experimental methods

2.1 SEM and XPS

Scanning electron microscopy (SEM) and X-ray spectroscopy (XPS) are used extensively for materials testing. SEM works by accelerating electrons towards a sample, with an electron gun. Looking at it from an atomic perspective, each nucleus in the material is surrounded by an electron cloud, which is commonly described as electrons from the sample orbiting around the nucleus. The electrons from the gun collide against the ones in the sample, and though the orbiting electrons gain energy from the collision, they eventually fall back to their original orbital, emitting a photon at a given wavelength in the process [10, 26]. The photons are detected by an energy dispersive X-ray detector (EDS) and linked to their corresponding chemical element to generate elemental maps. The scattered electrons are also detected, and an image is formed based on their characteristics coming back, such as angle and momentum [26, 30, 31]. The two main operating variables to consider for SEM analysis for this project are the magnification and accelerating voltage. A greater accelerating voltage allows exciting higher energy electrons and a deeper penetration into the sample, while the magnification sets the size of the window of interest.

In contrast, the XPS works by extensive use of the photoelectric effect. Monochromatic soft X-rays impact the sample and allow its valence electrons to be emitted. Because solid samples have such a short electron mean free path, the emission comes only from

the very surface and goes as shallow as just a few atoms deep. The kinetic energy from each emitted electron can be found with an energy balance

$$KE = h\nu - BE - \varphi_s$$

where $h\nu$ equals the photon energy from the well-known Einstein formula, BE is the binding energy, and φ_s stands for the work function of the spectrometer. The BE can be seen as the amount of energy lost from the moment the electron leaves the atom. Each element has a different electron configuration, ergo different binding energies; this allows XPS to identify the elements on the surface and evaluate their concentration [30]. From Hackleman, the equipment used can be seen in Figure 20 [16].

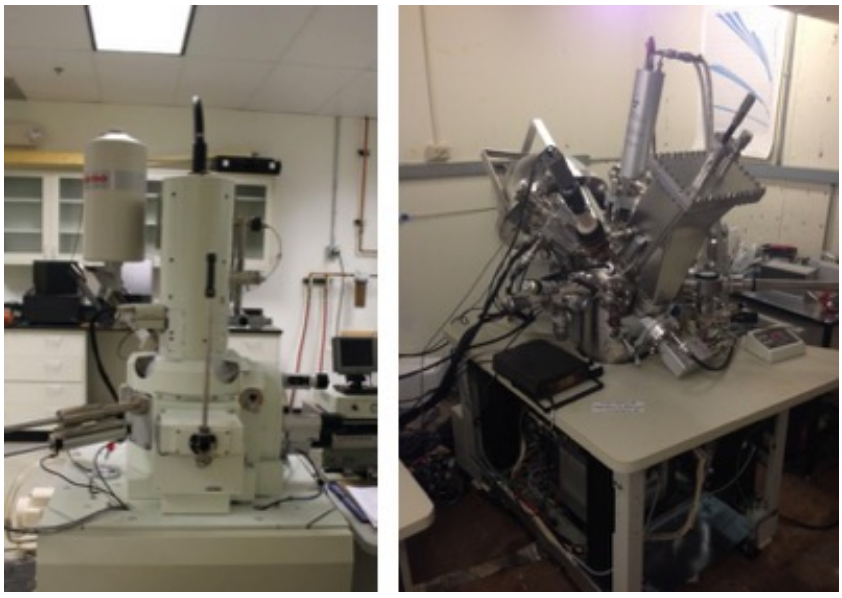

Figure 20: Used scanning electron microscope on the left, and X-ray spectroscope on the right [16].

Furthermore, XPS provides accurate concentration measurements of the surface composition, but SEM is able to go deeper into the sample and reveal a picture of the sample. SEM also provides concentration information, but it is rather qualitative and

should be used to identify trends [26, 30]. Long collection times minimize the amount of noise and are used with both XPS and SEM for accuracy purposes.

On a separate note, both of the catalyst units being tested were aged together, but only one of them was disassembled and the top corrugated sheets were removed for further analysis. However, removing the top sheet damages the remaining corrugated top sheets in the unit, as they are moved excessively and are often scratched by the sheet being pulled. The damage seen is a patchy wash-coat with exposed naked substrate areas. To prevent further handling damage, several sheets at the top were removed, both damaged and in perfect conditions, for future SEM and XPS testing. The unit was then reassembled to resemble a structurally sound aged catalyst. The handled catalyst unit is therefore now shorter than the untouched unit and is depicted in Figure 21. The reassembled shorter unit is Unit A, and the untouched catalyst is Unit B.

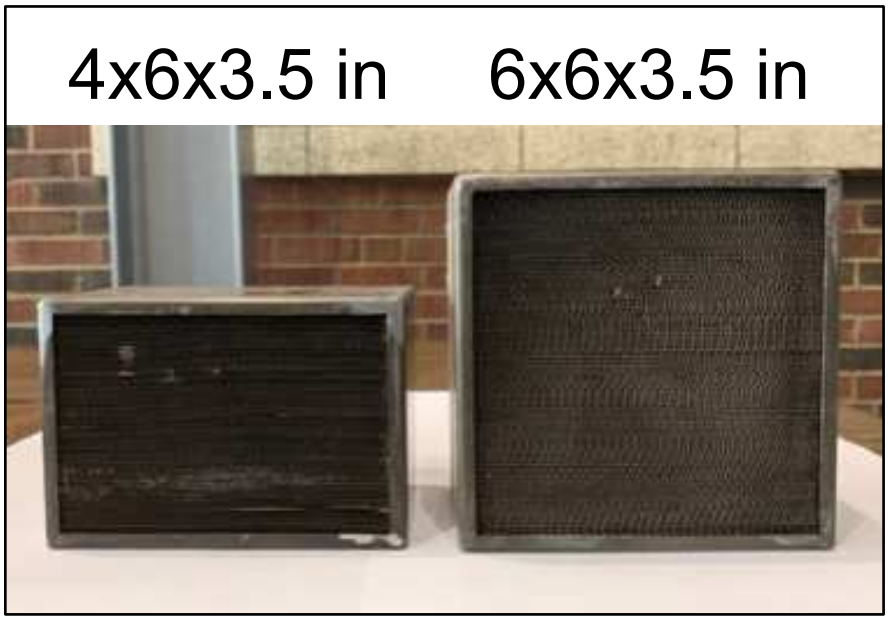

Figure 21: The reassembled catalyst Unit A on the left, and the untouched catalyst Unit B, on the right

2.1.1 Depth analysis

As mentioned before, the accelerating voltage and magnification are the most significant variable parameters for these SEM scans. For the depth analysis the goal is to find out how the poisons of interest differ in their deposition, specifically focusing on how deep they can go into the wash-coat. To perform this analysis, SEM is used with a magnification of 50x over a fixed window, and variable accelerating voltages ranging from 4 to 20 kilovolts (kV) in 4kV increments. The accelerating voltage determines how deep the impinging electrons go into the sample. When the accelerating voltage is higher, the electrons have more kinetic energy, and consequently their velocity increases. This allows the electrons to go deeper into the sample. The depth also depends on the chemical properties of the elements of interest. This relation is explained by Castaing's formula

$$Z_m = 0.033 \times (E_0^{1.7} - E_c^{1.7}) \frac{A}{\rho z},$$

where Z_m is the electron penetration range, E_0 is the acceleration voltage, E_c is the critical excitation energy, A stands for the atomic mass, the density is expressed with ρ, and Z is the atomic number [32].

The depth the electrons from the SEM electron gun reach into the sample is simulated using the program Monte Carlo Simulation of Electron Trajectory in Solids (CASINO) version 2.5.1.0. [33].

Please note that the results are estimates, as the simulation does not take into account the imperfections of the alumina wash-coat, nor does it consider the uneven distribution of elements, poisons in this case, that are deposited onto the surface of the wash-coat. The baseline accelerating voltage, 4kV, is selected considering all the elements of

interest: Al, C, O, Zn, S, P, and Pt. These elements are identified in Figure 22, which is a cutout from a periodic table used for EDS analysis and provided by JEOL, the spectrometer manufacturer [32].

For this application, the most important piece of information in Figure 22 is the characteristic X-ray energy level of each element. According to the personnel at the Central Instrument Facility at Colorado State University, an accelerating voltage two to three times the amount of characteristic X-ray energy levels is enough to excite the valence electrons in that element for EDS detection for lower energy orbitals. Platinum is included out of its proper location in the periodic table for informational purposes of its characteristic X-ray energy levels only.

Figure 22: Parts of the periodic table provided by JEOL for EDS analysis [32]

Therefore, aluminum and platinum constrain the accelerating voltage to be at 4 kV or higher. Starting at any lower accelerating voltage and incrementally going higher would give an increase in aluminum when passing the 4kV barrier due to finally exciting the valence electrons and not because there is more aluminum deeper into the sample. Platinum is added to Figure 22 to show that the *M* shell X-ray energy levels in Pt are extremely close to the *K* shell levels in P, 2.04 kV versus 2.01 kV. For this reason, it is almost impossible to differentiate between the two using EDS. To get around this, only the higher energy, *L* shell electrons are used to detect Pt, which translates into using an accelerating voltage of at least 15kV to be able to see Pt.

2.1.2 Linear analysis

The goal of the linear analysis is to determine the difference in poison deposition from inlet to outlet, with several data acquisition points along the line referenced in Figure 23. XPS is used as it provides more accurate information about the composition of the surface.

A short survey scan is taken first to find out what elements are on the surface of the wash-coat of the sample and to identify any charging effects. After finding the best configurations for each element, the equipment is set to run a longer high-resolution scan that focuses only on the configured elements. The elements of interest are carbon, oxygen, phosphorus, zinc, and sulfur. The high-resolution is set to run for 60 to 70 minutes to minimize noise.

Figure 23: Linear analysis schematic, performed with XPS to obtain poison atomic percent distribution from inlet to outlet

2.1.3 Half-pipe analysis

SEM is used for this analysis with a magnification of 50 times and an accelerating voltage of 4 kV. A sideview schematic of this half-pipe analysis is seen in Figure 24.

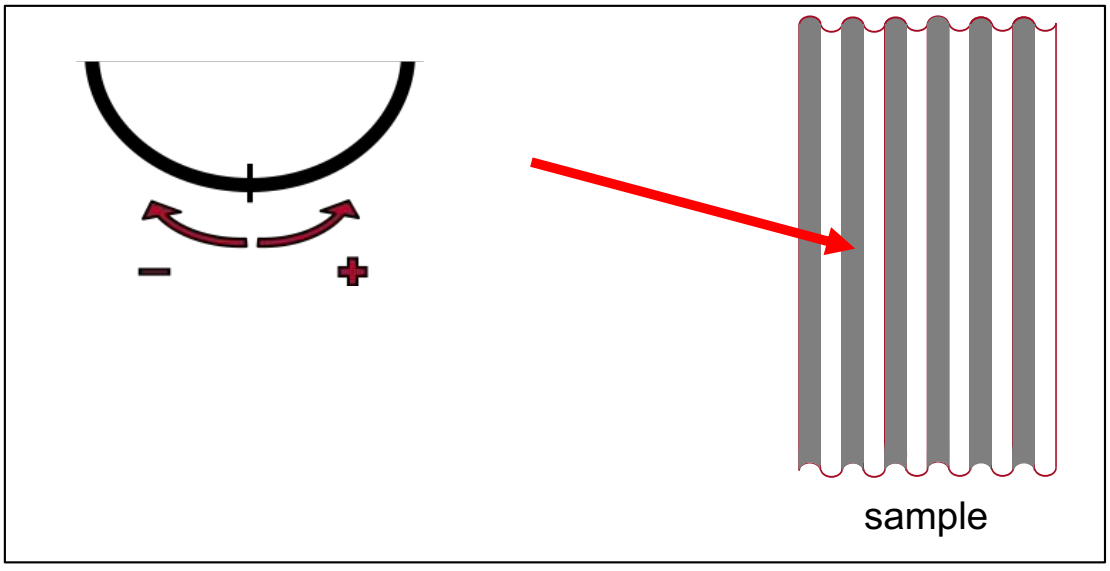

Figure 24: Side view of corrugated metal valley describing the half-pipe analysis

The analysis is analogous to an observer moving down a half-pipe, collecting data across several points while moving from side to side, taking the first datapoint at the top,

and then moving down one of the walls of the valley until the flat bottom is reached. After reaching the bottom, the point of interest keeps moving in the same direction and starts going up the opposite wall, until the top is reached.

2.2 Carbon baking

Different components that foul and poison the catalyst that are deposited onto the wash-coat during the aging process leave the surface at dissimilar baking temperatures. Since carbon oxidizes and leaves the surface at a lower temperature than the other elements, a bake out procedure can help analyze the amount of carbon in the catalyst deposited from the exhaust, formed presumably at the surface of the wash-coat [11], [17]. Though 450°C is the baking temperature suggested by the literature, there is evidence noted in Table 1 (presented earlier) that shows crystallite growth occurs at temperatures above 400°C for this catalyst, and this effect is significantly higher above 450°C. Hackleman et al. baked the samples at 450°C for one hour first, and then the reduction of carbon levels was achieved at 425°C. Only the latter temperature is used in the following baking processes not to promote crystallite growth but only heat up the sample enough to promote the oxidation of its carbon layer. An FB1315M Thermo Scientific Thermolyne furnace is used to bake the samples, which is depicted in Figure 25.

A scale measures the weight of a sample pre- and post-baking. The scale of choice is a Mettler Toledo MX5, pictured in Figure 26. The resolution of the scale is one microgram, which makes it sensitive to static charges otherwise imperceptible. A radioactive deionization strip is used in order to remove these, whose decay of alpha particles discharges each sample before being placed on the scale [3]. The measurement is

performed three times to account for random error. Moreover, these samples lose weight every time they are handled and reweighed, likely due to attrition; however, no change in weight is observable while the sample is on the scale, so the possibility of sublimation of any parts of the sample is discarded. The loss is more significant the first few times the sample is handled but stabilizes after the majority of loose wash-coat particles leave the sample. Each of the samples is treated with care to minimize the loss of loose wash-coat pieces.

Additionally, the sample is developed by extracting a sheet of corrugated metal from the catalyst unit and cutting rectangles out of the sheet of approximately 200mg, which translates to approximately 2 x 1.5 cm catalyst sheet cutouts. These were selected based on the ideal dimensions for SEM analysis, and the size of the scale. A schematic of an average carbon baking experiment sample can be seen in Figure 27.

Figure 25: FB1315M Thermo Scientific Thermolyne furnace used to bake samples

Weighing and baking of a sample at 425°C for two hours is performed iteratively until the weight is relatively stagnant. At this point the carbon layer is declared to be removed from the sample and this is supported by SEM measurements of the carbon atomic percent at the surface. After removing the layer of carbon, only the poisoned wash-coat and the substrate remain. The wash-coat is completely removed from the substrate surface with a wire brush, and so the weights of the wash-coat and the substrate are obtained.

The porous samples lose all of the previously absorbed humidity after being exposed to 425°C for two hours. This is seen on the scale as a continuously increasing transient weight reading of the samples when placed in the scale immediately after baking them, as they absorb the humidity in the air. For this reason, before weighing the samples they are left for 48 hours in an equilibrating tub at semi-constant humidity levels; this is simply a closed container with air filters attached to the sides, which allows for air exchange but lowers the risks of the environment contaminating the sample. The relative humidity is kept at a maximum level in a room at a fairly constant temperature of 25°C, which allows the dewpoint and the relative humidity in the air to remain unchanged. The room temperature is not actively monitored, but it is rather passively controlled with insulation. The scale is located in the laboratory basement, which reduces temperature fluctuations and vibrations. A lab blank is made to check for consistency in the humidity in the room. The lab blank is the same type of sample but baked for 5.5 hours at 425°C. The weight of the lab blank being constant on different days ensures the samples have comparable levels of absorbed humidity.

Figure 26: Mettler Toledo MX5 scale, with a readability of 0.001 mg

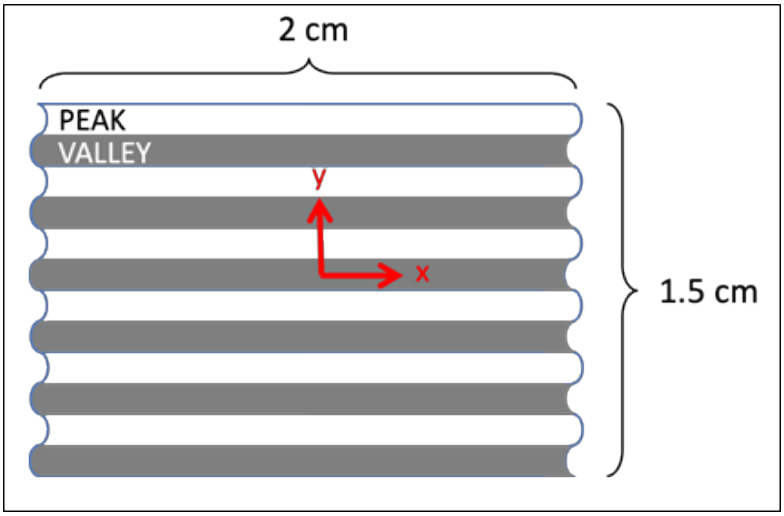

Figure 27: Average sample, cutout from a larger catalyst sheet metal substrate

2.2.1 Carbon baking with additional gas purging

Carbon is known to oxidize and leave the surface between 400 and 450°C [11]. At a higher O_2 concentration than that of air, the amount of carbon oxidized and removed may increase. This is further tested by adapting the furnace to purge gases into the chamber. This gives the experimenter the ability to control what gases are in the chamber during baking.

A schematic of the modified baking set-up is shown in Figure 28. The first additional gas purging test consists in purging industrial grade nitrogen through the furnace while baking a catalyst sample at 425°C for eight hrs. The eight-hour period is selected based on the results of the carbon baking and weighing iterative test, which are included in the next chapter. The hypothesis is that the carbon will not oxidize and will not leave the surface when deprived of O_2. The weight should remain constant to prove the hypothesis.

The second test consists in purging air through with a pump while baking. This renews the amount of O_2 molecules readily available in the chamber. The third carbon baking test consists in purging a mix of 40% O_2 and 60% N_2 through the furnace while baking. Weighing is performed before and after baking each sample, and the results are compared to find the most successful carbon removal baking method. All three tests consist of a baking temperature 425°C and a baking time of eight hours.

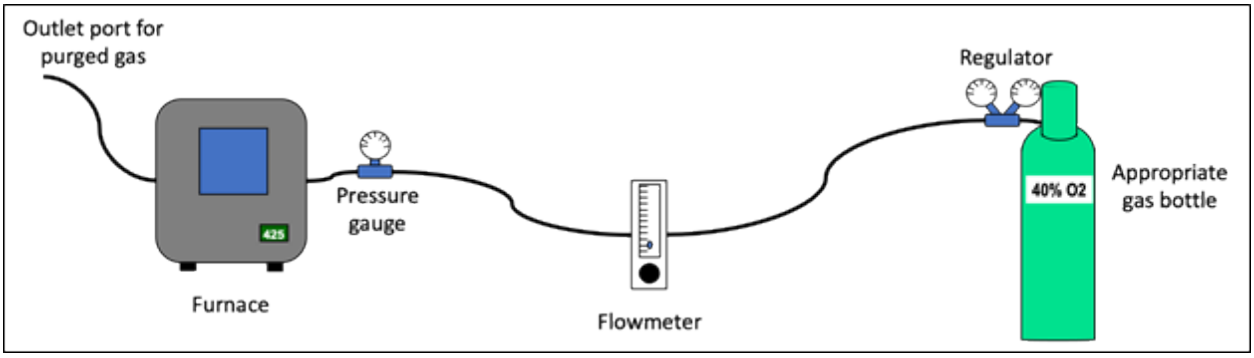

Figure 28: Set up for baking experiments with additional gas purging

2.2.2 Hydrogen reduction

One way to detect whether a catalyst unit contains oxidized crystallites is to attempt a hydrogen reduction and measure the reduction efficiency of the catalyst unit before and after. The reduction efficiency for this test is measured at AGES.

With the same baking setup (Figure 28) a hydrogen purge is tested. The selected temperature for this hydrogen reduction is 450°C for a period of two hours, while purging a mix of 5% H_2 diluted in N_2. The reduction initiates in between 400°C and 450°C and peaks near 550°C [23, 24, 25]. According to Table 1, sintering occurs at slow rates above 400°C for this catalyst but the sintering rate rapidly increases after 450°C. For these reasons, 450°C is selected as the reduction benefits will likely outweigh the amount of sintering after a single two-hour long exposure. If the reduction improves performance significantly, this two-hour baking process is added to the carbon baking procedure.

The available information in the literature regarding the oxidation temperature of platinum is inconclusive. The reason seems to be that bonding of oxygen and platinum occurs at both low and high temperatures, but the bonding structure is different depending on the temperature and pressure. A study by Matthijs A. van Spronsen et al. shows bonding with oxygen takes place at room temperature and also at ~255°C. The study also suggests the bonding requires prolonged exposure to oxygen, which indicates most of the oxidation occurs during the degradation period in the Cooper-Bessemer GMVH-12 instead of during the shorter carbon bake-out procedure. This is not proven experimentally since the carbon bake-out procedure with ambient air was applied to the unit before the hydrogen reduction took place [34].

2.3 OCEC analysis

An analysis of the ratio of elemental versus organic carbon helps decipher the source of the carbon deposited onto the surface of the wash-coat. Carbon in the exhaust stream

is operationally classified in this type of study as either elemental or organic. Refer to Figure 29 for a visual representation of the process [35]. Elemental carbon (EC) is composed of light-absorbing heavy chains of HCs, colloquially known as black carbon or soot. Organic carbon (OC) on the other hand is composed of more volatile chains of HCs, like the ones from atomized lubricating oil droplets. So volatile that it is common for samples to be stored at extremely low temperatures after being acquired to avoid loss of OC [36].

The OCEC analysis consists in a stepped increase in temperature in an inert H_2 environment. The sole increase in temperature in the non-oxidizing environment is enough for the volatile OC to leave the sample. After reaching 870°C the temperature is decreased and O_2 is introduced as a 2%O_2/H_2 mix, and the stepped increase in temperature is repeated in an oxidizing environment to measure levels of EC.

The OC is catalytically converted to CO_2 and then reduced to CH_4, which is quantified by a flame ionization detector (FID). EC levels are measured similarly, with the difference that the carbon oxidizes and leaves the surface as CO_2 in the second scenario.

Carbonate (CC) is typically a sub-division within OC, unless the user wishes to differentiate between the two. Some OC has the tendency of charring and creating additional light-absorbing carbon at high temperatures. Not to count for this as EC originally present, the equipment counts with a diode laser and a photodetector in case charring occurs. The light-absorbing carbon formed interferes with the transmittance of the laser, bringing the transmittance down. Once the char is eliminated and accounted

for as OC, the transmittance levels go back to the same levels measured at the beginning of the procedure.

The split line in Figure 29 is set by the transmittance of the laser getting to its initial value after getting rid of the char formed in the process. Any carbon desorbed to the left of the line is considered OC, and any quantification to the right of the line is EC; this is the reason why it is an operational classification [35]. A picture of the thermal-optical analyzer is shown in Figure 30.

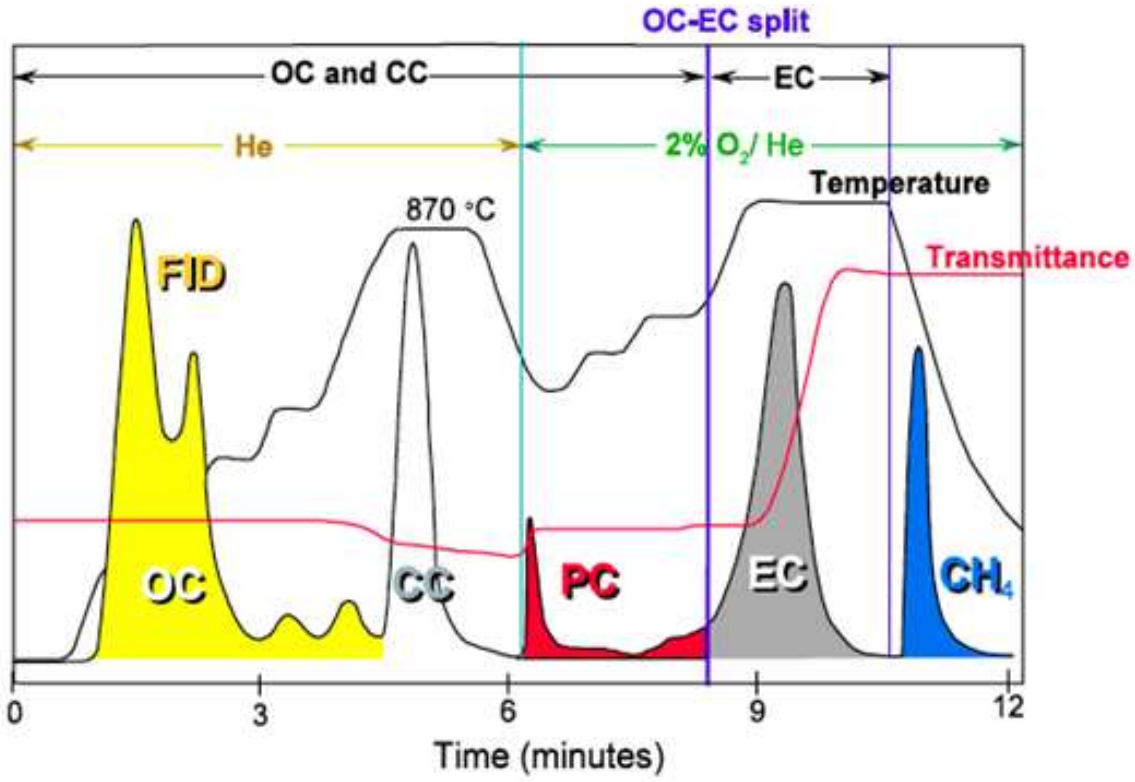

Figure 29: Thermogram of a sample with organic carbon, OC; carbonate, CC; pyrolyzed char formed, PC; and elemental carbon, EC [35]

Figure 30: OCEC thermal-optical analyzer

2.4 Fine washing matrix

Due to the proximity in the results of the coarse washing matrix, more permutations of the washing variables are explored. The experiments are performed in a small scale by removing strips of corrugated sheet metal from Unit A (Figure 21). The chemical baths are contained in 500 mL beakers and samples are supported by a retort stand. The pH levels are altered by varying the ratio of chemical to water. The temperature and agitation are controlled by a Scilogex hot-plate stirrer, model MS-H280-Pro, with an agitation range of 200 to 1500 rpm, and a maximum plate temperature of 280°C. The instrument and the washing setup are seen in Figure 31. An external thermocouple is used to measure the temperature of the bath. Based on the results of the carbon baking experiments of this study, the samples are baked at 425°C for eight hours before

washing them chemically; this information is further explored in the carbon baking results section. Fresh deionized water us used for every rinse.

Figure 31: Scilogex hot-plate stirrer and washing setup

The second washing matrix version is called the *fine washing matrix*, and it includes lower bath temperatures than previously tested [29], lower increases in concentration of the chemical baths in comparison to the industry standard, and further evaluation of various agitation rates, ranging from 200 to 1000 rpm. The fine washing matrix is summarized in Table 6. The room temperature and the pH are measured at the time of washing. Reduced washing times are evaluated in some of the experiments. There is some variability in the pH of the experiments, this is attributed to the water source.

Table 6: Fine washing matrix

Name	Temperature (F)	Aggitation (rpm)	Concentration	pH	Time
R0 (Baseline)	Room Temp. (≃ 74)	0	Standard	Caustic Soda (12.50) Acetic Acid (1.85)	Standard
R1	≃100	0	Standard	Caustic Soda (12.45) Acetic Acid (1.88)	Standard
R2	Room Temp. (≃ 74)	200	Standard	Caustic Soda (12.97) Acetic Acid (2.14)	≃1/2
R3	Room Temp. (≃ 74)	0	Lower	Caustic Soda (12.88) Acetic Acid (2.26)	Standard
R4	Room Temp (≃ 76)	200	Standard	Caustic Soda (12.53) Acetic Acid (1.83)	Standard
R5	Room Temp (≃ 77)	750	Standard	Caustic Soda (12.48) Acetic Acid (1.83)	Standard
R6	Room Temp. (≃ 74)	500	Standard	Caustic Soda (12.48) Acetic Acid (1.84)	Standard
R7	Room Temp. (≃ 74)	1000	Standard	Caustic Soda (13.04) Acetic Acid (2.18)	Standard
R8	Room Temp. (≃ 74)	0	Higher	Caustic Soda (12.61) Acetic Acid (1.77)	Standard
R10	Room Temp. (≃ 74)	200	Lower	Caustic Soda (13.01) Acetic Acid (2.18)	≃1/2
R11	Room Temp. (≃ 78)	200	Lower	Caustic Soda (12.94) Acetic Acid (2.16)	Standard

2.5 Catalyst washing box

Besides testing variations of the industry standard catalyst washing procedure, the procedure itself is analyzed to have as a reference. A small sample placed in a 500 mL container does not resemble the actual washing method, because the ratio of volume of chemical to surface of wash-coat is much greater when the sample is placed in an open container when compared to the fully assembled catalyst unit. When the unit is

immersed in the bath, the channels formed by the corrugated metal are much smaller than the volume available in the beaker. The amount of liquid that each channel is exposed to is minuscule without recirculation or agitation.

Therefore, to better resemble the fully assembled catalyst unit immersed in the bath without agitation, a catalyst washing box is created. The box needs to be resistant to the diluted acetic acid and caustic soda solutions. And more importantly, the box needs to have the proper dimensions in order to obtain the same ratio of volume of chemical to surface of wash-coat. To do this, the corrugated sheet metal is measured, and the catalyst washing box is manufactured with the appropriate dimensions out of stainless steel, and it can be seen in Figure 32. An O-ring is used in order to prevent the escape of the washing solution, and screws are used to clamp the two halves of the box together. The hole observed in Figure 32 on the lid side is there to allow all the air to escape as the screws are tightened, and it is closed with a screw-on lid when the experiment is setup, in order to avoid any contact with the exterior. Refer to Figure 33 to see the catalyst washing box fully assembled.

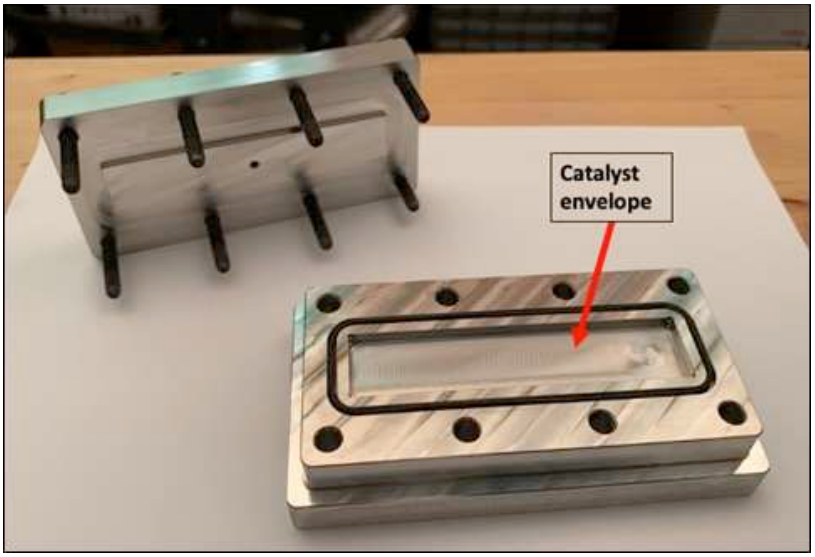

Figure 32: Stainless steel catalyst washing box

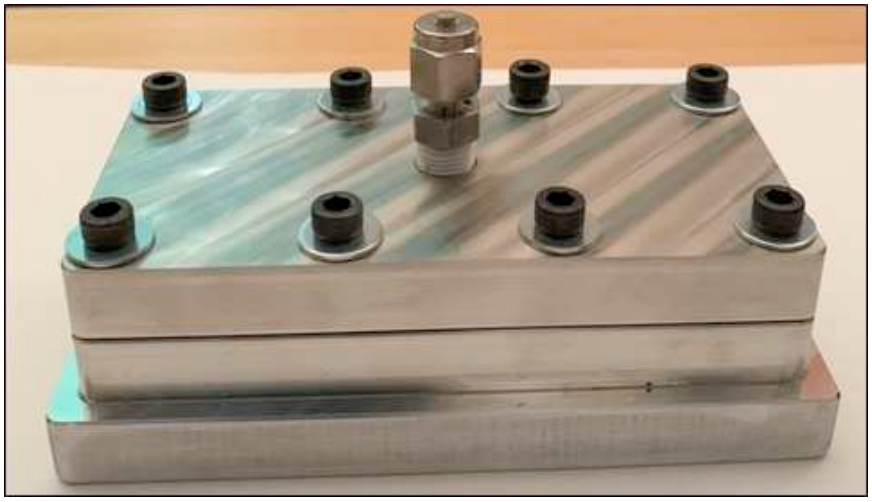

Figure 33: Catalyst washing box fully assembled

Moreover, since the catalyst unit is built by placing one corrugated sheet in between two flat sheets, the catalyst washing box is used in the following order: fill the catalyst envelope in Figure 32 with the appropriate catalyst solution, either caustic soda, acetic acid, or deionized water. Then place a flat substrate cutout of the appropriate size in the catalyst envelope, then add more solution if needed and place the corrugated substrate on top. Then add more solution if needed and place the top flat sheet on top. After this proceed to place the lid on top with the cap unscrewed. Tighten all eight screws in and then screw in the cap at the very top in Figure 33. This entire process minimizes the possibilities of mass diffusion being responsible for the slight recirculation of fresh chemical onto a sample, as it likely happens when a small individual sample is placed in a beaker.

The samples are baked for eight hours at 425°C before being washed in the box, for this test to be comparable to all washing tests performed in the fine washing matrix (Table 6). After washing, the corrugated piece is analyzed with XPS and these results are compared against the ones for the coarse washing matrix, which were performed in

the open beaker. The catalyst washing box experiment determines whether the lack of agitation reduces the effectiveness of the washing process.

2.5 Washing and baking

Besides finding the most successful washing and baking procedures independently, the combination of the two is tested. This implies comparing poison removal levels and investigating whether the processes are commutative, and is done with SEM analysis, which is qualitative more than it is quantitative. However, it has been proven in previous experiments that the results of both XPS and SEM line up closely [17], and the SEM can reveal pictures of the samples that help identify damage to the wash-coat.
There is a trade-off based on the selected operation order. On one hand, from a financial standpoint baking after washing helps reduce costs as it shortens the drying time significantly. On the other hand, from a chemical standpoint it makes more sense to remove the carbon layer before washing, so that the chemicals are able to interact directly with wash-coat during the washing process. Furthermore, the literature suggests hydrogen is more resistant to acid in its metallic form as “acid treatment does not remove active metal (Pt), which would occur if the surface platinum were partially oxidized” [13].

2.6 Activity scan

Diesel Controls Limited (DCL) performs an activity test where they turn the wash-coat into a powder. This breaks through the physical barriers of the layers that compose the catalyst sheet, and the powder is obtained by means of a brush-headed drill bit. Drilling through several random areas of the catalytic converter allows for the powder to

represent the average condition of the wash-coat across the unit, which is not achieved with the previous XPS analysis. Different analyses reveal the characteristics of the wash-coat: BET for the surface area, XRD for crystal phases, and PIXE for elemental analysis. BET refers to the Brunauer–Emmett–Teller theory, “applicable on a monolayer followed by multi-layers and further capillary condensation” [37]. XRD refers to X-ray diffraction, and PIXE refers to particle-induced X-ray emission [38].

2.7 Performance testing

2.7.1 Activity testing

AGES has been a contributing partner to this research project. They provide with catalyst fitting, washing, and recycling options to their customers and have helped by providing the usage of their facilities to further test Unit A and evaluate each step of the restoring process, along with SEM and XPS analysis. Their test stand (Figure 34) utilizes gas bottles to simulate exhaust gases; CO bottles are used for oxidation catalysts, and NO, CO, and H_2O are used for TWCs; the fixture is able to measure the equivalence ratio for TWCs. The test stand heats up the catalytic converter by purging hot air through, and once the catalyst is at the desired temperature the flow changes to the heated fluid of interest. The stand measures pre- and post-catalyst levels of the fluid of choice by means of a *Testo 340*, providing the user with an approximate reduction efficiency value for the catalyst unit.

The most successful baking restoration method, the hydrogen reduction, and the most successful washing method of the washing matrix are applied to catalyst Unit A and then shipped to AGES for an analysis of the reduction efficiency of the unit after each

restoration step. The temperature ranges from 500 to 700°F for most reduction efficiency tests performed at AGES.

Figure 34: Test stand used at AGES with a zoomed in picture of Unit A being tested

2.7.2 Engine slipstream performance testing

This procedure is explained in chapter 1.5.3. The engine used for the test is introduced in chapter 1, a Cummins QSK19G with 159 mm of bore and stroke that runs on natural gas, with a 19 L displacement and a rated power of 350 kW at 1800 rpm.

In addition, a slipstream is used in the lab to better control the temperature and space velocity. This is done with a liquid-gas heat exchanger, a bypass control valve, and a space velocity flow control valve. From Baumgardner, Figure 35 shows a schematic of the slipstream. Omega K-type thermocouples are used, and a Rosemount differential

pressure transducer (0 to 0.136 bar range) measures the pressure drop across the catalyst.

The oxidation catalyst used (Unit B) is placed in the small catalyst housing of the slipstream due to its size. The small catalyst housing dimensions are $0.152 \times 0.165 \times 0.482\ m$. The quality of the emissions is measured with a Rosemount five-gas analyzer and a Nicolet Fourier Transform Infrared (FTIR). The first measures CO, CO_2, NO_x and THC, and the latter is used to measure methane, ethane, propylene, propane, and formaldehyde. Propane, propylene, and ethylene constitute the volatile organic compounds for this study (VOCs), as mentioned earlier.

A temperature sweep ranging from 150 to 430 °C at a fixed space velocity of $150{,}000\ h^{-1}$ is tested with the fixture in Figure 35. Previous studies in this project show that the space velocity has a small effect in the reduction efficiency [16], so the team considered a space velocity sweep to be unnecessary.

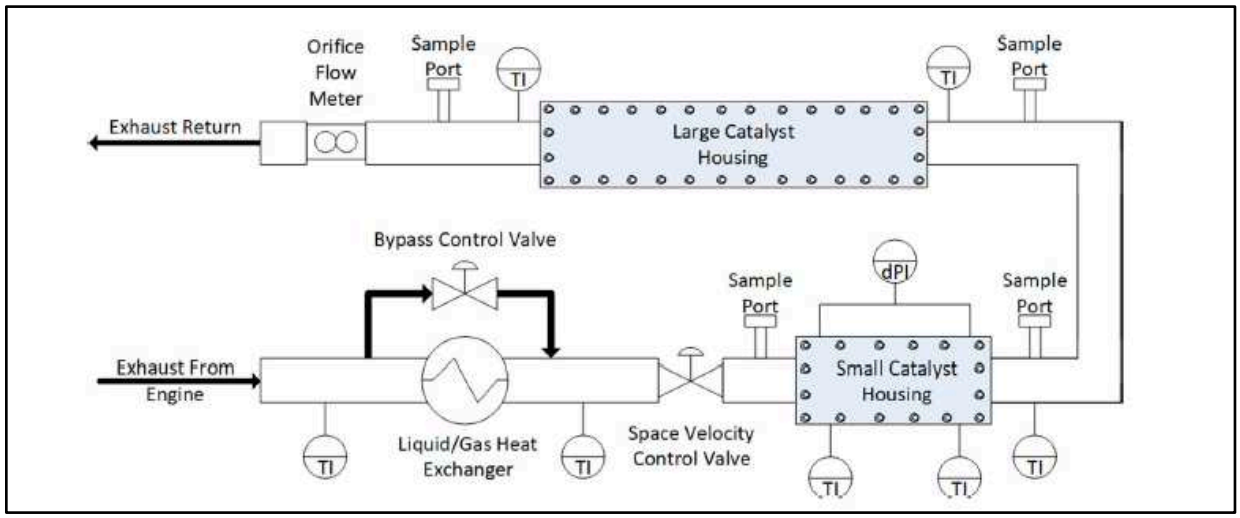

Figure 35: Laboratory slipstream schematic [17]

3. Characteristics of poison deposition

3.1 Depth analysis

The atomic percent for all three poisons is presented as a function of accelerating voltage in Figure 36. Utilizing CASINO 2.5.1.0, the accelerating voltage is converted into a depth value, in units of nm. As stated before, the simulation is useful to approximate the dept that the shot electrons penetrate into the sample. The simulation does not take into account the lack of uniformity of the sample nor does it consider the impact of the uneven deposition of poisons, but it uses the accelerating voltage during acquisition and the density of the sample to evaluate how deep the electrons from the SEM go. As an example, with the density of a highly porous alumina catalyst monolith, 0.825 $\frac{g}{cm^3}$ [39], and for an acquisition at an accelerating voltage of 16 kV, the electrons are declared to go as deep as $7000\ \mathrm{nm}$ into the alumina wash-coat (Figure 37).

Following the logic introduced in the previous paragraph, the CASINO simulation values replace the accelerating voltage to generate Figure 38. The vertical axis in this figure shows the percentage of each poison with respect to the initial most superficial value, starting with 100% at 4 kV. As the scan goes deeper, the atomic percent of each poison is greatly reduced in value. This indicates there is a layer of poisons that builds up superficially, and a smaller amount of each poison makes it through the physical barrier at the surface and gets adsorbed deeper into the wash-coat. Zinc shows the most dramatic drop, meaning it is the most superficial of the three poisons, phosphorus goes deeper into the wash-coat than zinc, and sulfur proves to penetrate the deepest.

a)

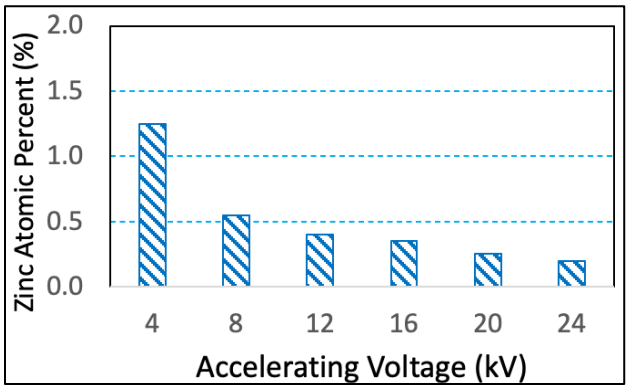

b)

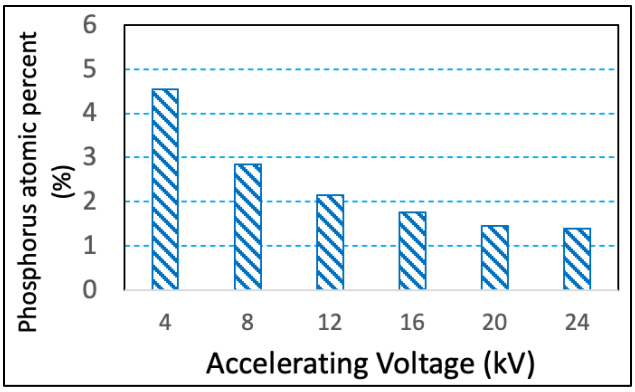

c)

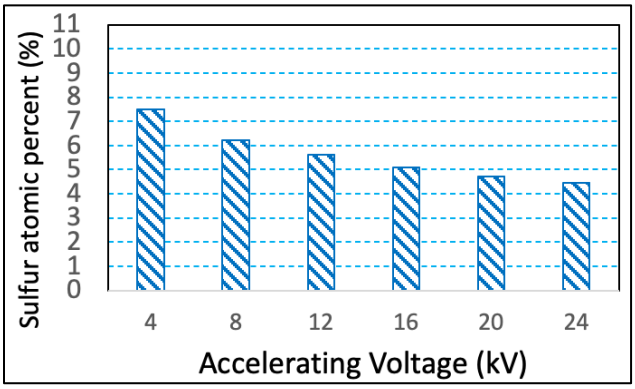

Figure 36: Atomic percent of poisons as a function of accelerating voltage of a) zinc, b) phosphorus, and c) sulfur

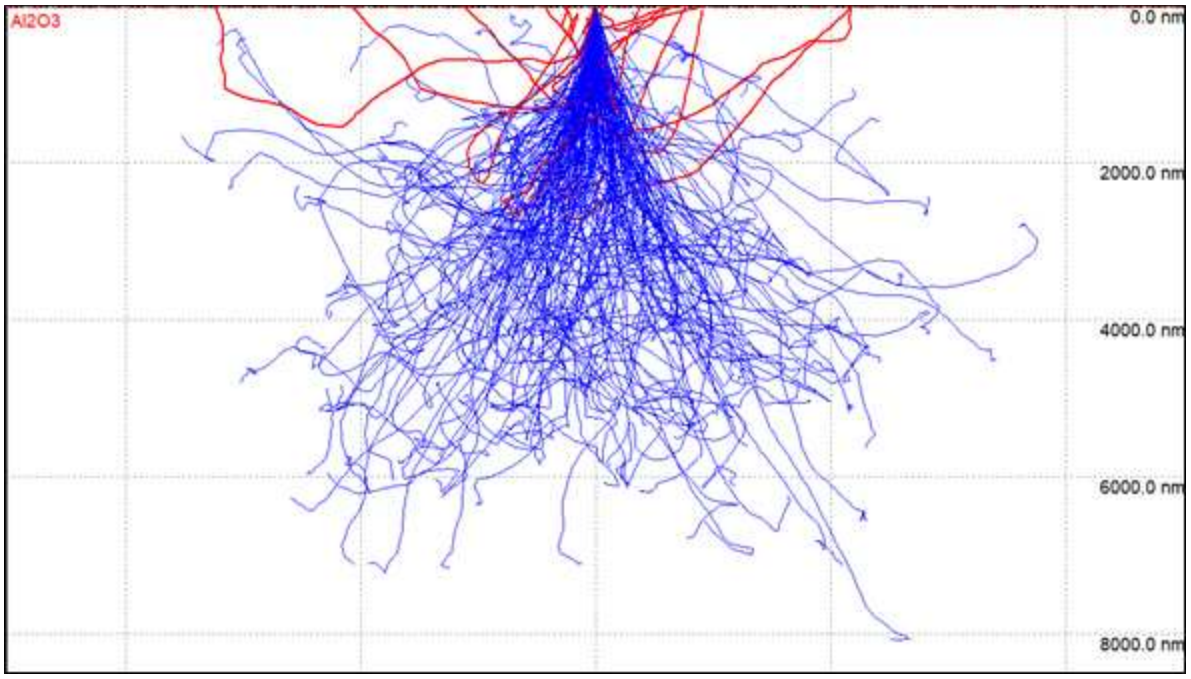

Figure 37: CASINO 2.5.1.0 simulation of electrons going into the sample at 16kV, showing depth in nm

Figure 39 shows that the level of aluminum is consistent throughout the scans. This adds robustness to the depth analysis as it shows what it is supposed to show, an alumina wash-coat with a small fraction of poisons added. These facts agree with the literature to the extent of alumina being used as a sulfur scavenger and zinc being highly superficial [11]; however, an approximate value of the depth achieved by each poison is not stated in the literature, nor is the depth of sulfur and phosphorus mentioned to the knowledge of the author. The result also explains the observation made by Baumgardner et al. stating sulfur reaches a deposition limit, while the atomic percent of phosphorus and zinc keeps on increasing as the catalyst is aged; presented previously in Figure 8. As mentioned earlier, the XPS is highly superficial. The amount of sulfur does not reach a limit but rather keeps on increasing while penetrating deeper into the wash-coat than phosphorus and zinc, interfering with the superficial XPS scan

and providing inaccurate values for the atomic percent of each poison. This superficiality aspect is circumvented with the activity scan, by converting the wash-coat into a powder and getting a more representative elemental analysis of the wash-coat. The depth analysis figures do not include error bars due to the characteristic of the SEM. The SEM is qualitative and used to identify trends. The results from the depth analysis are supported by the activity scan and are explained further in section 3.5.

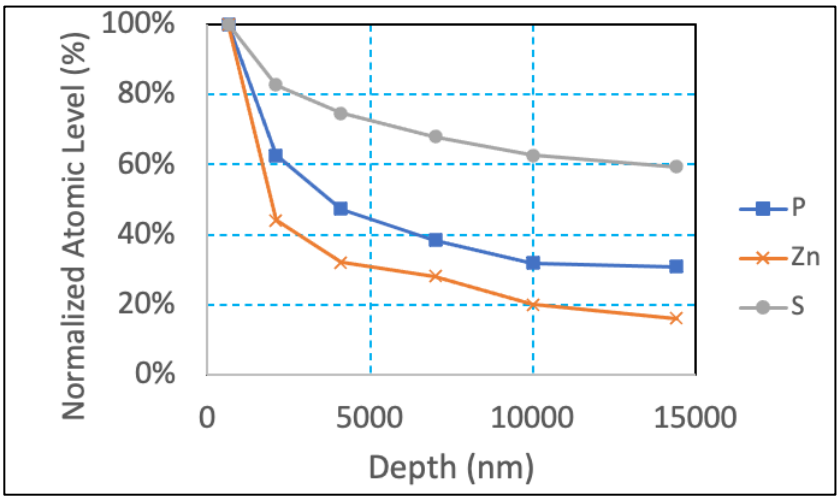

Figure 38: Percentage of poisons relative to the surface versus depth, based on Casino simulation

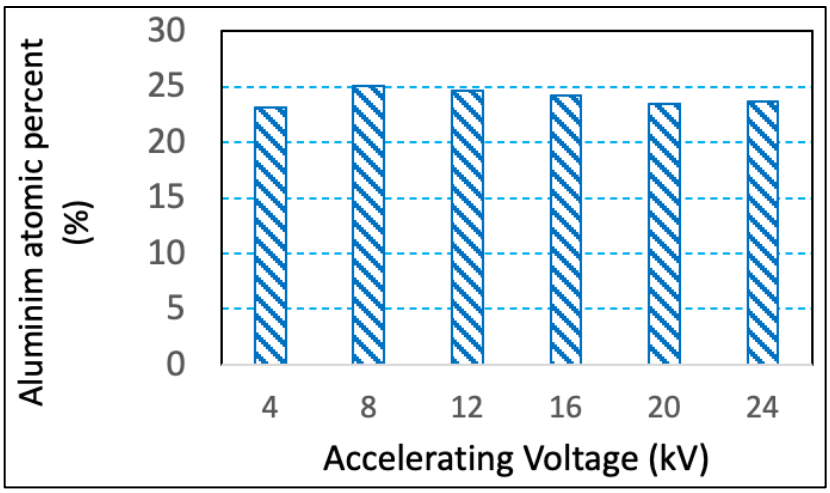

Figure 39: Atomic percent of aluminum (%) as a function of accelerating voltage (kV)

3.2 Linear analysis

The literature suggests phosphorus and zinc deposit towards the inlet of the catalyst, and that sulfur distributes evenly [11]. Previous studies from Davies and Hackleman confirm the phosphorus trend and mention sulfur builds up towards the back of the catalyst (Figure 13) [10, 16]. Two samples were scanned for the linear analysis, but the results are inconclusive. No clear trend is identified in the deposition of poisons from inlet to outlet in aged Unit A. More samples ought to be analyzed to discard what is suggested by the literature or identify new trends.

3.3 Half-pipe analysis

The distance from the center is expressed as a negative or positive number, respectively left or right from the center of the valley. Figure 40 and Figure 41 compare to each other complementary. The higher the amount of carbon, the lower the amount of aluminum, expressing that the carbon lays on top, forming a layer. In addition, the amount of deposition is lowest near the top of the walls of the valley, then increases greatly near the center of each valley, possibly indicating this is where the most amount of exhaust flow occurs. The lack of repeatability as more samples are not available make it impossible to draw other conclusions, but the most significant finding from this analysis is the identification of the carbon layer that deposits on top of the wash-coat of aged catalysts. Please consider this is a lean burn engine oxidation catalyst. The low levels of soot make the carbon layer deposit somewhat counterintuitive, but as was mentioned by Baumgardner et al., this deposition of carbon is likely due to the atomized

lubrication oil particles making their way to the catalyst [17]. As with the depth analysis, the error is not estimated due to the qualitative characteristics of the SEM.

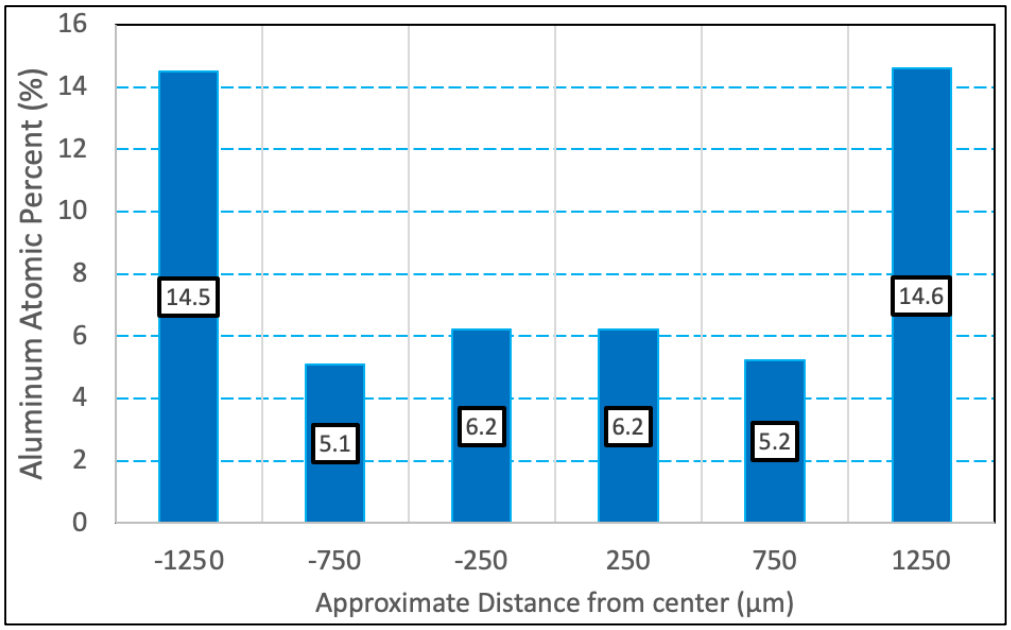

Figure 40: Aluminum atomic percent (%) as a function of distance from the center of the valley (µm)

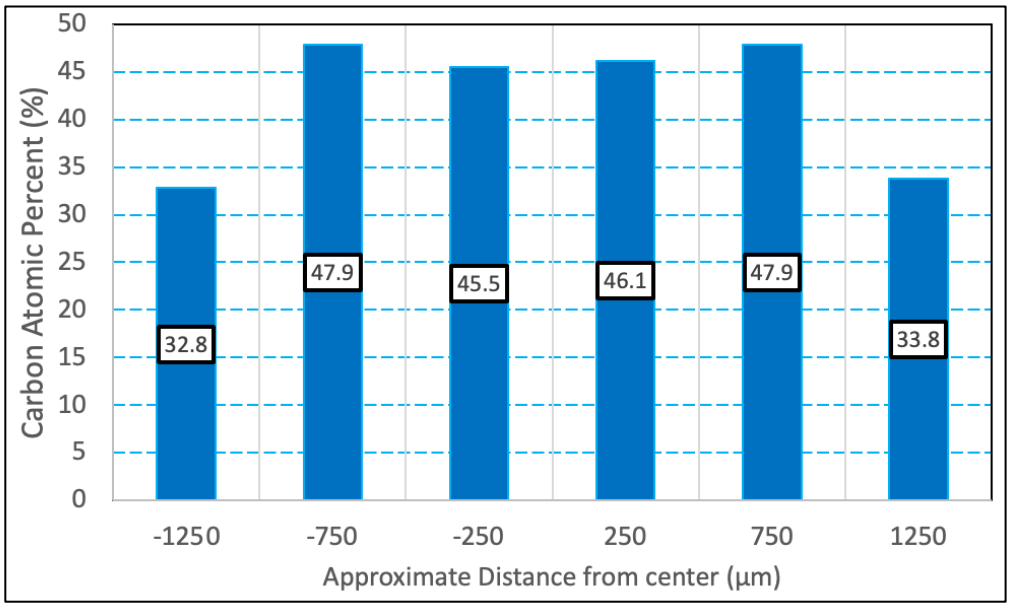

Figure 41: Carbon atomic percent (%) as a function of distance from the center of the valley (µm)

3.4 Location of poisons with respect to active catalyst sites

Using SEM with a high magnification and at the maximum accelerating voltage of the equipment (30 kV), it is possible to take pictures of the platinum crystallites. Figure 42 is a picture of the wash-coat magnified 8500 times. Using this image and EDS, it is possible to generate elemental maps that are enhanced with colors that show the distribution of that element in the sample. Figure 43 shows the elemental maps for iron and aluminum, indicating that the irregular layers seen in the sample correspond to the porosity of the wash-coat. And Figure 44 shows the elemental maps for platinum, phosphorus, and sulfur. These indicate that the brighter objects observed in the sample correspond to platinum crystallites. Furthermore, the distribution of phosphorus is in line with that of platinum, but this is not the case for sulfur. This implies that the alumina is indeed acting as a sulfur scavenger, but phosphorus is able to chemically react and poison the platinum crystallites.

Please note that the alignment of platinum and phosphorus is not due to the proximity in the excitation energy between the two. As referenced earlier in Figure 22, the characteristic X-ray in the M orbital of platinum is aligned with that in the K orbital of phosphorus (2.013 versus 2.048 keV), which tends to generate confusion when using EDS, as it is difficult to differentiate between the two elements. However, a high accelerating voltage of 30 kV is used so that the higher energy electrons in platinum can be excited. The elemental map for platinum is based off the L orbital, which has a much higher characteristic X-ray of 9.441 keV and therefore requires a much higher excitation energy than that of phosphorus, which makes it possible for the equipment to differentiate between the two.

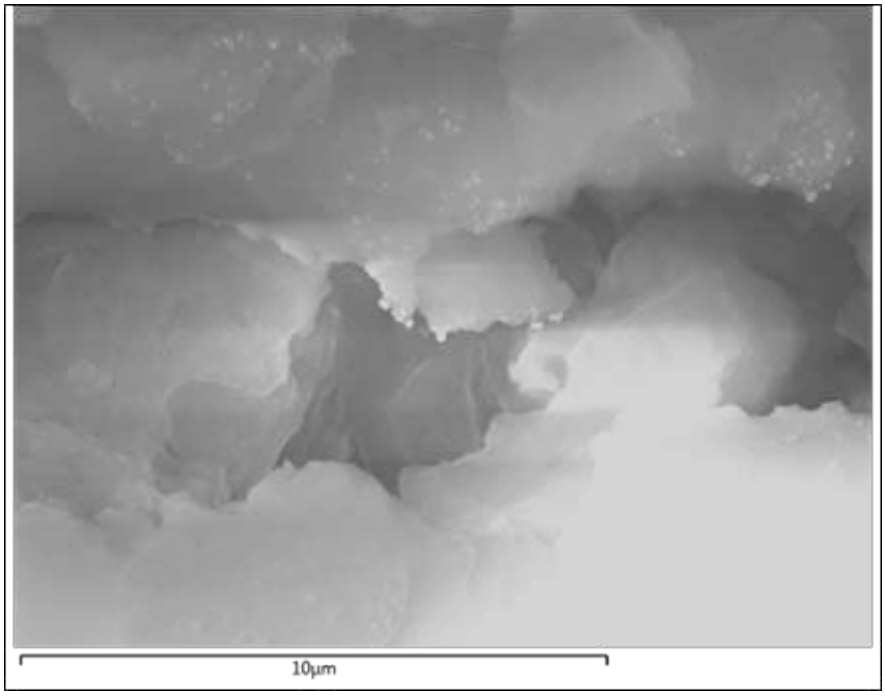

Figure 42: Electron image of the wash-coat with a magnification of 8500x and an accelerating voltage of 30 kV

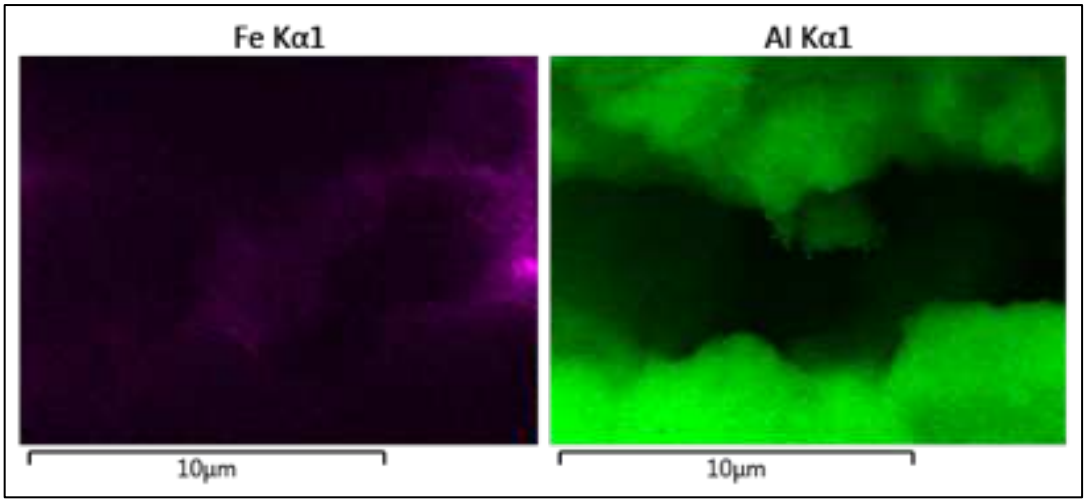

Figure 43: Elemental maps for Iron and aluminum of a catalyst wash-coat sample at 30 kV and a magnification of 8500x

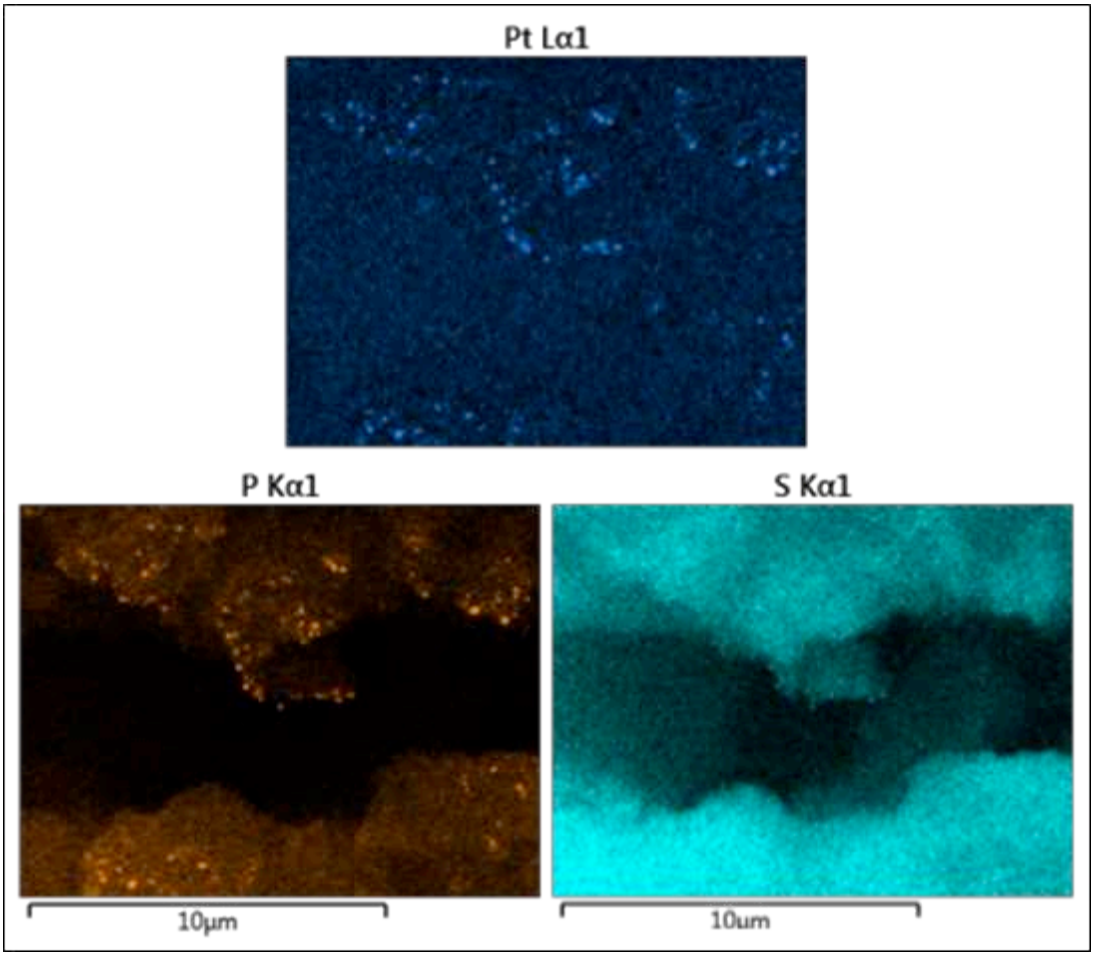

Figure 44: Elemental maps for platinum, phosphorus, and sulfur of a catalyst wash-coat sample at 30 kV, with a magnification of 8500x

3.5 Pre-restoration activity scan

Table 7 shows the maximum acceptable poison levels versus the levels found in Unit A. The activity scan results line up with the depth analysis by showing there is greater amounts of sulfur than phosphorus and zinc overall. For almost every single superficial XPS scan performed on these samples, the levels of phosphorus show higher values than those of sulfur. The powder from the wash-coat containing high sulfur levels indicates that this element must be going deeper into the wash-coat than the rest of the poisons, interfering with the XPS. Furthermore, sodium shows higher levels than in

most superficial scans, and the only source of sodium in this case is from the caustic soda that is used in the washing process. Moreover, Unit A was previously washed with reused rinse water with a high pH level, indicating the possible contamination of the catalyst during previous work performed on the units. Ever since the utilization of reused rinse water was identified as a possible poisoning source, fresh deionized water has been used for rinsing off chemicals. Regardless of the higher sodium levels, the slipstream performance test will determine whether the higher levels of sodium have a negative impact on the reduction efficiency and the light-off temperature.

In addition, there is severe catalytic performance loss due to the loss of surface area. According to the personnel at DCL, the surface area of the wash-coat can be lowered up to approximately 75 $\frac{m^2}{\mathrm{g}}$ before the catalyst unit is no longer in compliance with the EPA reduction efficiency regulations, but the BET surface area analysis for Unit A shows a surface area of approximately $32\ \frac{m^2}{\mathrm{g}}$.

Table 7: Elemental analysis of the wash-coat by the DCL activity scan

Element	DCL recommended atomic %	Unit A atomic %	Error (%)
Phosphorus	1.0	2.551	0.030
Zinc	1.0	0.232	0.002
Sulfur	2.0	8.972	0.090
Phosphorus + Zinc + Sulfur (collectively)	2.0	11.755	--------
Sodium	0.5	2.389	0.106

The loss of surface area can be due to a combination of factors, such as high temperature exposure, ash masking, and poisoning. The operating temperature of the

catalyst has never reached the required levels for this to happen (900 to 1000 °C), but the fluctuations in temperature have likely induced attrition. This is observed when the unit is moved around, as loose wash-coat particles fall down from the unit continuously. Raw data from the activity scan performed by DCL can be found in Appendix A.

3.6 Carbon layer

3.6.1 Iterative carbon baking

After baking the samples iteratively for a total of eight hours at 425°C, the baking procedure starts showing diminishing returns (Figure 45). The optimal amount of baking time is therefore determined to be eight hours. Moreover, the total amount of weight removed from the sample by baking corresponds to the carbon layer deposited by the exhaust, and it constitutes approximately 2% of the weight of the sample. After scratching off the wash-coat of the sample with a wire brush, the total amount of mass removed equals roughly 13%, leaving a steel substrate that constitutes approximately 85% of the total. This is shown in Figure 46. The catalyst units are made out of stacks of alternating corrugated and flat sheets of metal, and the ratio expressed in Figure 46 applies to the corrugated sheets only.

The error bars in Figure 45 are minimal due to the readability of the scale and the low standard deviation of the data. For this reason, the amount of error is low once the sample is on the scale, but there are unquantifiable sources of error too. The samples might contain different ratios of organic versus elemental carbon.

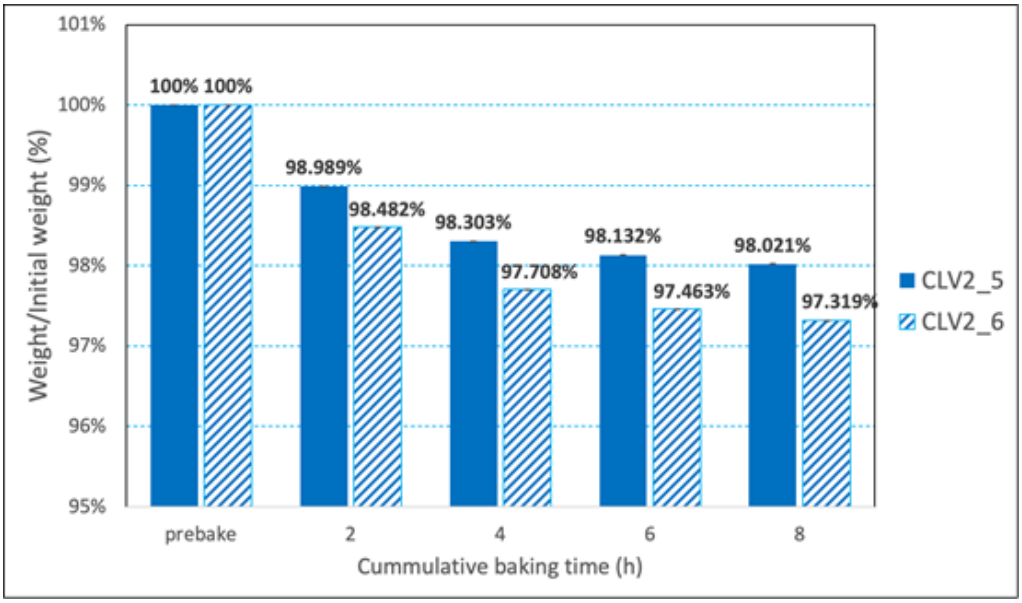

Figure 45: Iterative carbon baking procedure at 425°C

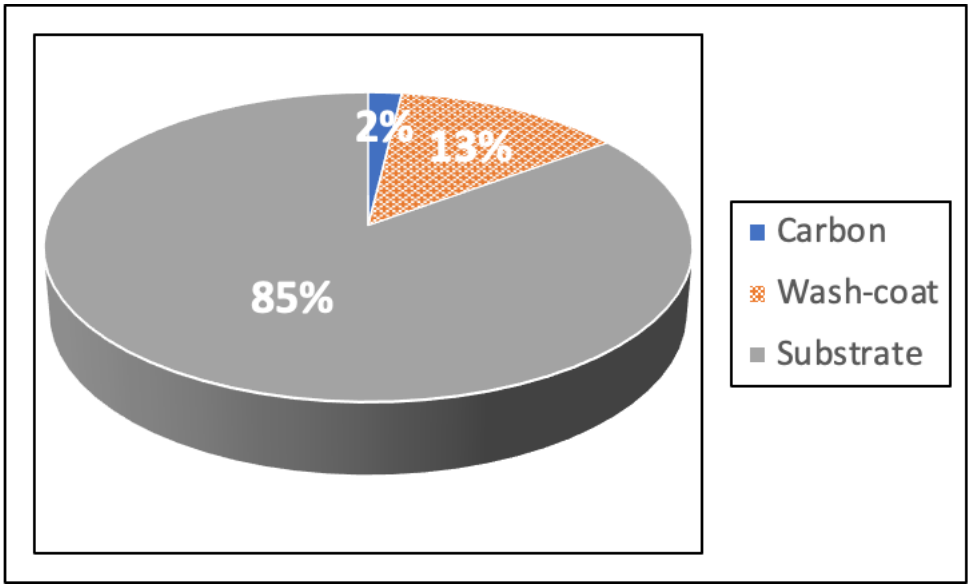

Figure 46: Weight distribution illustration of sample determined with the carbon baking procedure

Furthermore, the samples contain loose wash-coat pieces that are removed by simply moving the sample around, and the amount of mass that is lost in between measurements is not accounted for and is minimal. The samples are handled with care

to reduce this source of error, but this test contains several iterations, which involves moving the sample from the furnace to the scale several times. The impact is believed to be minimal when a single eight hour bake out procedure is performed, and the amount of weight removed is comparable. Those results are discussed in Section 4.1.

3.6.2 OCEC analysis

The procedure is applied to aged Unit A and to a brand-new catalyst with zero hours of use of the same substrate/wash-coat/crystallite combination as Unit A (Figure 47). The total amount of carbon is higher for degraded Unit A when compared to the unused unit, but there are no qualitative differences when it comes to the OCEC ratio. The ratio of organic to elemental carbon is slightly higher for the aged unit, likely due to the lean burn exhaust and elevated temperatures to which the unit has been exposed during the aging process.

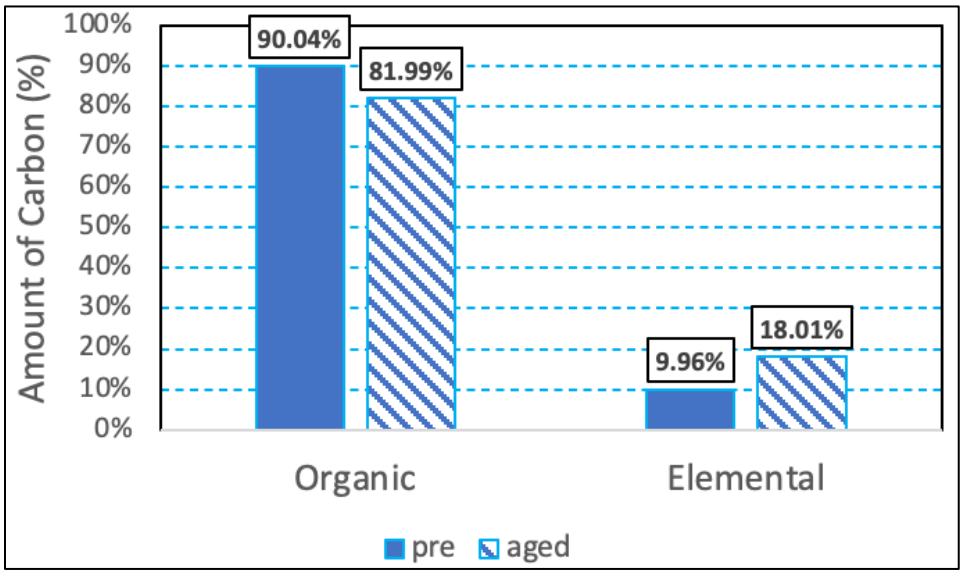

Figure 47: OCEC analysis carbon distribution for a new and an aged catalyst

Additionally, the amount of organic carbon present in Unit A suggests the carbon layer mentioned earlier is composed of atomized oil droplets that stick to the surface of the catalyst unit but do not charr [35]. The error propagation is not evaluated, but the results greatly favor organic carbon over elemental. The main sources of error are the accuracy of the analyzers and the lack of proof of repeatability, as more samples need to be evaluated to have a more representative result of the quality of the carbon deposited onto the catalyst unit.

4. Catalyst regeneration improvement

This section describes the experiments performed to evaluate restoration practices and not poison nor carbon deposition.

4.1 Carbon baking

Various baking procedures were evaluated. The results are presented in Figure 48. The data indicate the amount of carbon removed by purging different gases through the furnace while baking, as a percent value with respect to the wash-coat total weight. A *no purge* test is also evaluated, in which the volume of the furnace is not purged. This test is different to the one mentioned earlier (Figure 45) because the procedure is not done in intervals but rather in eight continuous baking hours at 425°C.

The Nitrogen purge shows similar removal levels to the rest of the baking experiments. This demonstrates that oxidation is not the only means by which carbon leaves the surface at 425°C. The results showing equal amounts of carbon removal in an oxygen free environment are supported by the OCEC analysis results. The removal of volatile

hydrocarbons is highly temperature dependent [36] and the sample shows on average that 82% of the carbon in the wash-coat is organic (Figure 47).

All of the baking procedures show very close results quantitatively and likely within the experimental uncertainty, which makes the results inconclusive. The OCEC ratio might differ for each sample, which changes the temperature sensitivity of the carbon removal. One way to circumvent this problem is to test enough samples to obtain more accurate average results, but that is beyond the scope of the present study. Furthermore, the amount of carbon removed in all of these tests is comparable to that of the iterative procedure that was used to find out the optimal carbon removal baking time, suggesting that the removal of loose wash-coat particles does not significantly affect the weight measurements. No error bars are added after considering the unquantifiable uncertainty in the OCEC ratio for each sample and the low measured variability in the data previously measured.

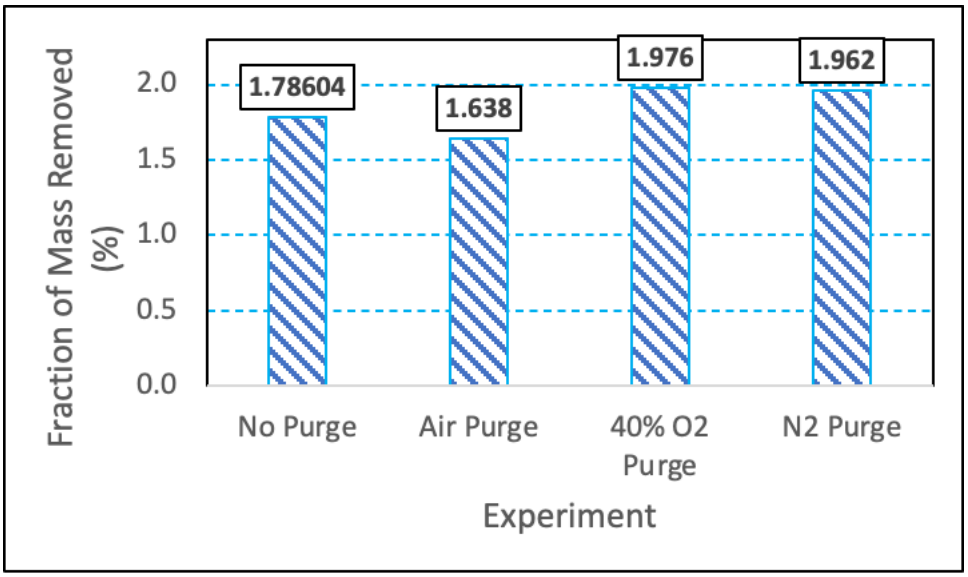

Figure 48: Different baking experiments to record the removal of carbon

4.2 Catalyst washing

4.2.1 Fine washing matrix

The coarse washing matrix results are presented earlier in section 1.5.6. The finer version is summarized in Table 6 and its results show that a bath temperature of 100°F is enough to remove most of the wash-coat of the sample, leaving only the steel substrate. The sample is so damaged that elemental analysis is not performed. Since the difference between 100°F and the average room temperature is minimal, any increase in temperature is declared unsuccessful and this is not explored further. Additionally, Figure 49 shows the levels of poisons (sulfur, phosphorus, and zinc) after baking for eight hours at 425°C and washing. The results make apparent a systematic problem in these tests (Table 6). The distribution of poisons is uneven and there is no way of accurately scanning the exact same location with the XPS once the sample is removed for washing. This makes it nearly impossible to compare the pre- and post-wash poison levels. Samples have different poisoning levels due to the uneven and highly porous wash-coat surface, and a post-wash low atomic percent of poisons in a sample may be due to lower pre-wash poisoning levels. The error bars are found by taking this into consideration by scanning several areas of three similar samples from the front area of the catalyst unit. The COV of each poison is used to find the error bars in these graphs when analyzing poisons independently, and the highest poison COV is used when the addition of poisons is evaluated.

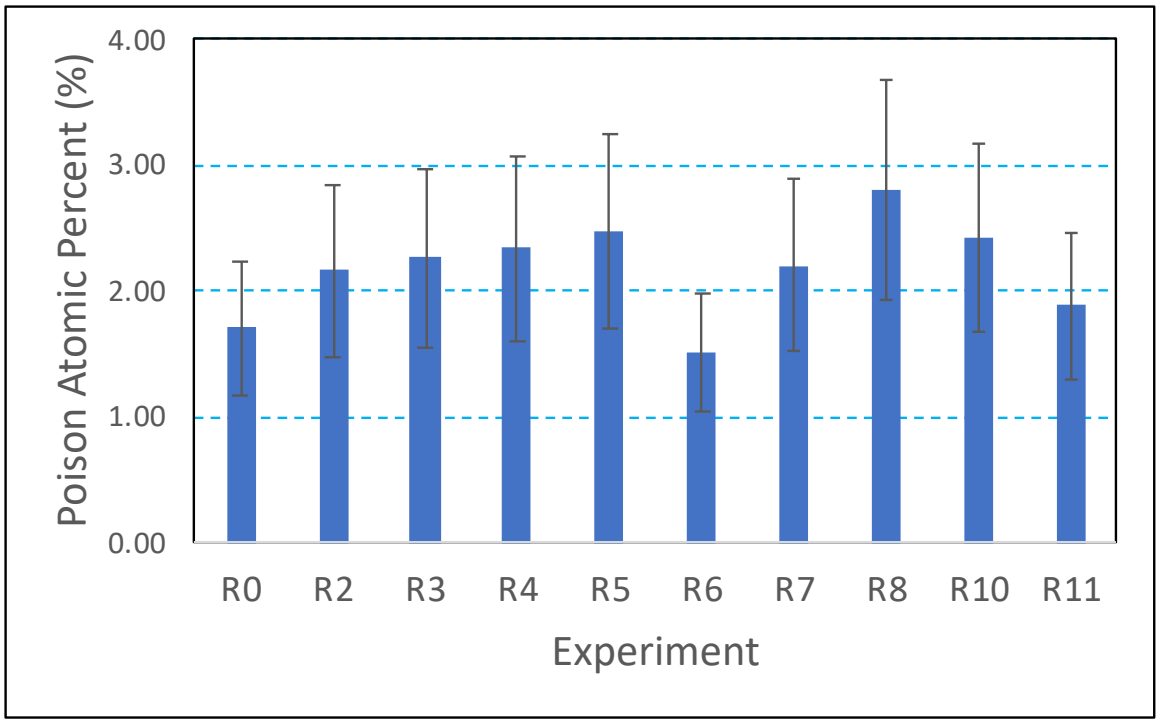

Figure 49: Washing experiment results for the fine washing matrix

The coarse washing matrix results (Figure 19) previously showed a possible indication of agitation being a successful addition to the standard process, but the variation in the data prevented definitive conclusions. Furthermore, the finer matrix results are all statistically equivalent due to the uneven distribution of poisons (Figure 49), calling into question the conclusion that adding agitation improves the washing process. The results do not support the modification of the industry standard washing procedure.

4.2.2 Catalyst washing box

Figure 50 shows the post-wash levels of poisons (P, S, and Zn) of the catalyst washing box versus the fine washing matrix results. The levels of poisons are comparable for both experiments, indicating there is no benefit in renewing the chemical that interacts with the wash-coat. This is the final indicator of agitation not being a beneficial addition

to the chemical washing process and this is not further studied. The results from this test combined with the fine washing matrix outcome show that there is not enough evidence to move away from the industry standard washing procedure.

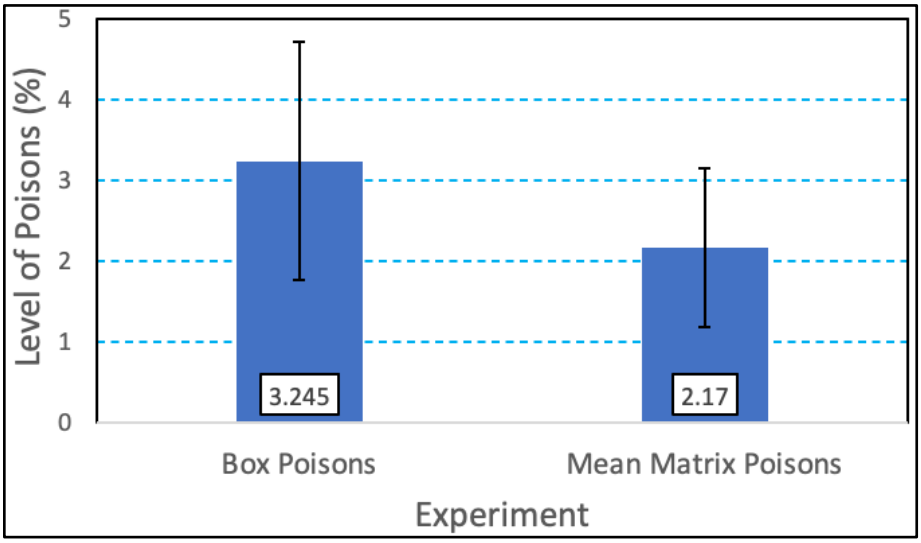

Figure 50: Catalyst washing box versus fine washing matrix poison levels

4.3 Order of washing and baking

The most successful washing procedure evaluated is the industry standard, and the most successful carbon baking procedure is at 425°C for eight hours; the combination of the two procedures is tested. Sample BW1 is baked first and then washed, and sample BW2 is washed first and then baked. The amount of poison removal is comparable and so this is not a determining factor. However, considering the integrity of the wash-coat of utmost importance, BW1 (baking before washing) is shown to be more efficient. The integrity of the wash-coat seems intact in both inlet samples (Figure 51), but it seems to be compromised in Figure 52 and Figure 54 for the middle and outlet samples that have been baked after washing. Though the sample BW1 is also damaged in Figure 52, one can see the damage is greater for sample BW2. Using EDS analysis,

one can see in Figure 53 that the iron and aluminum levels are complementary, demonstrating that the areas of the sample with lower aluminum levels are indeed locations where the aluminum is removed and the steel substrate is exposed. The damage to the wash-coat is attributed to the phase change of the absorbed liquid by the porous surface when baking after washing.

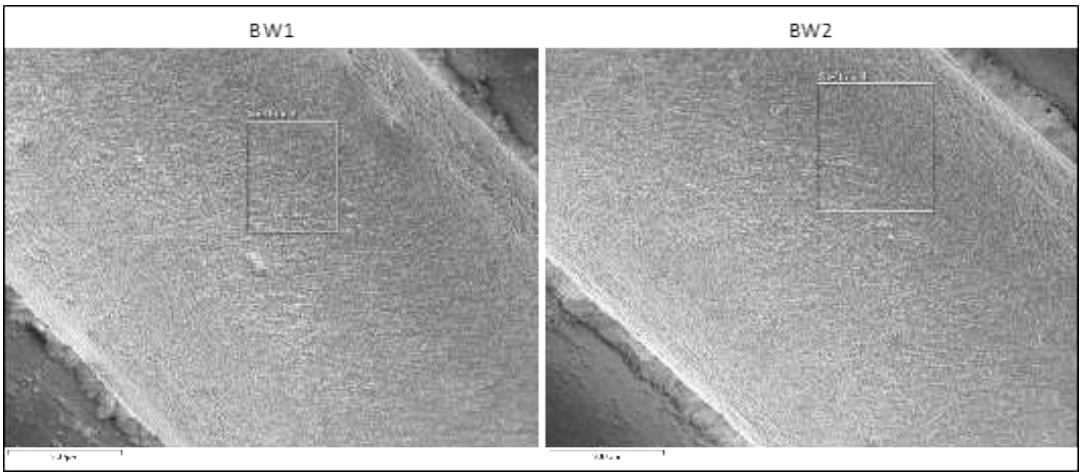

Figure 51: Electron image of inlet samples baked first and then washed (BW1), and washed first and then baked (BW2)

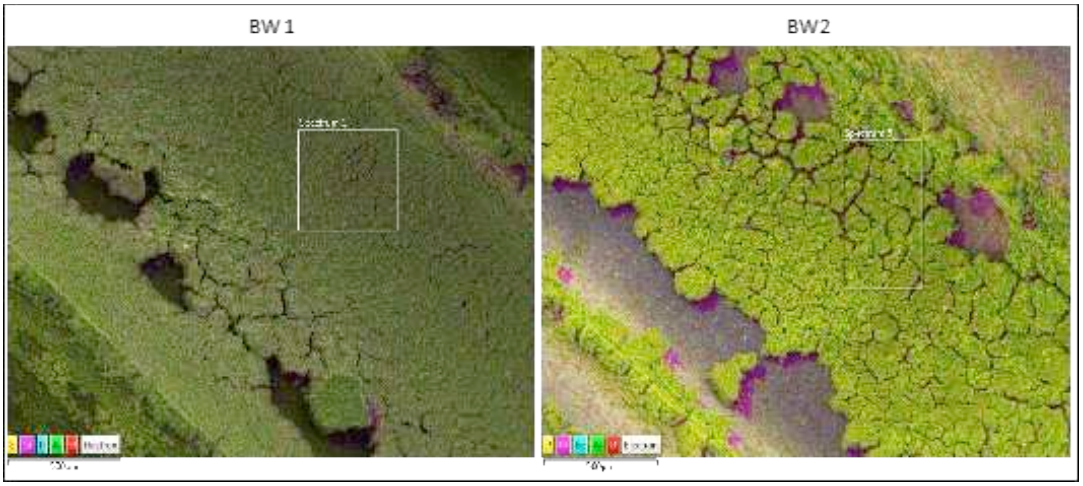

Figure 52: EDS layered image of middle samples baked first and then washed (BW1) and washed first and then baked (BW2)

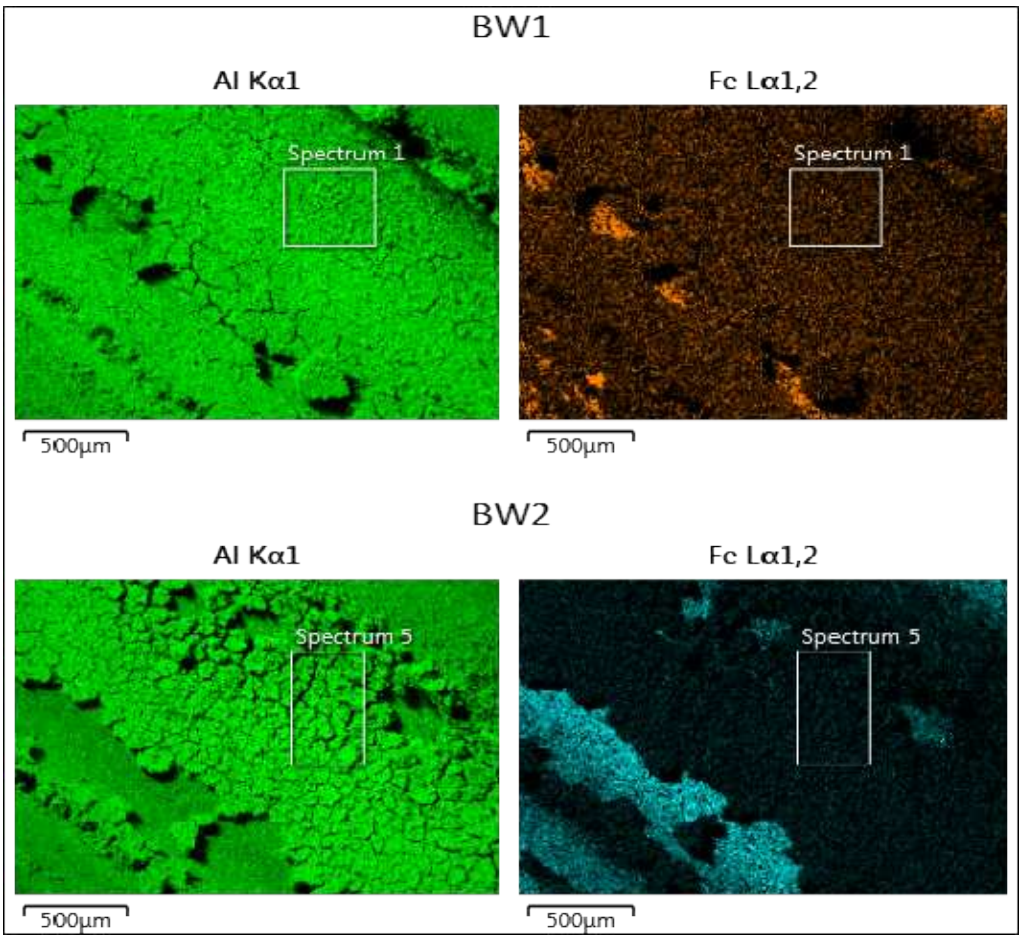

Figure 53: Elemental Maps of middle samples baked first and then washed (BW1) and washed first and then baked (BW2), exposing damage to the wash-coat.

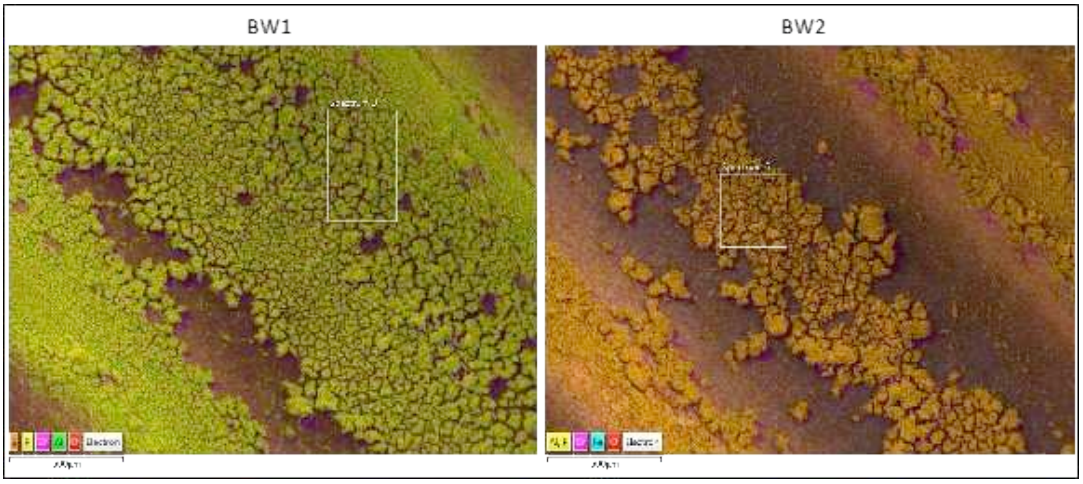

Figure 54: EDS layered image of outlet samples baked first and then washed (BW1) and washed first and then baked (BW2).

The damage is confirmed in Table 8 with higher iron levels in the samples that are baked after washing. Furthermore, the poison removal levels are similar and the choice of washing after baking as the most successful procedure is based solely on the integrity of the wash-coat. Another positive point comes in relation to reusing the chemical baths. It is not illustrated in these experiments, but it appears to be the case with a visual inspection that there is less carbon contamination in the baths when the carbon is removed first by baking. An elemental analysis of the baths must be done in order to evaluate this, which is beyond the scope of this study.

Table 8: Baking and washing order experiments, SEM results

Element	BW1 - inlet (atomic percent)	BW2 - inlet (atomic percent)	BW1 - center (atomic percent)	BW2 - center (atomic percent)	BW1 - outlet (atomic percent)	BW2 - outlet (atomic percent)
P	1.1	1.1	1.4	0.6	0.8	0.6
Fe	0.4	0.4	0.4	1.1	2.0	2.5
Zn	0.1	0.1	0.1	0.1	0.1	0.1
S	0.2	0.2	0.5	0.3	0.5	0.4

4.4 Activity testing at AGES and hydrogen reduction

Figure 55 shows the performance results of each restoration step declared successful in the lab by looking at small scale samples, then applied to Unit A and tested at AGES. The red horizontal line along the 50% reduction efficiency mark is there to help identify the light-off temperatures. These curves are built by averaging the regular and flipped catalyst orientations, and the error bars are made considering the error propagation of the analyzer ($\pm 20\ ppm$ or 5% for CO). The baseline shows a damaged catalyst with almost no activity at 500°F and a light-off temperature of approximately 585°F at that unmeasured space velocity. After baking and removing carbon, Unit A shows an

increase in catalytic activity by shifting the light-off temperature to ≈540°F. The hydrogen reduction proves to be successful by further shifting the light-off temperature to ≈510°F. And the chemical washing further restores the unit by shifting the curve upwards and setting the light-off temperature to lower temperatures than the equipment is able to test.

The hydrogen reduction shows high levels of improvement and is added to the restoration process. The increase in catalytic activity observed by the reduction is not attributed to the slightly higher baking temperature, only 25°F higher than that of the carbon baking removal, since the carbon baking procedure lasts eight hours and the reduction is executed for two, and the restoration effects of the two are comparable and additive.

In addition, Unit A was left to dry without a fan for 48 hours and then shipped to AGES to obtain the post-wash results. Personnel at sight commented that the unit was still wet upon arrival, and for this reason the unit was baked at 230°C for one hour for drying purposes. This led to the conclusion of adding baking for drying to the process but at a lower temperature of 120°C after drying the catalyst unit with a fan for eight hours or longer. The lower amounts of liquid in the wash-coat after drying for hours with continuous airflow will likely induce little to no damage to the wash-coat, as it is seen in Figure 52 when baking is performed after washing.

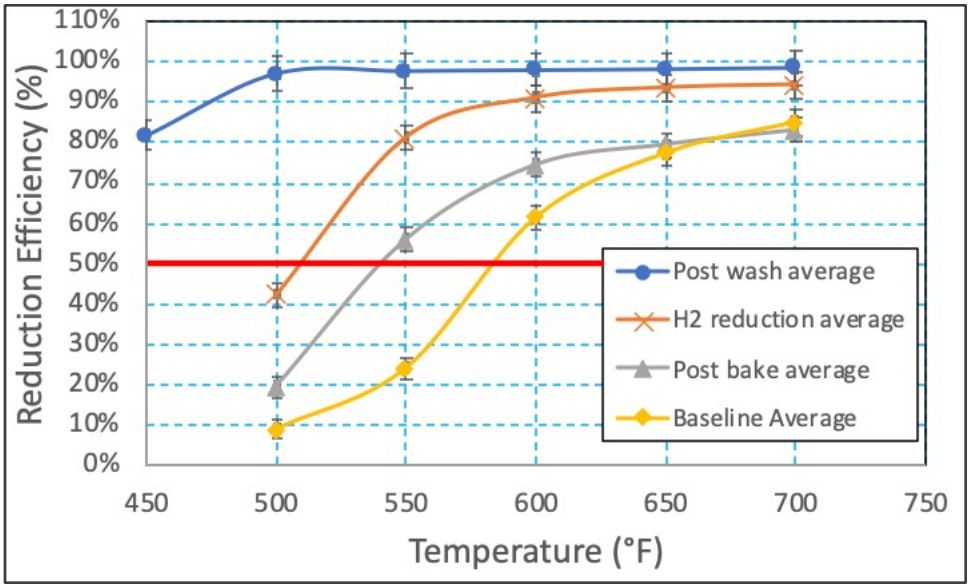

Figure 55: Performance testing at AGES showing all restoration steps, including the hydrogen reduction

4.5 Final restoration process

The carbon baking tests and the OCEC results show that the carbon removal is dependent on the temperature and not on the environment. Taking this and the eight hours required at high temperatures for the maximum removal of the carbon layer into consideration, the final restoration process to be tested in catalyst Unit B is summarized in Figure 56 and is the following:

- Unit is baked for six hours in atmospheric air at 425°C.
- Oxygen is removed by purging an inert gas into the chamber.
- The hydrogen reduction takes place in an oxygen free environment at 450°C for two hours, completing the eight hours at high temperatures needed for the removal of the carbon layer.
- The catalyst unit is washed with the industry standard chemical wash.

- Unit is dried with a fan for eight hours or longer (as long as possible).
- Unit is further dried before testing for one hour at 120°C.

The restoration process lasts 23 hours, which translates to three business days. The unit is baked on day one, washed on day two, then dried overnight, and baked for one hour for further drying on day three. The baking step adds one business day to the duration of the industry standard washing procedure.

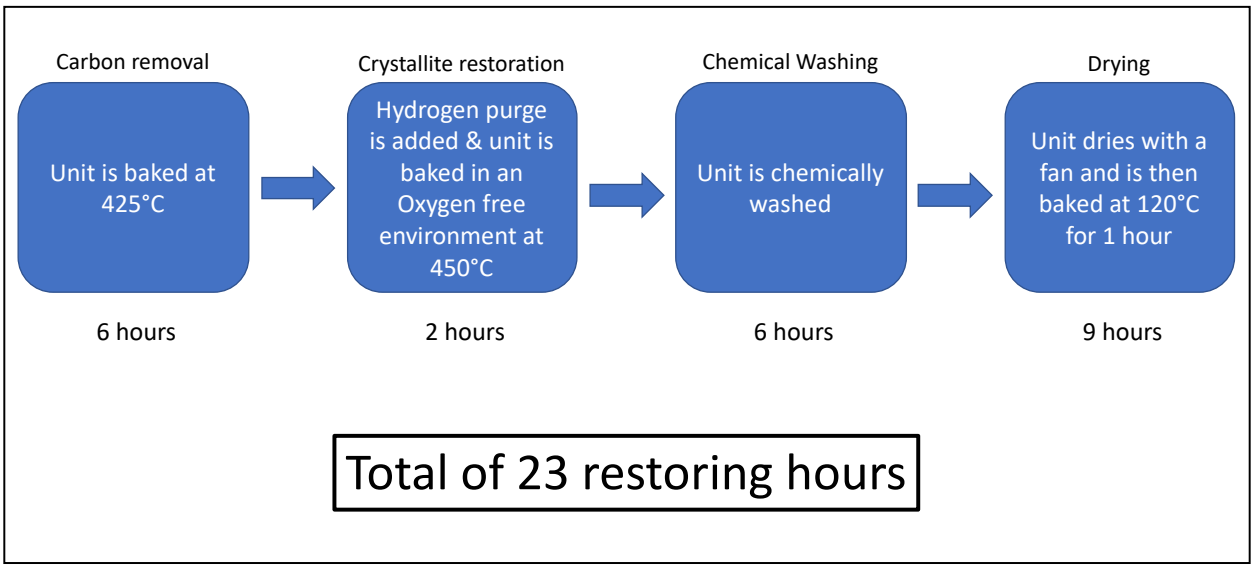

Figure 56: Summary of final restoration process on a flowchart

4.6 Post-restoration activity scan

The surface area of Unit A after undergoing the final restoration process went from 32 to 197 $\frac{m^2}{g}$. The major increase in wash-coat surface area is attributed to the removal of the carbon layer and poisons. The post-restoration PIXE elemental analysis show that sulfur and phosphorus are reduced to 0.692 and 0.689%, respectively. Zinc is reduced to 0.0484% of the wash-coat. The post-restoration poison levels make up 1.43% of the

wash-coat, which is under the 2% poison limit recommended by DCL for a healthy catalyst. Table 9 shows sodium is not detected after the final restoration is applied to Unit A, likely because the fresh-rinse water was sufficient to revert the sodium poisoning that occurred during the first wash of the unit, in which re-cycled instead of fresh rinse water was used.

Table 9: Post-restoration activity scan performed by DCL

Element	DCL recommended level (%)	Pre-restoration Unit A level (%)	Post-restoration Unit A level (%)
Phosphorus	1.0	2.551	0.689
Zinc	1.0	0.232	0.0484
Sulfur	2.0	8.972	0.692
Phosphorus + zinc + sulfur (collectively)	2.0	11.8	1.43
Sodium	0.5	2.389	Not detected

4.7 Slipstream performance tests

The final restoration process is applied to Unit B and the reduction efficiency of various gases is tested before and after restoring the unit. Due to complications with the five-gas analyzer during the pre-restoration test, only the FTIR values are used. The FTIR and the five-gas analyzer values relate closely before the malfunction.

The catalyst unit at elevated temperatures is able to reduce emissions to levels that are much closer to the background noise of the gas analyzers. For such reasons, the maximum reduction efficiency contains the highest amount of error and the more representative results are closest to the light-off temperature. Figure 57 shows the reduction efficiency of CO along the temperature sweep. Recall that Unit B was aged

until it was non-compliant, then chemically washed, and then it was re-aged until it was non-compliant with the NESHAP limits. Test 10 corresponds to the last aging period. The unit was then restored for a second time with the process described in section 4.5., and this corresponds to the second restoration.

Unit B was left untouched after test 10 by Hackleman [16]. The pre-restoration and test 10 performances are therefore supposed to be equal, but the uncertainty in measuring the lower post-catalyst emissions at higher temperatures is exposed when comparing the maximum reduction efficiencies. Figure 57 shows new catalyst levels are best for reducing CO, followed by the first restoration, and then the second restoration. This shows something that is known in the industry: a unit is restored best the first time and there is a finite number of times a catalyst unit can be restored. Recall that the first restoration consisted in the chemical washing only, and the second included the added baking steps. Similar tendencies are observed for the reduction efficiency of formaldehyde (Figure 58), where the unit shows improvement after the final restoration process, but the higher initial restoration levels are not achieved.

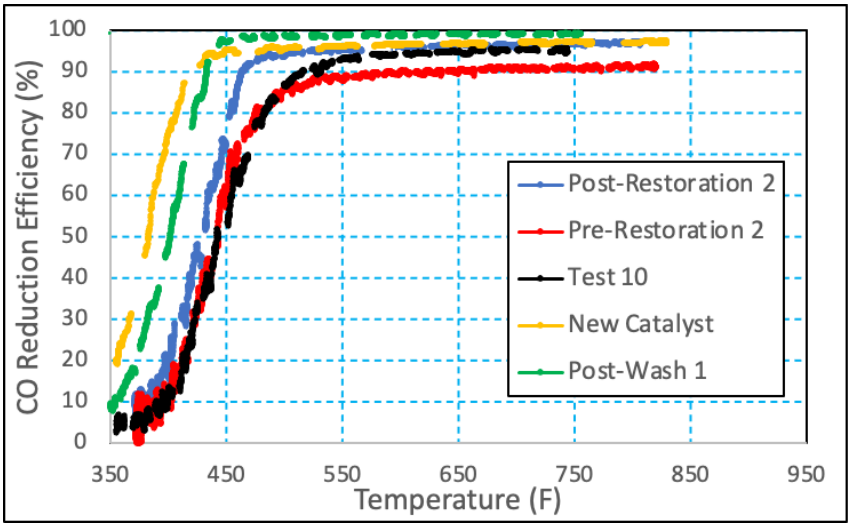

Figure 57: Reduction efficiency of CO as a function of temperature

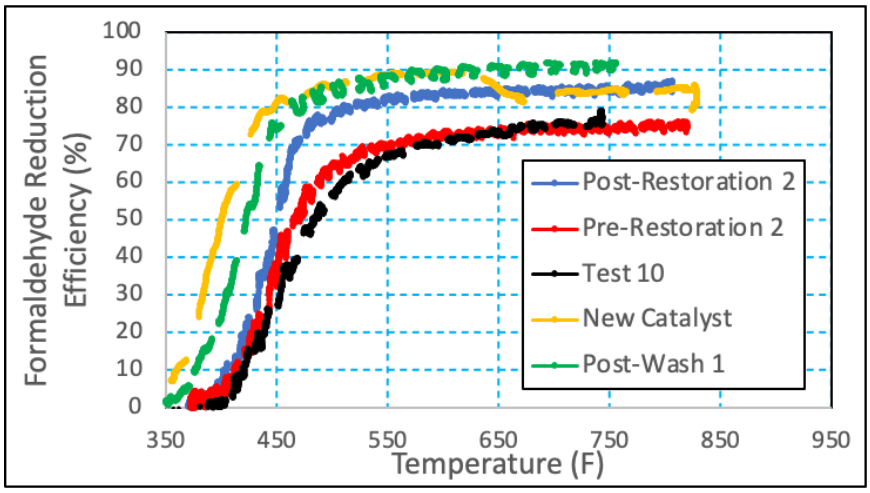

Figure 58: Reduction efficiency of formaldehyde as a function of temperature

In addition, VOCs in Figure 59 show major differences, but the reduction efficiency of VOCs is governed by the lack of catalytic activity for alkanes, propane in this case. The more propane is present, the lower the reduction efficiency. This is the main difference between test 10 and the pre-restoration test; 3.7 ppm for the pre-restoration versus 11.3 ppm of propane during test 10.

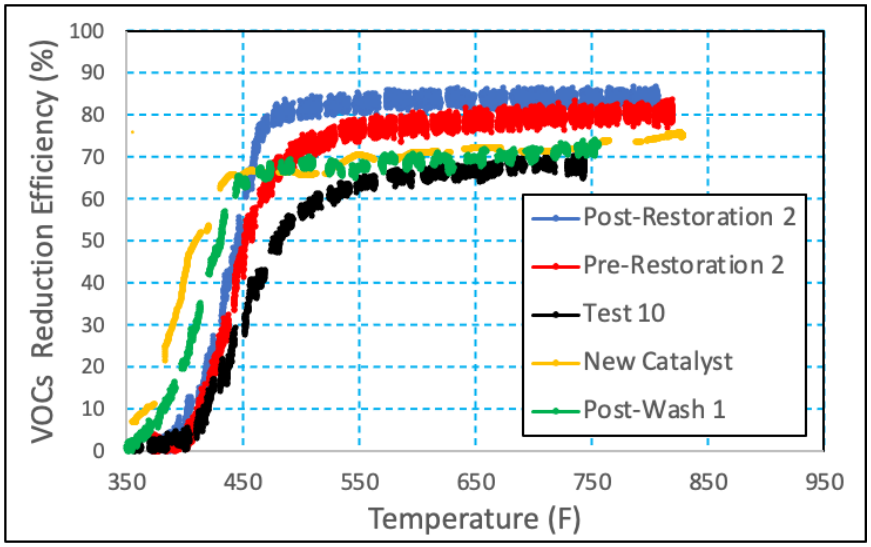

Figure 59: Reduction efficiency of VOCs as a function of temperature.

The end goal of the catalyst unit is to meet compliance with the NESHAP limits. The CO limit is a reduction efficiency of 58%, which depends heavily on the operating temperature. At a low operating temperature of 450°F, the catalyst is at the border of non-compliance with the CO reduction efficiency limit before being restored, and the unit does not meet compliance with the formaldehyde limit. Figure 60 and Figure 61 are modified from Hackleman to show the degradation [16]. The added arrows show the post-restoration results, as they are difficult to see vertically since three tests (test 10, and the final pre- and post-restoration tests) were taken at 505 million catalyst exchanges. The results highlight the amount of variation in the data. Test 10 and the pre-restoration test should be close to identical, as Unit B was not further degraded in between the two.

The improvement of the final restoration process is more apparent at 600°F (Figure 61), where the reduction efficiency reaches brand new levels for CO and approaches new catalyst levels for the formaldehyde 12 ppmd limit. These results also highlight the dependence of the catalyst unit on the operating temperature. At 600°F the unit does not need to be restored at 300 million catalyst exchanges. The catalyst should be well insulated and as close to the engine as possible, as this extends the life of the catalyst and alleviates the need for a restoration.

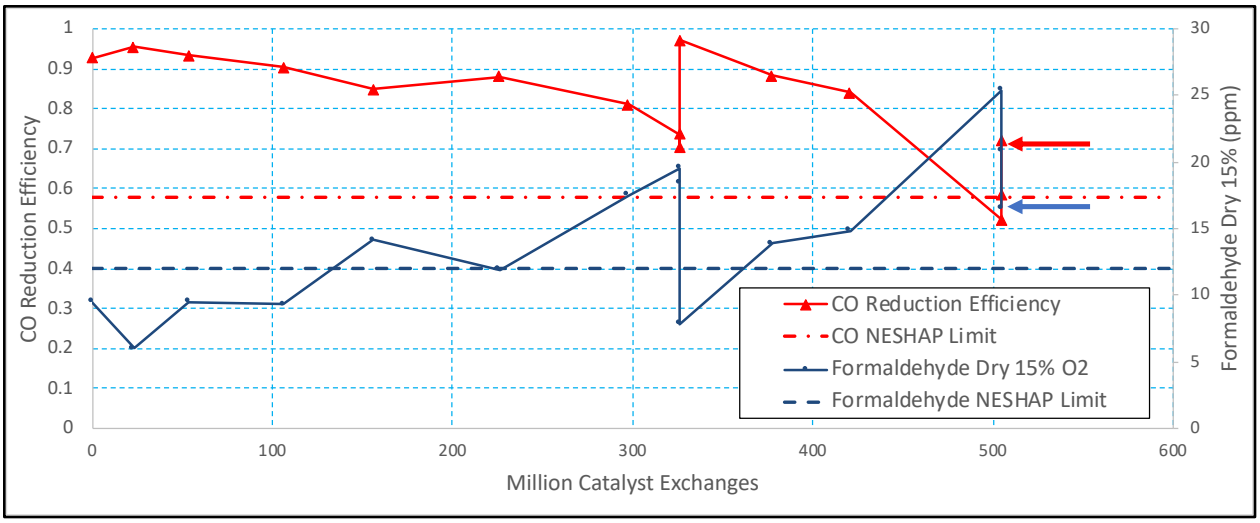

Figure 60: NESHAP limits with respect to million catalyst exchanges at 450°F

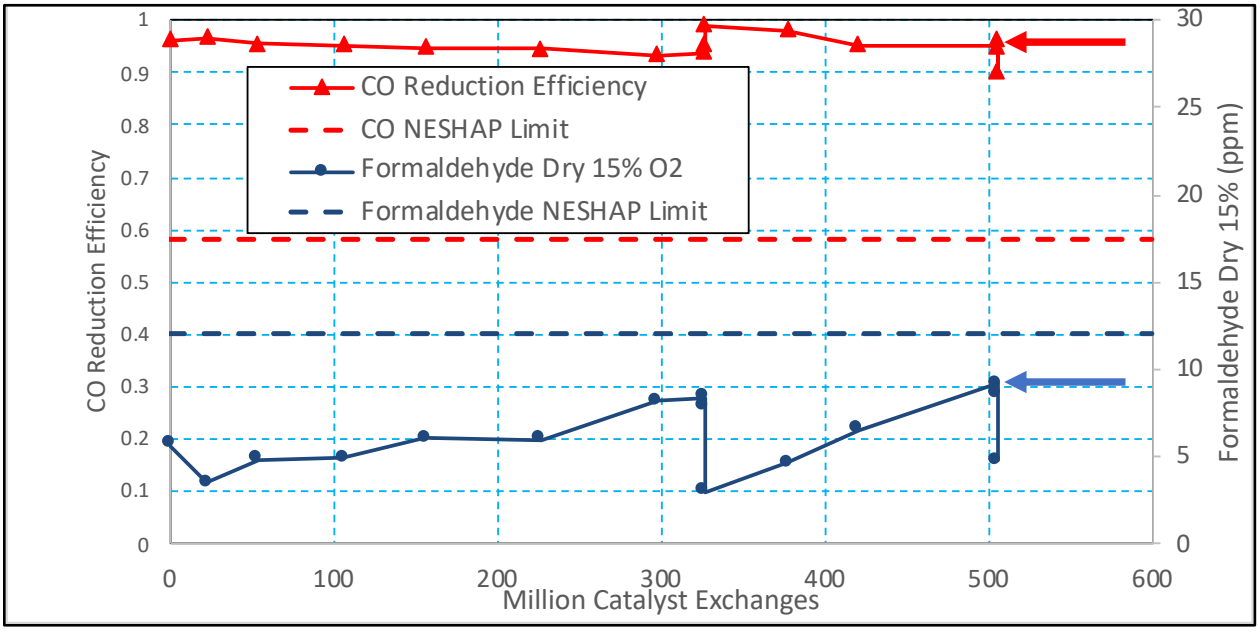

Figure 61: NESHAP limits with respect to million catalyst exchanges at 600°F

5. Conclusions

Two identical oxidation catalyst units, Units A and B, were aged in the field in a Cooper Bessemer GMVH-12 and were tested periodically in the lab for elemental analysis and performance in a Cummins QSK19G engine. The periodic tests allow the evaluation of

the degradation rate, and once the catalyst is non-compliant with the NESHAP CO limit, the units were chemically washed. The units were then re-aged until non-compliance with emissions was met, and lastly they were restored with a more intricate restoration process that involves the combination of baking and washing.

The most abundant poison is sulfur, followed by phosphorus and zinc. Sulfur penetrates much deeper into the wash-coat than the other poisons. This is illustrated by the depth analysis and confirmed by the fact that individual superficial XPS scans show comparable levels of phosphorus and sulfur, but when the wash-coat is turned into a powder to circumvent the superficiality of these scans, then the levels of sulfur are vastly superior. According to the activity scan performed by DCL to the degraded units, sulfur levels correspond to 8.97% of the wash-coat, while phosphorus is estimated to equate to 2.55%, and zinc only makes up 0.23% of the wash-coat. Levels of sulfur, phosphorus, and zinc are reduced by applying the final restoration process to 0.692%, 0.689%, and 0.048%, respectively. Though sulfur is more prevalent, phosphorus is estimated to be actively and objectively poisoning crystallites. This is a greater problem in the sense that most of the sulfur targets the wash-coat but not the active platinum pieces, so the wash-coat acts as a scavenger.

Carbon is considered a non-poison that fouls the catalyst, and it is estimated to settle as a layer on top of the wash-coat. This layer greatly reduces the surface area of the wash-coat, which minimizes catalytic activity. This is believed to be the cause of the carbon bake-out procedure being successful. Moreover, either the aging process or the carbon bake-out procedure oxidize platinum, as the platinum reduction greatly increases the efficiency of the unit before washing.

The slipstream performance tests show that there is less benefit in restoring the unit a second time, and this is known by the industry. The second restoration process still moves the catalyst to higher reduction efficiency levels, but the light-off temperature is not reduced greatly the second time the unit is restored. The second restoration is highly successful for both formaldehyde and CO at 600°F.

The slipstream performance tests do not provide enough evidence to move away from the industry standard, but the stepped testing process at AGES does suggest a shift from the chemical washing to a combination of baking and washing. The suggested restoration process for oxidation catalysts is to bake off the carbon layer first for six hours at 425°C, then restore the platinum crystallites with a 5% H_2 purge in an inert gas base at 450°C for two hours, and to finish the process with the industry standard chemical washing. After air drying, an additional baking step at 120°C for one hour is suggested before returning the catalyst to the customer.

Furthermore, though this text mentions an industry standard chemical washing process, there are vast differences among catalyst washing companies. The catalyst washing box experiment suggests there is no need to recirculate the washing fluid through the unit, which greatly reduces infrastructural costs. In addition, it is not suggested to expose a catalyst unit to elevated temperatures immediately after washing, as the accelerated phase change of the absorbed washing fluid after washing is attributed to the destruction of the wash-coat.

Lastly, in order to extend the life of an oxidation catalyst, the following process ought to be followed. Use the catalyst until it approaches either the CO 58% reduction efficiency or the 12 ppmd formaldehyde non-compliance NESHAP limit. Flip the catalyst at this

point, which ought to happen close to the 300 million catalyst exchange mark for the temperature range tested, in order to extend the life of the catalyst before restoring it. After the flipped catalyst approaches the NESHAP limits at another 250 to 300 million catalyst exchanges, proceed to fully restore the catalyst. Repeat this a second time when the catalyst reaches the non-compliance limits. The catalyst should be well insulated and as close to the engine as possible, as this extends the life of the catalyst and diminishes the need for a restoration. Flipping and restoring the catalyst units extends their lifespan for a fraction of the cost of replacing the unit, but it is likely that there are diminishing returns in restoring the catalyst a third time.

Specific conclusions and important quantitative results arrived at in this work are summarized below:

- Sulfur is the most abundant poison and constitutes 8.97% of the wash-coat, phosphorus follows and is estimated to equate to 2.55%, and zinc only takes 0.23% of the wash-coat.
- Levels of sulfur, phosphorus, and zinc are reduced by applying the final restoration process to 0.692%, 0.689%, and 0.048%, respectively.
- Sulfur penetrates the deepest into the wash-coat, followed by phosphorus and zinc.
- The surface area of the wash-coat goes from $32\ \frac{m^2}{\mathrm{g}}$ when fully degraded to $197\ \frac{m^2}{\mathrm{g}}$ after the final restoration process, increasing catalytic activity.
- It takes approximately 300 million catalyst exchanges to degrade an oxidation to the point of non-compliance catalyst with a LBNG two-stroke engine. Flipping

and restoring the unit can double the lifespan for a fraction of the cost of replacing the unit.

- A two-hour baking process at 450°C in an inert gas environment with 5% H_2 is enough to reverse the oxidation of the platinum crystallites that occurs during the aging process.

5.1 Suggested future work

The work presented in this paper is partly limited to oxidation catalysts, but there is great potential for TWC and the new restoration process, especially considering the baking step, as it is something that can be implemented easily in these units.

In addition, the ideal hydrogen reduction temperature has not been established. A reducing temperature of 450°C shows improvement, but it would be ideal to test 425°F and lower temperatures, as it might be less damaging to the catalyst. Moreover, Davies also indicates partly oxidized platinum is less susceptible to sintering, so it would be beneficial to do a follow-up project to test the degradation rate of the catalysts restored with hydrogen. Furthermore, flipping the catalyst indicates an increase in the reduction efficiency. The degradation rate of a flipped unit needs to be evaluated.

A Sulfur Scavenger Unit (SSU) should be evaluated as an addition to the exhaust after-treatment. The SSU consists of a smaller unit that contains all the same elements as the current oxidation catalysts but excludes the crystallites. The goal of this sacrificial unit is to act as a sulfur and carbon filter that can be restored without having any downtime. This reduces costs as the unit with the precious metals would have a longer lifespan, being degraded almost exclusively thermally.

References

[1] A. T. Kirkpatrick and C. R. Ferguson, Internal Combustion Engines, Fort Collins: Wiley, 2016.

[2] D. B. Olsen, G. Arney and A. Reining, "Oxidation Catalyst Performance Considerations: Catalyst Temperature, Space Velocity, and Fouling," in *Gas Machinery Conference*, Nashville, 2011.

[3] M. M. El-Wakil, Powerplant Technology, Singapore: McGraw Hill, 1985.

[4] "United States Environmental Protection Agency," 19 January 2017. [Online]. Available: https://www.epa.gov/stationary-engines/compliance-requirements-stationary-engines. [Accessed 3 July 2019].

[5] K. Badrinarayanan, Performance Evaluation of multiple Oidation Catalysts on a Lean Burn Narural Gas Engine, Fort Collins: Colorado State University, 2012.

[6] J. B. Heywood and E. Sher, Two-Stroke Cycle Engines, New York: Taylor and Francis, 1999.

[7] J. B. Heywood, Internal Cobustion Engine Fundamentals, New York: McGraw-Hill, 1998.

[8] J. Chen, R. M. Heck and R. J. Farrauto, "Deactivation Regeneration and Poison-resistant Catalysts: Commercial Experience in Stationary Pollution Abatement," *Catalysts Today,* no. 11, pp. 517-545, 1992.

[9] C. H. Bartholomew, "Mechanisms of catalyst deactivation," *Applied Catalysts A: General 212,* pp. 17-60, 2001.

[10] K. Davies, Oxidation Catalyst Degradation in the Exhaust Stream of a Large Bore 2-Stroke Natural Gas Engine, Fort Collins: Colorado State University, 2015.

[11] A. Kalantar Neyestanaki, F. Klingstedt, T. Salmi and D. Yu. Murzin, "Deactivation of postcombustion catalysts, a review," *Fuel 83,* vol. 83, pp. 395-408, 2004.

[12] J. Andersson, M. Antonsson, L. Eurenius, E. Olsson and M. Skoglundh, "Deactivation of diesel oxidation catalysts: Vehicle and synthetic aging correlations," vol. 72, pp. 71-81, 2006.

[13] F. Cabello Galisteo, R. Mariscal, M. Lopez Granados, J. L. Garcia Fierro and O. Salas, "Reactivation of a Commercial Diesel Oxidation Catalyst by Acid Washing," vol. 30, no. 10, pp. 3844-3848, 2015.

[14] C. H. Bartholomew, "Mechanisms of Nickel Catalyst poisoning," in *Catalyst Deactivation*, Provo, Brigham Young University, 1987, pp. 81-104.

[15] S. J. Eaton, B. G. Bunting and T. J. Toops, The Roles of Phosphorus and Soot on the Deactivation of Diesel Oxidation Catalysts, SAE, 2009.

[16] B. Hackleman, Two-stroke Lean Burn Natural Gas Engine Oxidation Catalyst Degradation and Regeneration via Washing, Fort Collins: Colorado State University, 2018.

[17] M. E. Baumgardner and D. B. Olsen, "Performance Degradation and Poison Build-Up of an Oxidation Catalyst in Two-Stroke Natural Gas Engine Exhaust," *Journal of Energy Resources Technology,* p. 22208, 2018.

[18] X. P. Auvray and L. Olsson, "Sulfur Dioxide Exposure: A Way To Improve the Oxidation Catalyst Performance," *Industrial and Engineering Chemistry Research,* no. 52, pp. 14556-14566, 2013.

[19] Y. Leng, "Transmission Electron Microscopy," in *Materials Characterization : Introduction to Microscopic and Spectroscopic Methods*, John Wiley & Sons, Incorporated, 2008, pp. 79-118.

[20] B. L. Dutrow, "X-ray Powder Diffraction (XRD)," 5 April 2019. [Online]. Available: https://serc.carleton.edu/research_education/geochemsheets/techniques/XRD.html. [Accessed 24 July 2019].

[21] E. Marceau, H. Lauron-Pernot and M. Che, "Influence of the Metallic Precursor and of the Catalytic Reaction on the Activity and Evolution of Pt(Cl)/δ-Al2O3 Catalysts in the Total Oxidation of Methane," *Journal of Catalysis,* no. 197, pp. 394-405, 2001.

[22] J. E. Benson and M. Boudart, "Hydrogen-Oxygen Titration Method for the Measurement of Supported Platinum Surface Areas," *Journal of Catalysis,* vol. Journal of Catalysis, no. 4, pp. 704-710, 1965.

[23] L. Liotta, A. Longo, G. Pantaleo, A. Martorana, S. Cimino, G. Russo and G. Deganello, "Alumina supported Pt(1%)/Ce0.6Zr0.4O2 monolith: Remarkable stabilization of ceria–zirconia solution towards CeAlO3 formation operated by Pt under redox conditions," no. 90, pp. 470-477, 2009.

[24] X. Wu, H.-R. Lee, S. Liu and D. Weng, "Regeneration of Sulfated MnOx−CeO2−Al2O3 Soot Oxidation Catalyst by Reduction with Hydrogen," no. 52, pp. 716-721, 2013.

[25] F. L. Chan and A. Tanksale, "Catalytic Steam Gasification of Cellulose Using Reactive Flash Volatilization," no. 6, p. 2727 – 2739, 2014.

[26] S. Swapp, "Scanning Electron Microscopy (SEM)," 16 May 2017. [Online]. Available: https://serc.carleton.edu/research_education/geochemsheets/techniques/SEM.html. [Accessed 2 July 2019].

[27] D. B. Olsen, B. Neuner and K. Badrinarayanan, Performance Characteristics of Oxidation Catalysts for Lean-Burn Natural Gas Engines, Albuquerque: Gas Machinery Conference, 2013.

[28] S. R. Turns, An Introduction to Combustion, Pennsylvania: Pennsylvania State University, 2000.

[29] B. Hackleman, R. Bauza Tellechea and D. B. Olsen, "Field Evaluation of Oxidation Catalyst Degradation on a 2-Stroke Lean-Burn NG Engine," in *PR-179-16207*, Fort Collins, 2019.

[30] J. F. Moulder, W. F. Stickle, P. E. Sobol and K. D. Bomben, Handbook of X-ray Photoelectron Spectroscopy, Eden Prairie: Physical Electronics, 1995.

[31] D. Henry, "Electron-Sample Interactions," 10 November 2016. [Online]. Available: https://serc.carleton.edu/research_education/geochemsheets/electroninteractions.html. [Accessed 11 July 2019].

[32] 2020. [Online]. Available: https://www.jeolusa.com/RESOURCES/JEOL-Posters-Calendars/lc/47251/lcv/s/jeol-eds-periodic-table. [Accessed 26 May 2020].

[33] R. Gauvin, "CASINO," Quebec, 1996.

[34] M. A. van Sprosen, J. W. M. Frenken and I. M. N. Groot, "Observing the oxidation of platinum," *Nature Communications,* vol. 8, no. 429, pp. 1-7, 2017.

[35] M. E. Birch and NIOSH, "CDC," NIOSH Manual of Analytical Methods, 15 March 2003. [Online]. Available: https://www.cdc.gov/niosh/docs/2003-154/pdfs/chapter-q.pdf. [Accessed 4 June 2020].

[36] B. D. Rice, J. Tillotson and D. B. Olsen, "Crankcase Blow-by Gas Particulate Matter Characterization and Filtration on a John Deere 4.5 l Diesel Engine," Fort Collins, 2017.

[37] A. Legras, A. Kondor, M. T. Heitzmann and R. V. Truss, "Inverse gas chromatography for natural fibre characterisation: Identification of the critical parameters to determine the Brunauer–Emmett–Teller specific surface area," vol. A, no. 1425, pp. 273-279, 18 November 2015.

[38] J. Goodge, "Energy-Dispersive X-Ray Spectroscopy (EDS)," 26 April 2017. [Online]. Available: https://serc.carleton.edu/research_education/geochemsheets/eds.html. [Accessed 02 July 2019].

[39] M. A. Ashraf, O. Sanz, M. Montes and S. Speccia, "Insights into the effect of catalyst loading on methane steam reforming and controlling regime for metallic catalytic monoliths," no. 43, pp. 11778-11792, 2018.

[40] D. B. Olsen, M. Kohls and G. Arney, "Impact of Oxidation Catalysts on Exhaust NO2/NOx Ratio from Lean-Burn Natural Gas Engines," *Air & Waste Management Association,* pp. 867-874, 2010.

[41] "Testo 340 - Combustion Analyzer for Commercial and Industrial Applications.," [Online]. Available: https://www.testo.com/en-US/testo-340/p/0632-3340. [Accessed 27 January 2021].

Appendix A: Activity scan

PIXE Test Report
Elemental Analysis, Inc.
2101 Capstone Dr. Ste. 110
Lexington, KY 40511
Tel: 1-800-563-PIXE(7493)

Date: 11/5/2020
Run: 469
Job: 6900-20
Name: DCL International Inc.
Project: Manasi Deval
Target: RD20201026-01

Element Name	Energy (keV)	Det. Limit 95% Conf.	Concentration Mass	Error
* O ----------			49.319%	
Sodium	1.041	0.136%	2.389%	0.106%
Magnesium	1.254	565.800 ppm	0.121%	0.045%
Aluminium	1.487	469.200 ppm	32.713%	0.327%
Silicon	1.740	218.000 ppm	0.361%	0.024%
Phosphorus	2.010	188.300 ppm	2.551%	0.030%
Sulphur	2.308	299.400 ppm	8.972%	0.090%
Cl	2.623	109.800 ppm		
Potassium	3.314	101.700 ppm	307.707 ppm	60.618 ppm
Calcium	3.692	131.500 ppm	894.694 ppm	84.370 ppm
Sc	4.091	78.840 ppm		
Ti	4.511	104.600 ppm		
V	4.952	191.800 ppm		
Cr	5.415	267.700 ppm		
Manganese	5.899	51.270 ppm	235.735 ppm	25.035 ppm
Iron	6.405	11.510 ppm	1.018%	0.010%
Co	6.930	44.390 ppm		
Nickel	7.478	1.517 ppm	90.781 ppm	2.696 ppm
Copper	8.048	2.651 ppm	291.391 ppm	4.662 ppm
Zinc	8.639	3.641 ppm	0.232%	0.002%
Ga	9.250	6.286 ppm		
Ge	9.887	2.643 ppm		
As	10.544	3.312 ppm		
Se	11.222	17.290 ppm		
Bromine	11.924	1.524 ppm	6.233 ppm	2.064 ppm
Rb	13.395	6.016 ppm		
Strontium	14.165	2.511 ppm	8.038 ppm	2.810 ppm
Yttrium	14.958	2.242 ppm	10.250 ppm	3.276 ppm
Zirconium	15.775	10.240 ppm	66.226 ppm	7.815 ppm
Nb	16.615	6.028 ppm		
Molybdenum	17.479	19.360 ppm	220.120 ppm	15.739 ppm
Tc	18.367	5.072 ppm		
Ru	19.279	9.963 ppm		
Rh	20.216	8.596 ppm		
Pd	21.176	9.798 ppm		
Ag	22.162	11.880 ppm		
Cd	23.173	3.041 ppm		
In	24.210	4.675 ppm		
Sn	25.271	25.220 ppm		
Sb	26.359	45.120 ppm		
Te	3.768	498.000 ppm		
I	3.937	288.000 ppm		
Cs	4.288	204.800 ppm		
Ba	5.157	0.160%		
Lanthanum	5.042	257.100 ppm	1.811%	0.027%
Ce	4.841	118.800 ppm		
Pr	5.034	308.700 ppm		
Nd	5.230	105.400 ppm		
Pm	5.431	175.400 ppm		
Sm	5.632	44.660 ppm		
Eu	5.841	71.950 ppm		
Gd	6.050	45.910 ppm		
Tb	6.271	93.620 ppm		

Figure A1: PIXE pre-restoration test report by DCL as a part of the activity scan

PIXE Test Report
Elemental Analysis, Inc.
2101 Capstone Dr. Ste. 110
Lexington, KY 40511
Tel: 1-800-563-PIXE(7493)

Date:	11/5/2020
Run:	469
Job:	6900-20
Name:	DCL International Inc.
Project:	Manasi Deval
Target:	RD20201026-01

Element Name	Energy (keV)	Det. Limit 95% Conf.	Concentration Mass	Error
Dy	6.492	119.500 ppm		
Ho	6.725	11.970 ppm		
Er	6.945	43.170 ppm		
Tm	7.182	33.220 ppm		
Yb	7.416	13.890 ppm		
Lu	7.655	6.029 ppm		
Hf	7.899	12.510 ppm		
Ta	8.149	18.280 ppm		
W	8.398	41.330 ppm		
Re	8.652	75.770 ppm		
Os	8.911	13.740 ppm		
Ir	9.174	10.730 ppm		
Platinum	9.442	61.470 ppm	0.299%	0.004%
Au	9.712	19.400 ppm		
Hg	9.989	8.876 ppm		
Tl	10.267	5.620 ppm		
Pb	10.551	7.668 ppm		
Bi	10.838	17.630 ppm		
Th	12.968	47.820 ppm		
U	13.616	7.970 ppm		

Figure A2: Continuation of the PIXE test report by DCL as a part of the activity scan

Element Name	Energy (keV)	Det. Limit 95% Conf.	Concentration Mass	Error
* O ----------			50.692%	
Na	1.041	0.148%		
Magnesium	1.254	532.600 ppm	0.225%	0.055%
Aluminium	1.487	418.300 ppm	45.080%	0.451%
Si	1.740	419.800 ppm		
Phosphorus	2.010	453.900 ppm	0.689%	0.027%
Sulphur	2.308	143.300 ppm	0.692%	0.018%
Cl	2.622	124.300 ppm		
K	3.314	95.210 ppm		
Calcium	3.692	126.300 ppm	307.829 ppm	66.583 ppm
Sc	4.091	105.300 ppm		
Ti	4.511	80.770 ppm		
V	4.952	119.600 ppm		
Chromium	5.415	131.100 ppm	0.100%	0.005%
Manganese	5.899	48.570 ppm	158.131 ppm	21.443 ppm
Iron	6.405	10.970 ppm	1.040%	0.010%
Co	6.930	45.960 ppm		
Nickel	7.478	2.119 ppm	152.710 ppm	3.436 ppm
Copper	8.048	2.933 ppm	31.516 ppm	2.688 ppm
Zinc	8.639	2.100 ppm	484.233 ppm	5.956 ppm
Ga	9.252	26.650 ppm		
Ge	9.887	2.564 ppm		
As	10.544	2.572 ppm		
Se	11.222	23.600 ppm		
Br	11.924	3.268 ppm		
Rb	13.395	8.041 ppm		
Sr	14.165	2.324 ppm		
Y	14.958	3.351 ppm		
Zirconium	15.775	5.431 ppm	89.798 ppm	8.199 ppm
Nb	16.615	4.729 ppm		
Molybdenum	17.479	13.080 ppm	48.935 ppm	9.645 ppm
Tc	18.367	3.996 ppm		
Ru	19.279	6.408 ppm		
Rh	20.216	9.180 ppm		
Pd	21.176	14.810 ppm		
Ag	22.162	10.560 ppm		
Cd	23.173	14.420 ppm		
In	24.210	23.460 ppm		
Sn	25.271	25.150 ppm		
Sb	26.359	26.030 ppm		
Te	3.768	370.800 ppm		
I	3.937	247.500 ppm		
Cs	4.288	212.800 ppm		
Ba	4.466	210.300 ppm		
Lanthanum	5.042	204.600 ppm	0.838%	0.019%
Ce	4.841	90.390 ppm		
Pr	5.034	221.400 ppm		
Nd	5.230	89.060 ppm		
Pm	5.431	191.900 ppm		
Sm	5.632	36.120 ppm		
Eu	5.841	60.530 ppm		
Gd	6.050	41.900 ppm		
Tb	6.271	95.950 ppm		

Figure A3: PIXE post-restoration test report by DCL as a part of the activity scan

Element Name	Energy (keV)	Det. Limit 95% Conf.	Concentration Mass	Error
Dy	6.492	124.700 ppm		
Ho	6.725	11.900 ppm		
Er	6.945	44.810 ppm		
Tm	7.182	35.210 ppm		
Yb	7.416	18.640 ppm		
Lu	7.655	6.472 ppm		
Hf	7.899	10.560 ppm		
Ta	8.149	11.100 ppm		
W	8.398	10.290 ppm		
Re	8.652	36.130 ppm		
Os	8.911	6.437 ppm		
Ir	9.174	13.400 ppm		
Platinum	9.442	28.830 ppm	0.516%	0.005%
Au	9.712	11.560 ppm		
Hg	9.989	9.966 ppm		
Tl	10.267	7.436 ppm		
Pb	10.551	8.378 ppm		
Bi	10.838	24.300 ppm		
Th	12.968	66.420 ppm		
U	13.616	11.290 ppm		

Figure A4: Continuation of the post-restoration PIXE test report by DCL as a part of the activity scan

Appendix B: Elemental analysis for fine washing matrix

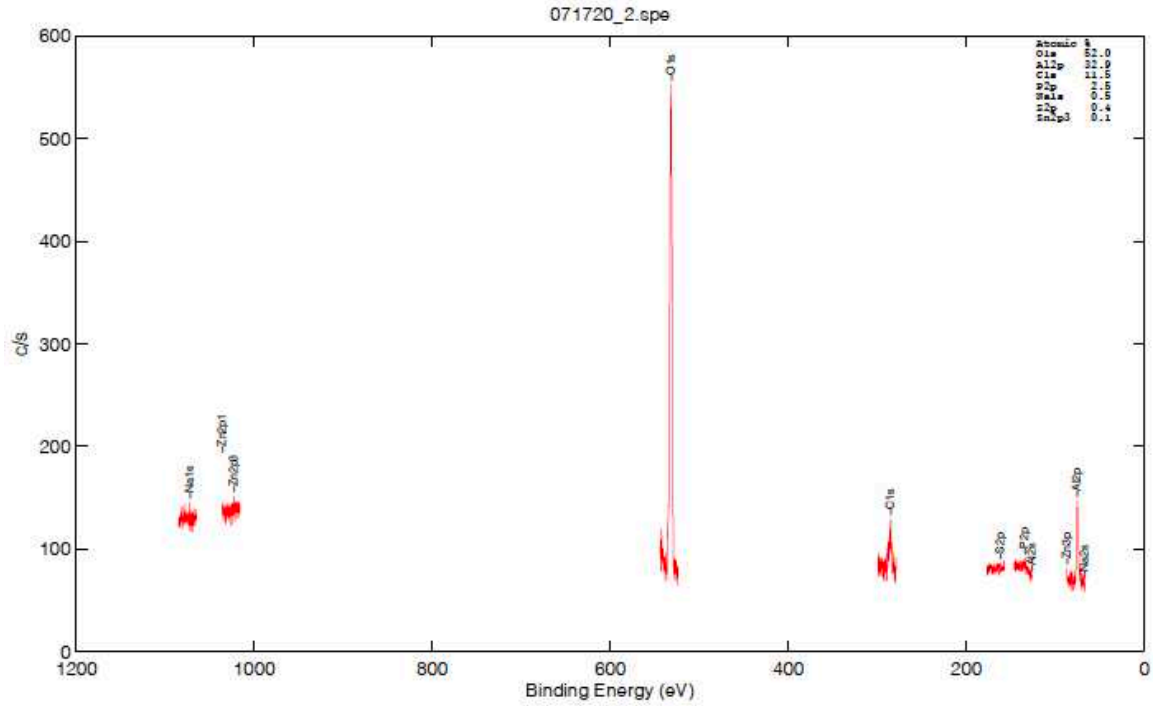

Figure B1: XPS analysis for test R0 from the fine washing matrix

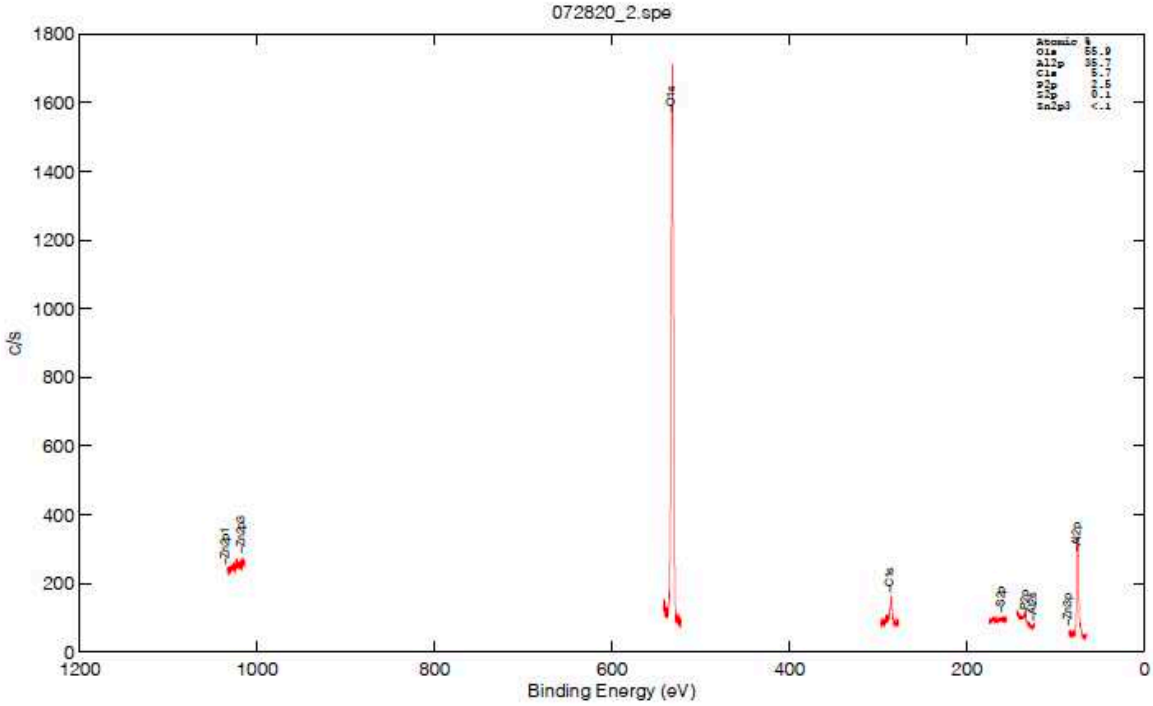

Figure B2: XPS analysis for test R2 from the fine washing matrix

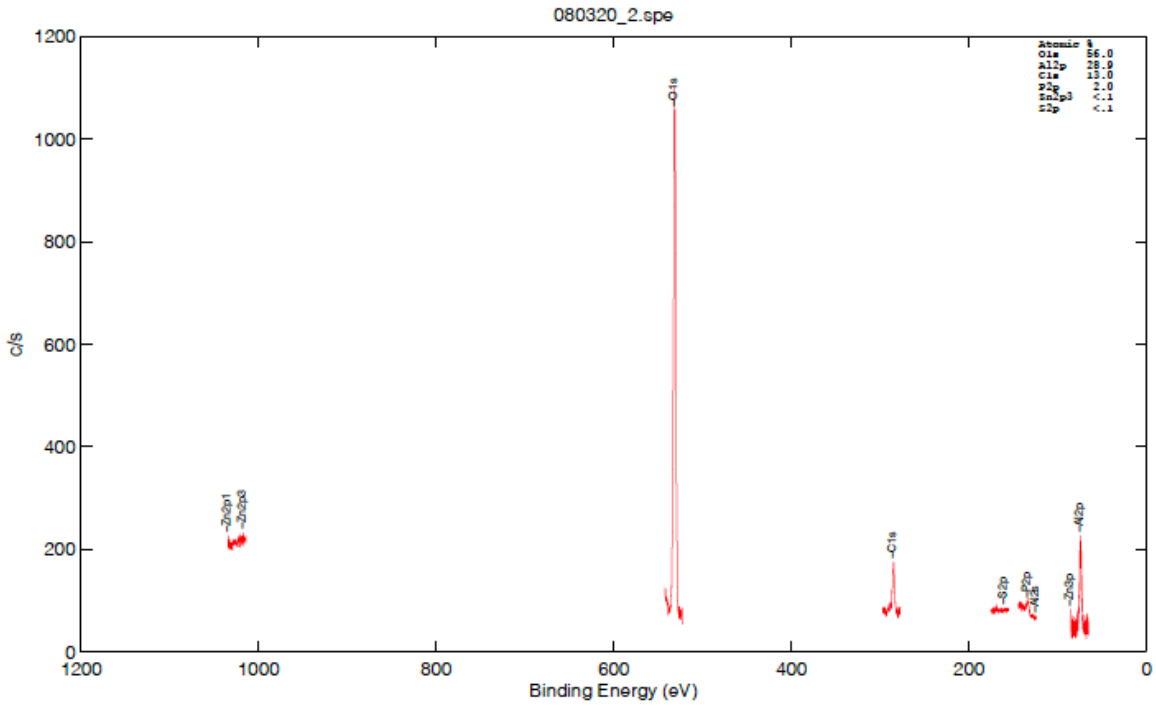

Figure B3: XPS analysis for Test R3 from the fine washing matrix

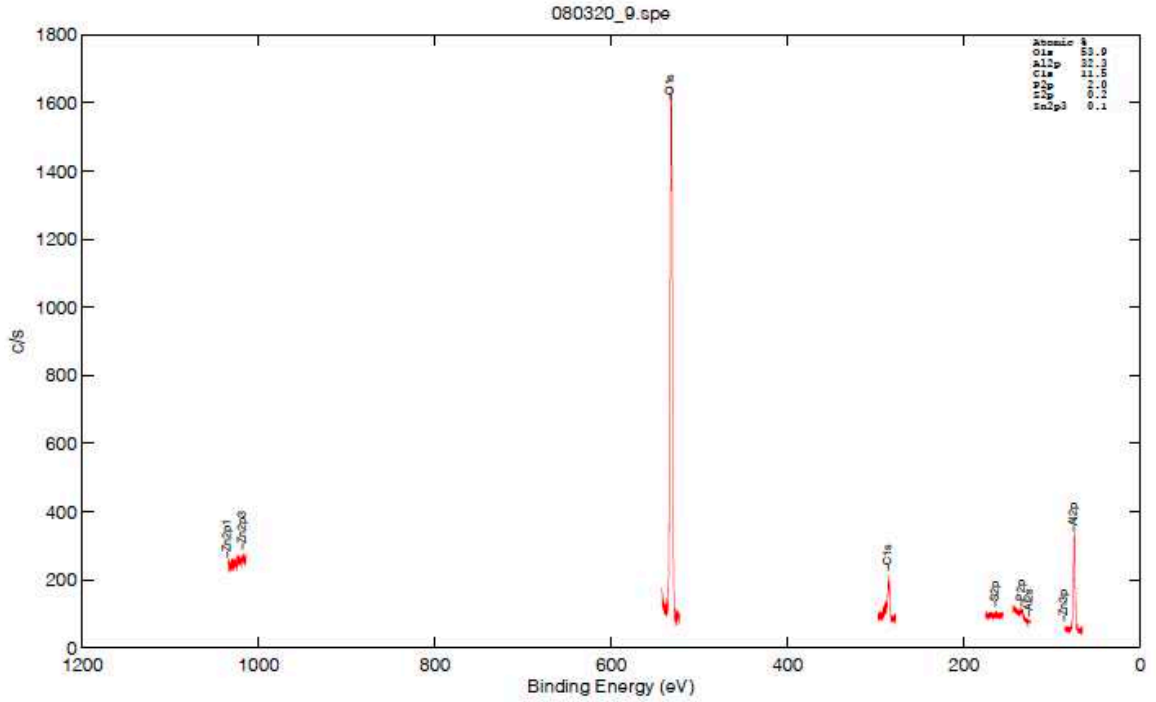

Figure B4: XPS analysis for Test R4 from the fine washing matrix

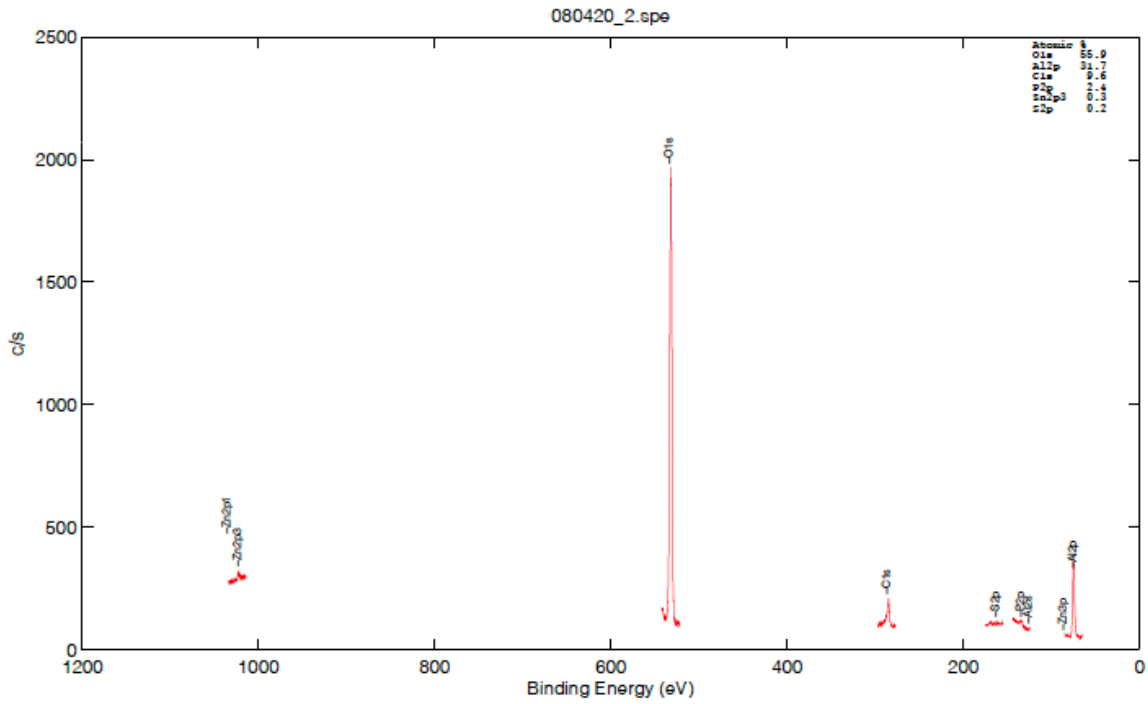

Figure B5: XPS analysis for Test R5 from the fine washing matrix

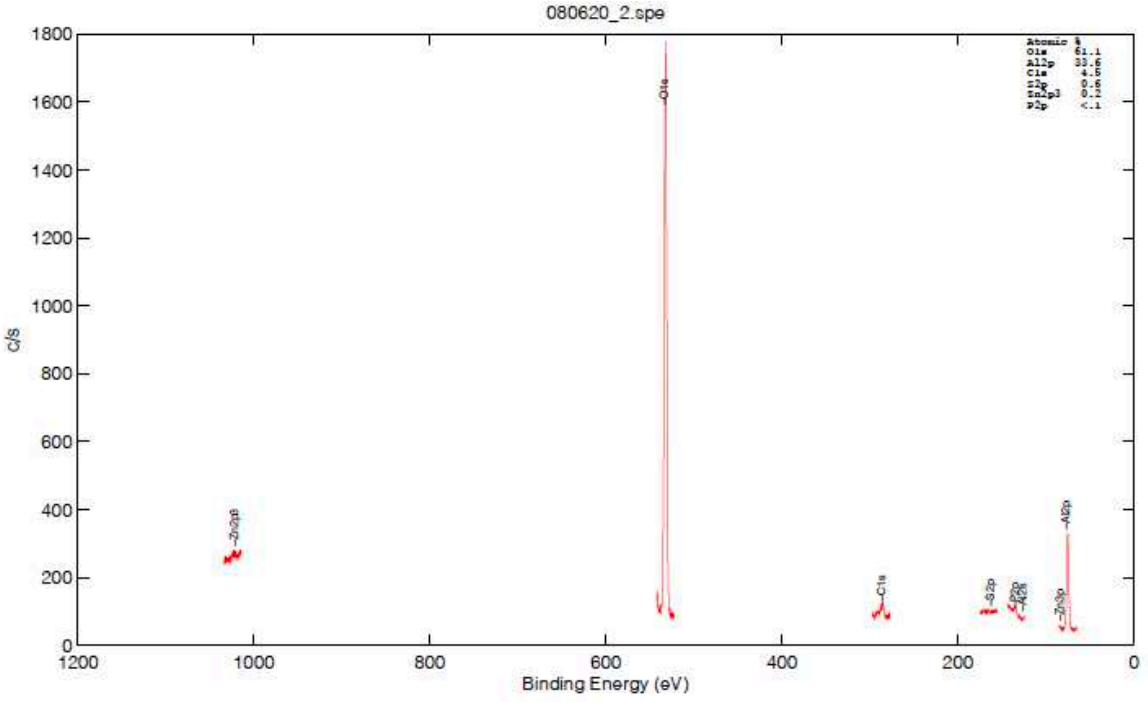

Figure B6: XPS analysis for Test R6 from the fine washing matrix

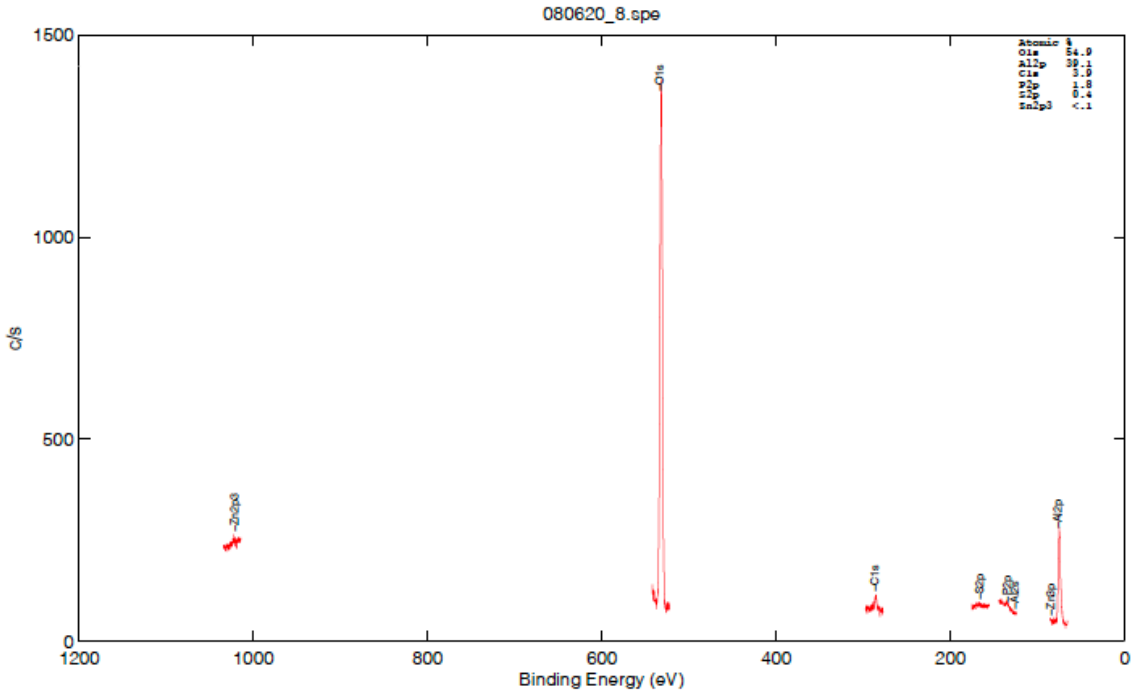

Figure B7: XPS analysis for Test R7 from the fine washing matrix

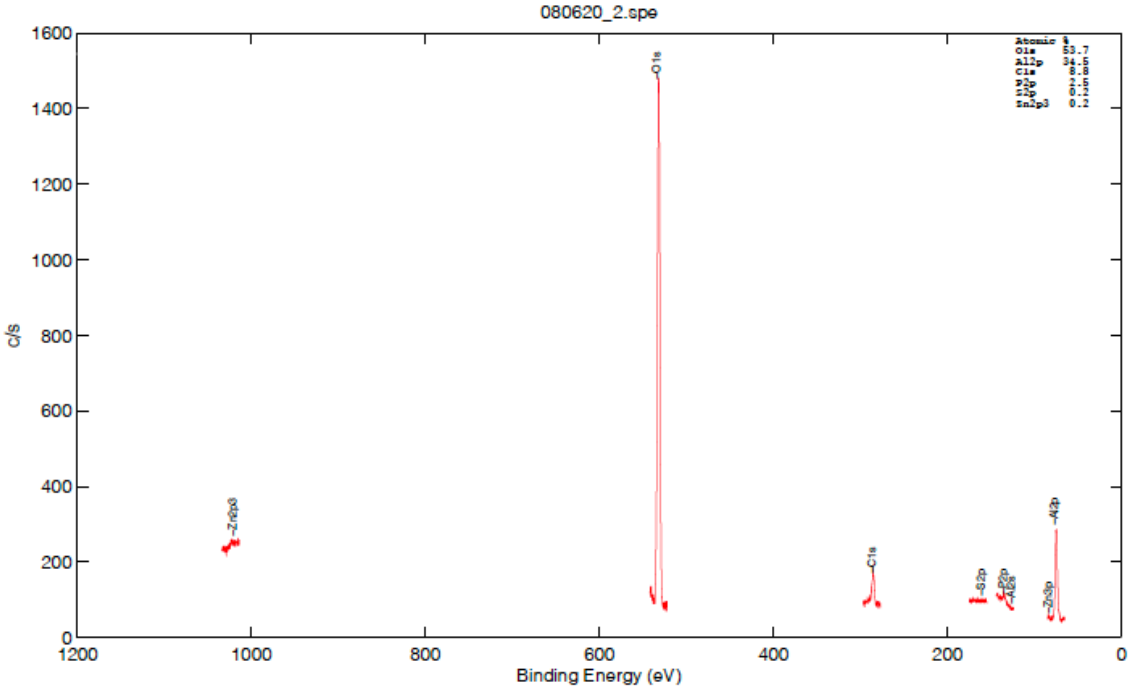

Figure B8: XPS analysis for Test R8 from the fine washing matrix

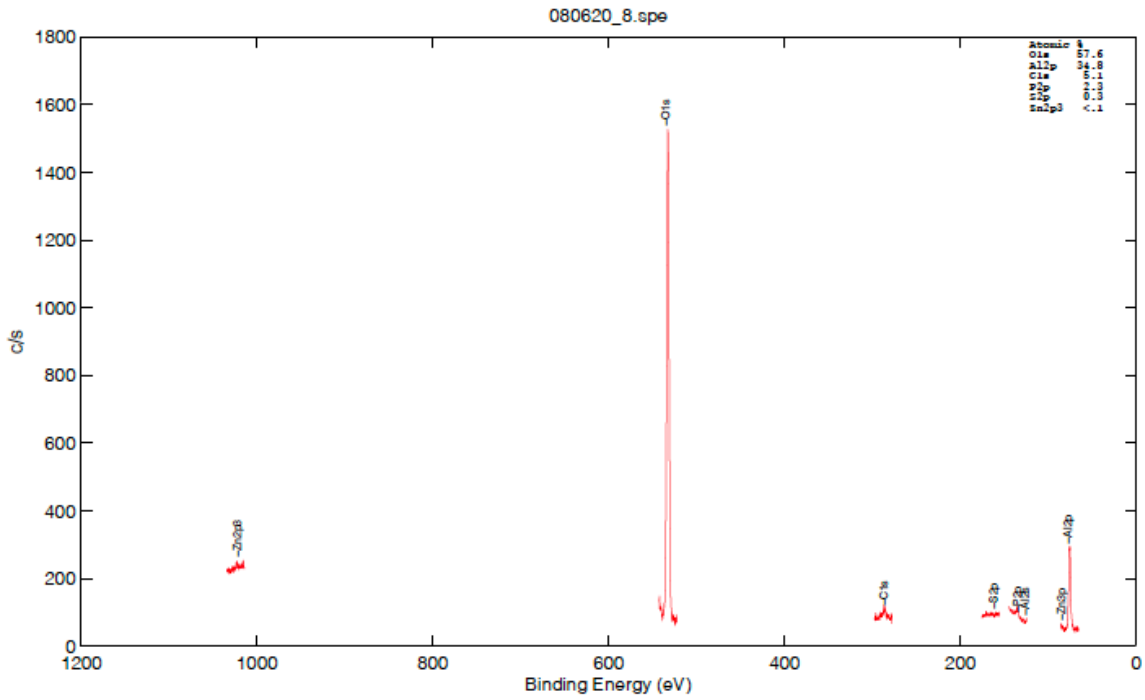

Figure B9: XPS analysis for Test R10 from the fine washing matrix

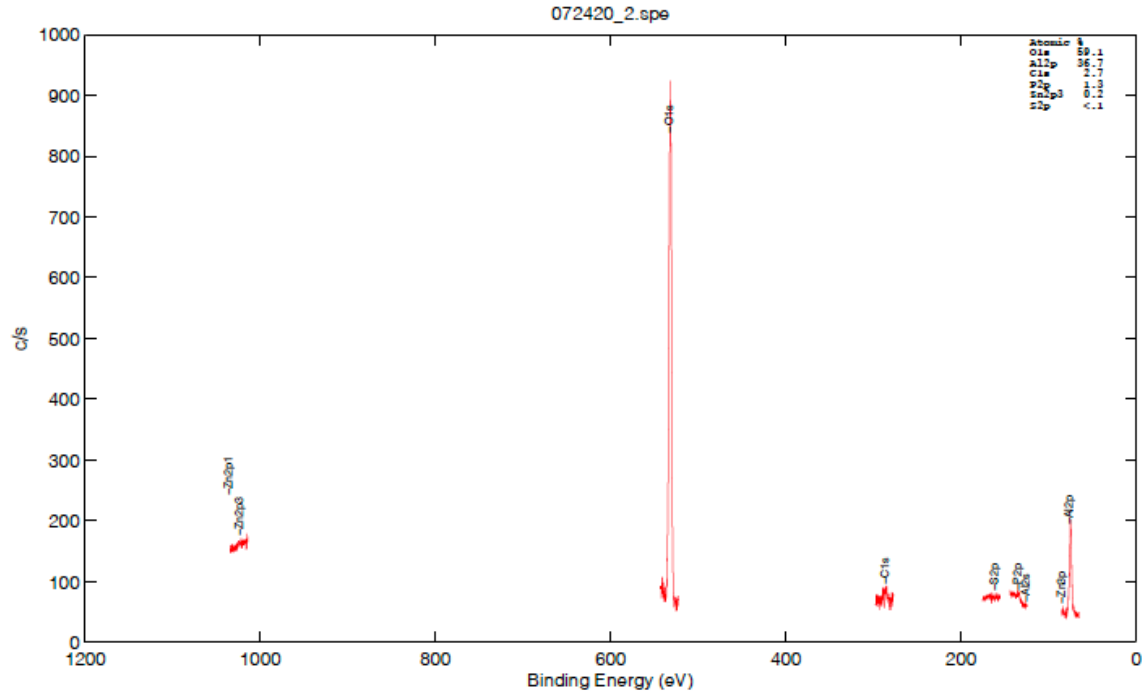

Figure B10: XPS analysis for Test R11 from the fine washing matrix

Appendix C: Additional emission analysis

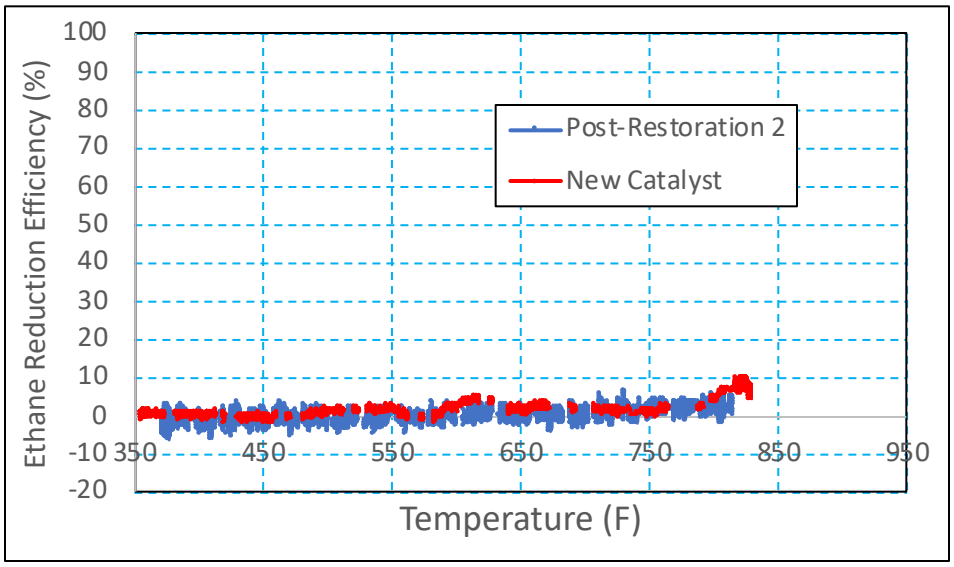

Figure C1: Ethane reduction efficiency as a function of temperature

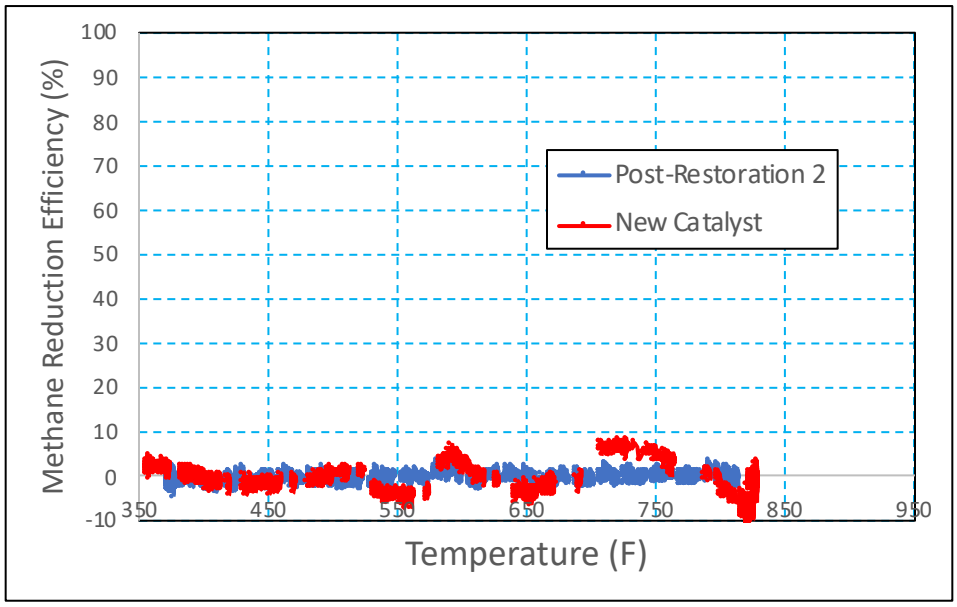

Figure C2: Methane reduction efficiency as a function of temperature

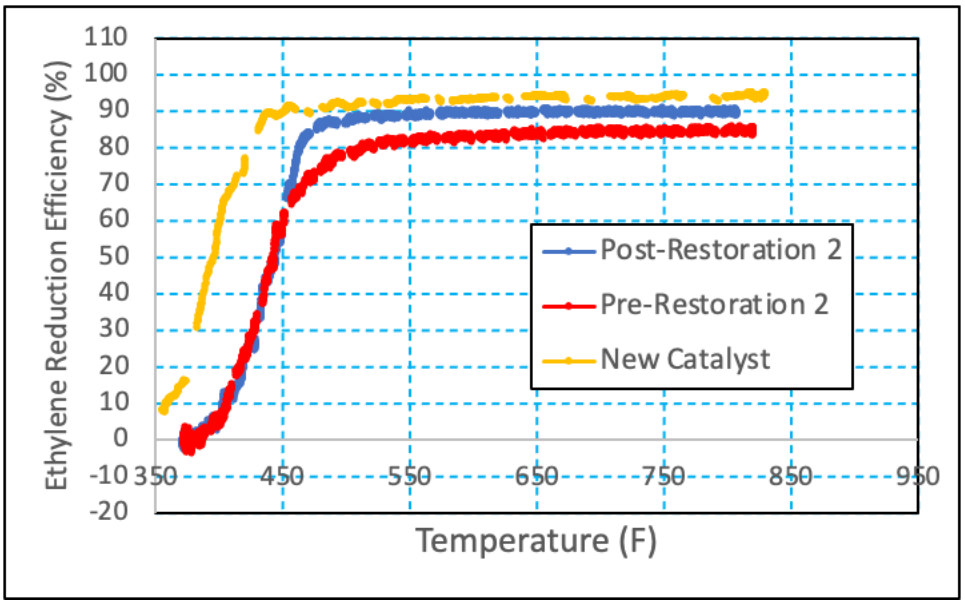

Figure C3: Ethylene reduction efficiency as a function of temperature

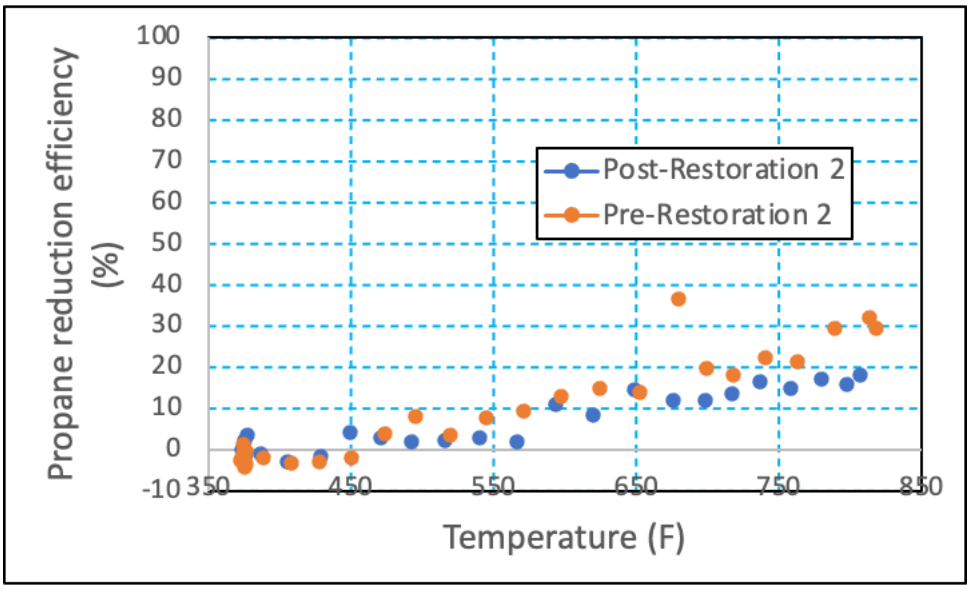

Figure C4: Propane reduction efficiency as a function of temperature